Novel Starch Nanocomposites

by

Sungho Park

A thesis
presented to the University of Waterloo
in fulfillment of the
thesis requirement for the degree of
Doctor of Philosophy
in
Chemical Engineering

Waterloo, Ontario, Canada, 2019

AUTHOR'S DECLARATION

I hereby declare that I am the sole author of this thesis. This is a true copy of the thesis, including any required final revisions, as accepted by my examiners.

I understand that my thesis may be made electronically available to the public.

Abstract

Thermoplastic materials using bio-derived renewable resources are studied intensively and are widely used in applications including packaging, agriculture and other consumer goods. Starch-based plastics exhibit a good balance between environmental benefits, mechanical properties, processability, and low cost. Recently, there have been numerous efforts to amplify the positive effects on the environment while maintaining competitive physical properties in order to meet the needs of the market.

Canadian companies have developed new starch-based products to amplify the positive environmental impacts. Polymer Specialties International developed a new thermoplastic starch copolymer resin with competitive characteristics. However, there is very little information on the reaction mechanisms and chemical compositions. Another Canadian company, Ecosynthetix, is producing starch nanoparticle materials for applications such as paper coating. Recent studies conducted by our research group showed promising results by applying these materials as filler in polyethylene composites. These research problems generated opportunities to investigate and develop new applications.

The goal of this research was to develop a technology to characterize and process environmentally friendly materials using starch as co-polymer and as nanoparticle. The research aimed to extend the range of properties of starch materials while maintaining environmental benefits and competitive physical properties for applications such as packaging and agriculture.

The first research objective was to characterize the new thermoplastic starch copolymer resin. In-depth characterization of its molecular structure and measurement of its thermal and mechanical properties were conducted. The material was also investigated in the presence of nanocellulose as reinforcement. Furthermore, the esterification process using maleic anhydride was done through three different systems: a reactive microwave reactor, a vacuum rotary evaporator, and a twin-screw extruder. A series of studies was conducted and the materials were compared via chemical composition analysis. Mechanisms for maleation were confirmed and this is an important step for manufacturing copolymer resin.

The second objective was to investigate the application of starch as nanoparticle. The focus was on the dispersion of starch nanoparticles in a green polyethylene matrix. Achieving uniform distribution and desired particle size through tuning of the processing conditions and additives were the keys. Detailed characterization of the composite materials were conducted. By designing and applying a systematic approach, uniform nano-sized dispersions of the fillers were achieved within the matrix, and this was confirmed by morphological analysis.

Acknowledgements

Throughout my graduate studies, I have received tremendous guidance, support, and encouragement. I would like to express my sincere gratitude and appreciation to my supervisor, Prof. Leonardo Simon, whose expertise was invaluable in every aspects of my research work.

I am also grateful to the members of my committee, Profs. Yuning Li, Ting Tsui, Jean Duhamel and Michael Thompson for their valuable guidance.

My colleagues in the research group, Bryon Wolff, Chong Meng, Andrew Finkle, Dr. Charles Dal Castel, Dinesha Ganesarajan and Douglas Casetta supported me throughout the time at Waterloo. I thank you all.

Special thanks to my co-op students James Kim and Xiao Zhao for their valuable help.

I would also like to thank my friends from Waterloo, JunGeun, Hyunki, Youngjae, Taejung, Hoonsub, Yunseok, Larry, Seyoung, Juhyeong, Dongun, Yongwook and Moongyu for all the great moments.

I thank Jiwon and her family for love and support.

Dedication

To my parents, Jukuk Park and Domi Seo, and my sister Sanghee Park.

Table of Contents

List of Figures

List of Tables

List of Abbreviations

°C	Degree Celsius
%	Percentage
ATR	Attenuated Total Reflectance
cm	Centimeter
CNC	Cellulose Nanocrystal
CNF	Cellulose Nanofiber
CO_2	Carbon Dioxide
DMTA	Dynamic Mechanical Thermal Analysis
DS	Degree of Substitution
DSC	Differential Scanning Calorimeter
ft	Feet
FTIR	Fourier Transform Infrared Spectroscopy
g	Gram
GPa	Gigapascal
H2O	Water
HDPE	High Density Polyethylene
in	Inch
J	Joule
kg	Kilogram
lb	Pound
LDPE	Low Density Polyethylene
LLDPE	Linear-Low Density Polyethylene
m	Metre
MFI	Melt Flow Index
mg	Milligram
MJ	Megajoule
mm	Millimetre
µm	Micrometre
MPa	Megapascal
nm	Nanometre
NMR	Nuclear Magnetic Resonance
PA	Polyamide
Pa	Pascal
PBAT	Poly(Butylene Adpate-Co-Terephthalate)
PC	Polycarbonate
PE	Polyethylene
PE-g-MA	Polyethylene Grafted Maleic Anhydride
PET	Polyethylene Terephthalate

PHA	Polyhydroxyalkanoates
PLA	Polylactic Acid
PMMA	Polymethyl Methacrylate
PP	Polypropylene
ppm	Parts Per Million
SEM	Scanning Electron Microscopy
SNP	Starch Nanoparticle
T_g	Glass Transition Temperature
TGA	Thermogravimetric Analysis
TPS	Thermoplastic Starch
UV	Ultraviolet
wt.%	Weight Percent

Chapter 1
Introduction

1.1 Motivation and Objectives

Plastics are important materials in today's economy because of their low cost and flexibility in their applications, and they constitute the second-largest petroleum application after energy [1]. However, plastic pollution in both aquatic and terrestrial environment is a growing issue globally. In western societies, on average, every person consumes 100 kg of plastics every year [2]. Among the uses, very small portions (9 to 26%) of plastics are recycled while 22 to 43% end up in landfills [2]. A projection shows that 9 billion metric tons will be recycled, 12 billion metric tons incinerated, and 12 billion metric tons discarded in landfills or exposed to the natural environment by 2050 [3]. Most plastics produced worldwide are not biodegradable and accumulation in the environment is a challenge to modern societies.

Academia and industry have attempted to replace the conventional petroleum-derived materials with more sustainable alternatives, such as bioplastics, for a very long period. The term bioplastics may refer to both plastics from bio-based feedstock (plants and animals) and biodegradable plastics from any source that compost after a certain period [4]. Some common bio-based plastics in today's market are poly(lactic acid) (PLA), polyhydroxyalkanoate (PHA), starch derived plastics, polyethylene (PE) derived from bio-

ethanol and poly(ethylene terephthalate) (PET) obtained via fermentation. Some of these materials already take a big portion of the market whereas others are still in the research and development phase. Table 1.1 illustrates some of these bio-based plastics with their applications and processing methods.

Table 1.1 Bio-based plastics with their major processing methods and applications

Polymer	Major Processing Methods	Major Applications
PLA	Inj. Mold., Blow Mold., Extrusion, etc.	Consumer goods, Packaging, etc.
PHA	Blow Mold.	Packaging, Medical uses, etc.
Starch-Base	Inj. Mold., Blow Mold., Extrusion, etc.	Consumer goods, Packaging, etc.
PET	Blow Mold.	Packaging (Bottles)
PE	Inj. Mold., Blow Mold., Extrusion, etc.	Packaging, Constructions, Automotive, etc.

Bio-based plastics could overcome many sustainability and environmental issues. However, the large scale continuous development of these materials is still facing challenges. Some of the challenges include poor mechanical performance, variability of properties and high production cost with a lack of infrastructure. It is thus necessary to develop and improve the manufacturing of these materials. There are different strategies that can be used to introduce a bioplastic to the market. One strategy that has been very successful is to take a

polymer that is well-known and then prepare its monomer using renewable feedstock. This is the case of polyethylene for example, where ethylene is made from dehydration of bio-based ethanol. Another strategy that has been successful is to take a polymer that is inherently made from a renewable feedstock and modify the polymer structure to adapt to common manufacturing processes (molding, extrusion, etc.). This is the case of PLA for example, where the monomer lactic acid is easily obtained by controlled fermentation [5], but the balance of cost and physical properties of PLA do not meet customer requirements to compete with other polymers very effectively. For better understanding, some of these thermoplastics are categorized based on their sources and compostability in Figure 1.1.

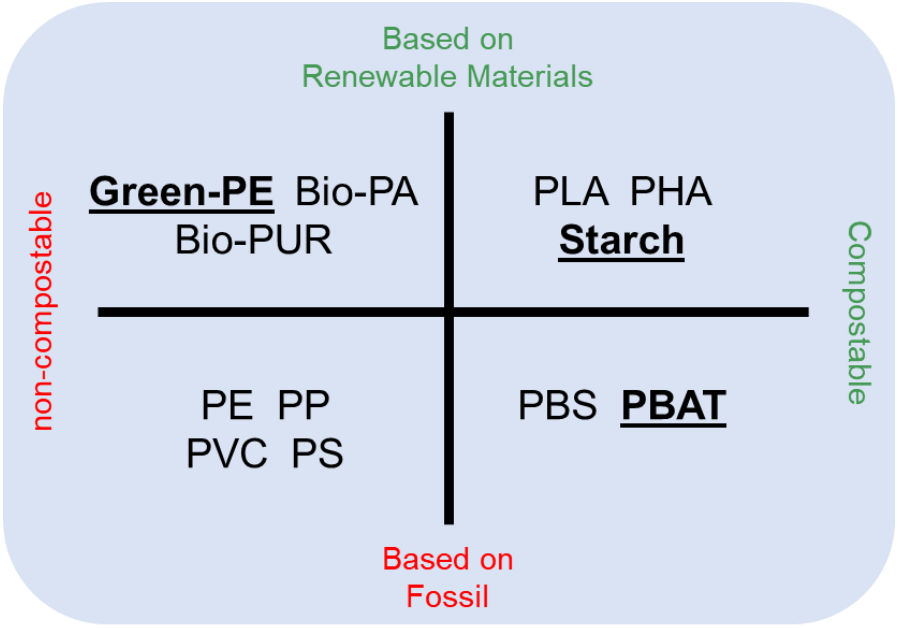

Figure 1.1 Categorization of plastics based on the sources and compostability

Thermoplastic starch (TPS) is an inexpensive bio-based material that is used in a wide range of applications. Despite its environmental benefits, TPS has many weak points such as its susceptibility to moisture [6]. A prolonged exposure to high moisture can alter its

properties and will lead to failure in end-use. Also, the long-term storage of these materials raises the issue of retrogradation [7]. Because of these critical weaknesses, blends of hydrophilic starch and hydrophobic conventional polymers such as polyethylene and polypropylene, are reported in the literature [8-10]. Furthermore, many efforts have been made to chemically modify starch and reduce its hydrophilic nature. This was typically done by replacing the hydroxyl groups on the starch molecules by other functional groups [11-13]. However, to the best of the author's knowledge, there are only a few reports in the literature about the characterization of TPS materials prepared by reactions with other polymers. Therefore, the preparation of TPS copolymers is not well known. This lack of knowledge and understanding precludes the manufacturing of TPS copolymers and the development of starch-based materials with improved properties, such as the resistance to moisture.

The first section of this research investigated a new type of thermoplastic starch copolymer recently developed by a Canadian company called Polymer Specialties International Inc. [14]. This new polymer shows great potential because it is based on starch but it has properties somewhat similar to polyethylene. The research focused on increasing the knowledge for the manufacturing of this new thermoplastic starch copolymer (aspect related to its preparation using reactive extrusion), the characterization of its molecular structure and its physical properties (thermal and mechanical). The material was also investigated in the presence of nanocellulose as reinforcement.

The second section of this research investigated the starch from the filler's point of view. Another Canadian company, EcoSynthetix prepared starch nanoparticles via reactive extrusion. The focus was on dispersing the starch nanoparticles in a green polyethylene

matrix. This approach was to incorporate starch into a thermoplastic that is non-compostable but is prepared from renewable sources. Achieving a uniform distribution and desired particle size through the tuning of the processing conditions and additives were key factors. The physical and chemical properties were related to the filler particle size.

The objectives of this research were to develop a technology to characterize and process environmentally friendly materials using starch as a polymer and as nanoparticle. The research aimed to extend the range of properties of starch materials while maintaining environmental benefits and competitive physical properties for applications such as packaging and agriculture.

1.2 Thesis Layout

This thesis is composed of 7 chapters. The layout is presented in Figure 1.2.

The first chapter describes the motivation and objectives of the overall study with the layout and the experimental plans. The second chapter reviews some literature about the materials, processing techniques, and analysis. Chapters 3 and 4 describe the study of starch utilized as co-polymer. Chapter 3 lists the materials used along with the preparation and testing procedures, and Chapter 4 provides experimental results and discussion. Chapters 5 and 6 correspond to the study of starch utilized as nanoparticle in composites. Finally, the last chapter reviews the conclusions reached in the study and recommends some future works.

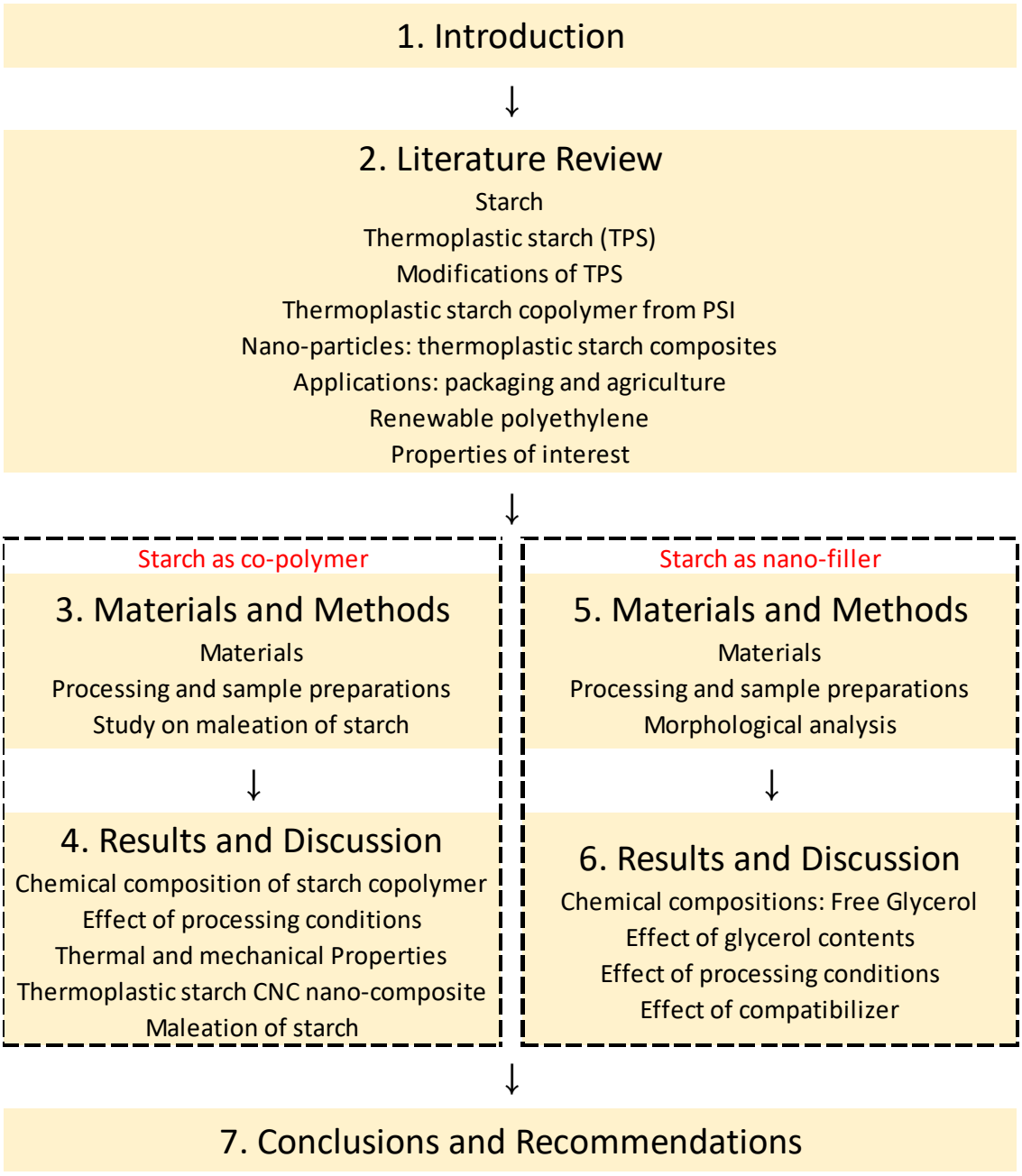

Figure 1.2 Thesis Layout with contents

Chapter 2
Literature Review

2.1 Starch

Starch is a carbohydrate that is found in many plant species including potato, corn, cassava, rice, etc. It is an important means of energy storage for these plants and thus many animals including humans consume the starch-containing components of these plants as food. Also, it is a natural polymer that has attracted a lot of attention lately as a possible alternative to petroleum-based plastics. Chemically, it has a large number of glucose units joined by glycosidic bonds. Figure 2.1 represents the molecular structure of the starch repeating units.

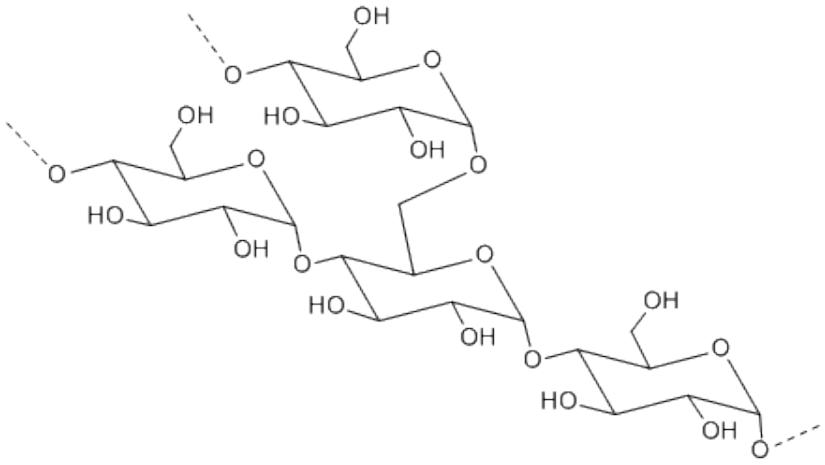

Figure 2.1 Molecular structure of starch (reproduced from [15])

As the figure illustrates, it is composed of a long chain of glucose units with a few branching points. Linear amylose and branched amylopectin are the two molecular building

blocks of starch. Depending on the sources, the contents of amylose and amylopectin differ, and thus the average weight chain length and degree of branching differ as well. In amylose, the glycosidic linkage is from carbon 1 to 4 (α-(1→4)), whereas amylopectin has the same backbone configuration as amylose with glycosidic linkages from carbon 1 to 4 (α-(1→4)), but also from carbon 1 to 6 (α-(1→6)), forming branch points.

The level of organization in starch granules is quite complex. Analytic techniques such as x-ray diffraction (XRD) and electron microscopy have contributed to analyze the native form of the starch found in the granule. Figure 2.2 illustrates the levels of organization of a starch granule. Amylose and amylopectin molecules are organized in granules as alternating amorphous and semi-crystalline concentric growth layers. The semi-crystalline layers consist of ordered regions composed of double helices formed by short amylopectin branches. The semi-crystalline layers are further ordered into crystalline structures (crystalline lamellae) and amorphous lamellae. The amorphous regions of the semi-crystalline layers and the amorphous growth layers are composed of amylose and non-ordered amylopectin branches [16, 17].

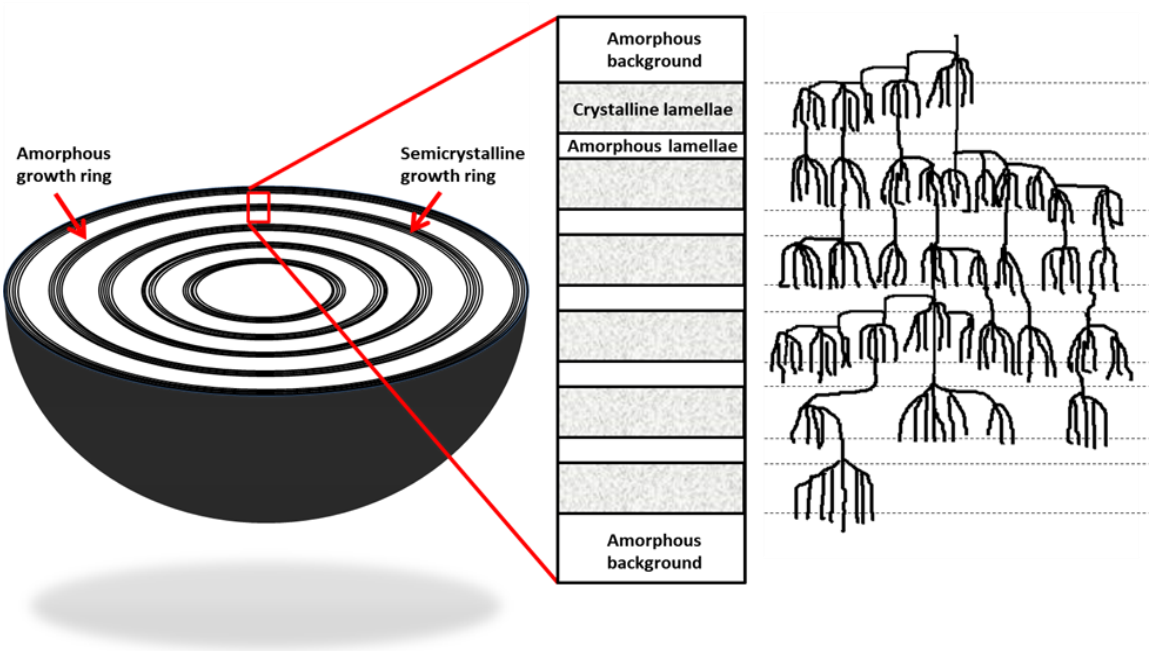

Figure 2.2 Starch granules organization (reproduced from [17])

Starch granules have numerous pores present on the surface (Figure 2.3). In fact, starch granules can be considered as porous material exhibiting both external and internal surface areas. The external surface area can be determined by microscopic analysis and light scattering techniques. Again, the geometry and quantity of these pores vary depending on the sources of starch granules [18].

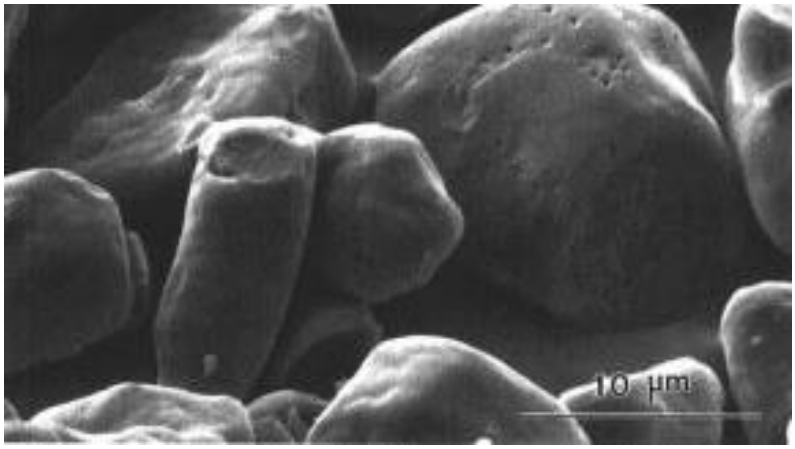

Figure 2.3 Scanned electron microscopy image of corn starch granules [19]

2.2 Thermoplastic Starch

The crystalline regions in starch disappear when it is subjected to temperatures greater than ~70 $^{\circ}$C in the presence of plasticizers such as water or glycerol. The plasticizers break hydrogen bonds between starch macromolecules, accompanied by partial depolymerization of the starch backbone. This helps to lower the melting and the glass transition temperature of starch below its decomposition temperature of 230 ^{o}C. The product of this transformation is called thermoplastic starch (TPS). Gelatinization is the process of breaking intermolecular bonds of starch molecules using plasticizers such as water and glycerol, and high temperature. The heat helps the plasticizer molecules to diffuse into the crystalline domains of the starch molecule. Because of its high molecular weight, high plasticization levels are required for gelatinized starch to flow. Using extrusion that provides a closed pressurized environment with high temperature and shear stress that breaks down the crystalline structure and renders starch completely amorphous, gelatinization along with some molecular weight reduction can be achieved. Once the starch is gelatinized and plasticized, the TPS can flow

just as any other molten thermoplastic polymer and thus is suitable for conventional molding and other thermoplastic processing technologies.

The role of plasticizer is crucial to improving the mechanical, thermal and water absorption of TPS. A study was conducted to see the effects of different plasticizers on TPS using monohydroxyl alcohols, high molecular weight glycols, and low molecular weight glycols. In general, products using low molecular weight glycols exhibited a superior outcome whereas monohydroxyl alcohols and high molecular weight glycols failed to plasticize the starch in the first place. Among many other alcohols, ethylene glycol was the most effective. The quantity of plasticizer did not affect the crystallinity of the products but affected the mechanical properties. Tensile testing revealed improvements in tensile properties as ethylene glycol contents increased up to 40% (Figure 2.4) [20].

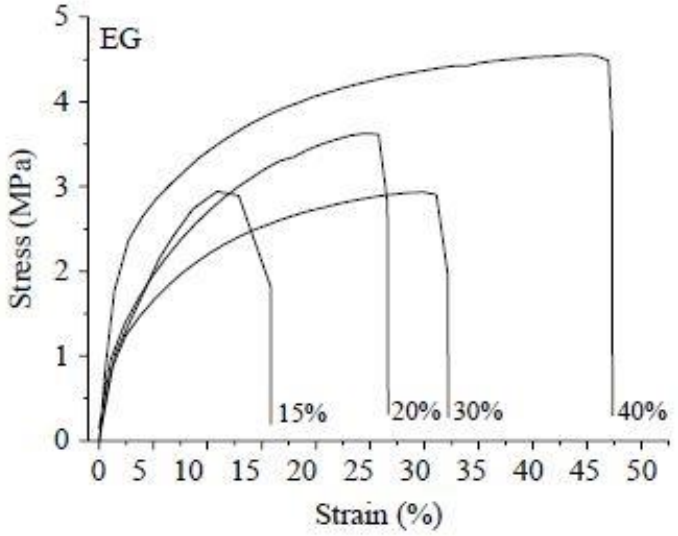

Figure 2.4 Stress-strain curve of TPS, plasticized using ethylene glycol as plasticizer at different concentrations [20]

2.3 Modification of Thermoplastic Starch

Natural starch is inherently unsuitable for most plastic applications. Therefore, it is often modified either chemically or physically. Modified starch can enhance the positive attributes of starch while minimizing its drawbacks. Many starch derivatives are used in food processing, papermaking, the pharmaceutical industry and as adhesives. As a replacement to conventional petroleum-derived plastics, TPS is also modified in order to meet the properties required for specific applications. The hydrophilic nature of TPS makes it susceptible to moisture attacks and significant changes in dimensional stability and mechanical properties [21-23].

Chemical modification of TPS generally involves esterification, etherification or oxidation of the hydroxyl groups. The addition of reactive and organic reagents to an aqueous slurry of starch is done to produce most commercial derivatives. Tuning the reactive environment is necessary as well. Typically, pH of 7-9 is required for esterification whereas more basic environment of pH 11-12 is required for etherification. A relatively mild temperature of 60 °C or less is common to prevent oxidation and degradation of the polymer chain. Neutralization using strong acids such as hydrochloric acid and sulfuric acid is often done, followed by washing with water and drying in the end [24, 25].

2.3.1 Starch Esters

Traditionally, starch esters have low degrees of substitution (DS) and are prepared in aqueous media via batch processes [26]. Nowadays, continuous processes via reactive extrusion (REX) have become a popular tool for the modification of starch. Esterification with anhydrides, carboxylic acids, and vinyl esters have been studied extensively.

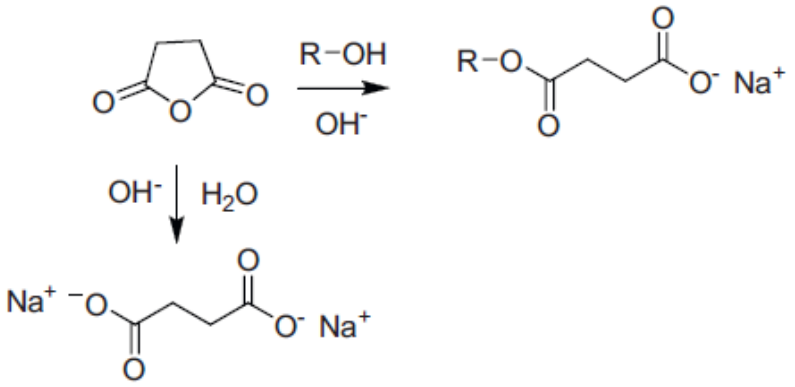

Figure 2.5 Base-catalyzed esterification of succinic anhydride (ring-opening) [27]

The esterification of starch by anhydrides may be catalyzed by acid or base. The overall reaction is shown in Figure 2.5 for a base-catalyzed esterification with succinic anhydride. This process has a clear advantage that there are no byproducts formed since it is a ring-opening reaction. There are numerous anhydride esterification processes done using different anhydrides and catalysts with an extrusion [28, 29].

Maleic anhydride is also quite popular in starch-polymer composites. The reaction for the grafting of maleic anhydride is illustrated in Figure 2.6. One or more hydroxyl groups can be replaced by ring-opening of maleic anhydride. However, the C6 position is the most preferential position. The product of this reaction has been studied extensively. For example, polyethylene grafted maleic anhydride with starch was used to produce biodegradable polyolefins and polyesters. Poly(butylene adipate-co-terephthalate) (PBAT) grafted maleic anhydride was used as an additive to prepare starch foams [30].

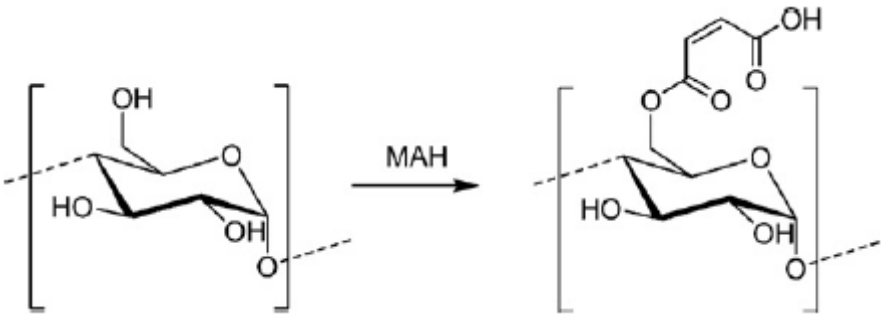

Figure 2.6 Grafting maleic anhydride to starch [29]

2.3.2 Blends and Composites

Often starch is blended or put into composites with other polymers to enhance the environmental benefits and retain desirable physical properties. There are a few literature reports for these blends and composites [31-33]. While retaining its granular structure, starch is put into composites or thermoplastic starch (TPS) is blended with another polymer. The main obstacle facing the blends or composites is the hydrophobic nature of most synthetic polymers. Simply mixing these polymers with hydrophilic starch results usually in a composite with poor properties and morphology due to phase separation. In order to reduce phase separation, interfacial agents are used. These interfacial agents should contain some chemical motives that are similar to the starch and other polymers. However, due to the difference in nature between motives, it is extremely difficult to co-polymerize these products. Reactive extrusion helps to overcome this problem.

Use of maleic anhydride and maleic acid as coupling agent (interfacial agents) was reported in a few studies [29, 30]. These reagents functioned as esterification catalysts and a grafted co-polymer (Starch-PBAT) product was successfully produced. Furthermore, maleic anhydride with a peroxide radical initiator was added to starch and PBAT in an extruder. The

addition of the peroxide resulted in better properties. Table 2.1 shows some of the starch-synthetic polymer compositions processed with maleic anhydride. Also, there are a number of studies with maleic anhydride modified polymers (polyolefin-*g*-maleic anhydride, PLA-*g*-maleic anhydride, PBAT-*g*-maleic anhydride, etc.) blended with starch [34, 35].

Table 2.1 Synthetic plastic-starch blends/composites processed with maleic anhydride

Compositions	Reference
PLA-starch-maleic anhydride-2,5-bis(tert-butylperoxy)-2,5-dimethylhexane	[34]
PLA-plasticized starch-maleic anhydride-2,5-bis(tert-butylperoxy)-2,5-dimethylhexane	[34]
PLA-glycerol-plasticized starch-maleic anhydride-peroxide	[36]
PE-maleic anhydride-peroxide	[37]

2.4 Thermoplastic Starch Copolymer from PSI

The term thermoplastic starch copolymer was coined by Polymer Specialty International Inc (PSI), a Canadian company with a research and development center located in Newmarket, Ontario. The company developed and patented a new material while the process of making the material is described in their patent [14]. The process uses a mixture of at least one of a dicarboxylic acid and a dicarboxylic acid anhydride with starch to yield a starch mixture. Adding a liquid mixture including water and polyol to the starch mixture produces a functionalized starch. Mixing the functionalized starch with a resin produces the starch-resin copolymer. The material produced by this method is biodegradable and compostable. Table 2.2 provides examples of the compositional range of the raw materials in each reaction stage.

The material and the process developed by PSI will be the basis for the research project proposed for this Ph.D. thesis.

Table 2.2 Compositional formulation of PSI starch resin copolymer [14]

Raw material	Stage 1	Stage 2	Stage 3
Starch	85-99.8%	65-85%	40-60%
Maleic Anhydride	0.2-15%		
Glycerol		10-25%	
Water		4-12%	
Peroxide		0-0.3%	
Polyester			40-60%
Total	100%	100%	100%

Studies taken from the literature showed that maleation of starch is known to cleave the starch backbone by hydrolysis and thus the degree of grafting is greatly enhanced by maleic anhydride [29, 30, 38]. Figure 2.7 shows the schematics for the maleation, hydrolysis and glucosidation reactions occurring during the reactive extrusion of maleated thermoplastic starch.

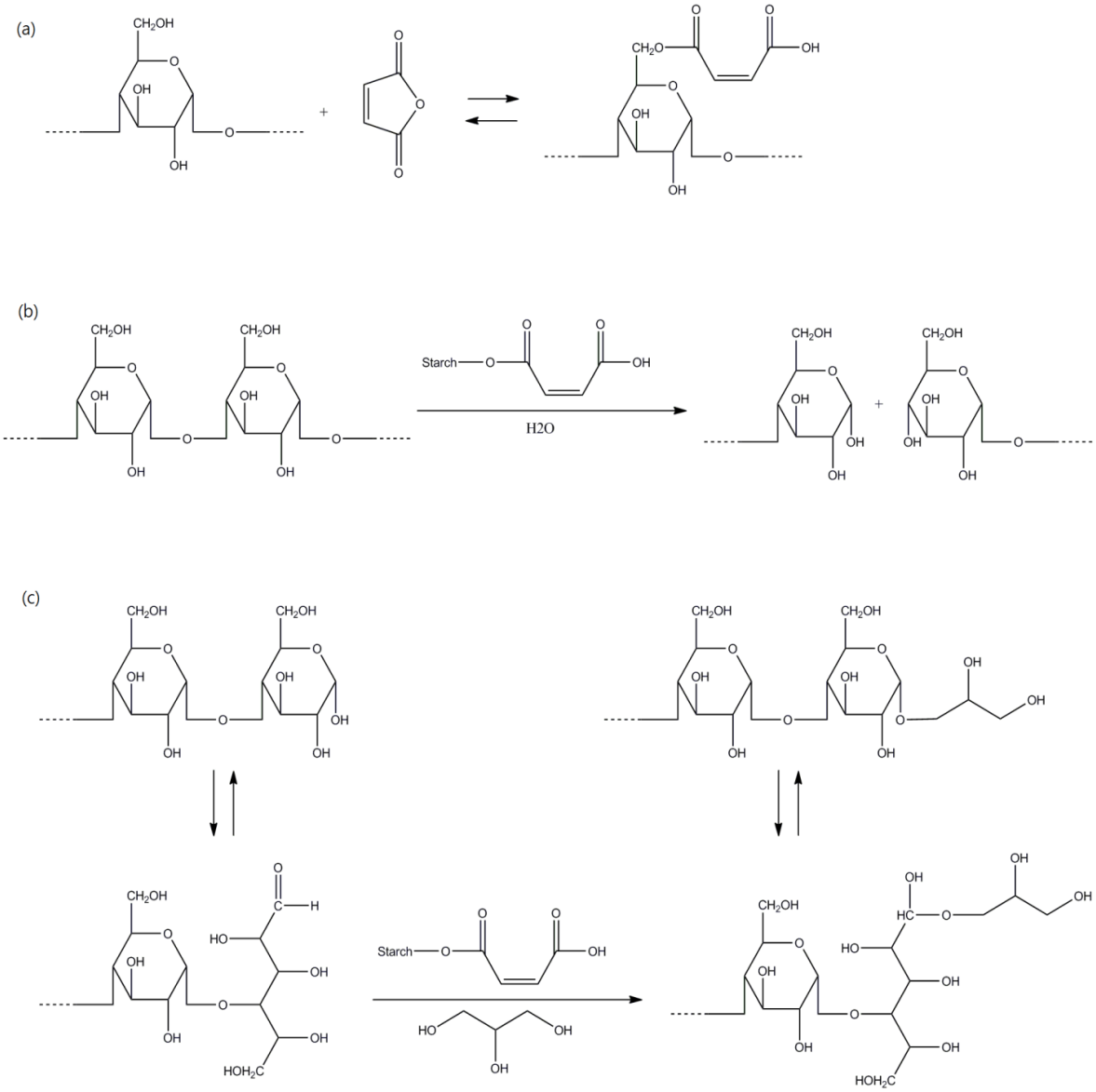

Figure 2.7 Maleation, hydrolysis and glucosidation reactions occurring during the reactive extrusions of maleated thermoplastic starch

This chemically modified starch has a high reactivity toward polyesters such as biodegradable poly(butylenes adipate-co-terephthalate, PBAT) that can yield graft copolymers [30]. Blending the modified starch with PBAT is an easy process to reduce the hydrophilic nature of starch and give environmental benefits at the same time.

Hablot et al. also proposed mechanisms of transesterification reactions between modified thermoplastic starch and PBAT. They suggested that graft copolymers were formed by covalent bonds through acid-promoted transesterification reactions between the ester functionalities of PBAT and the hydroxyl groups of the thermoplastic starch (Figure 2.8). These reactions were confirmed from the analysis of the ATR-FTIR spectra of the products.

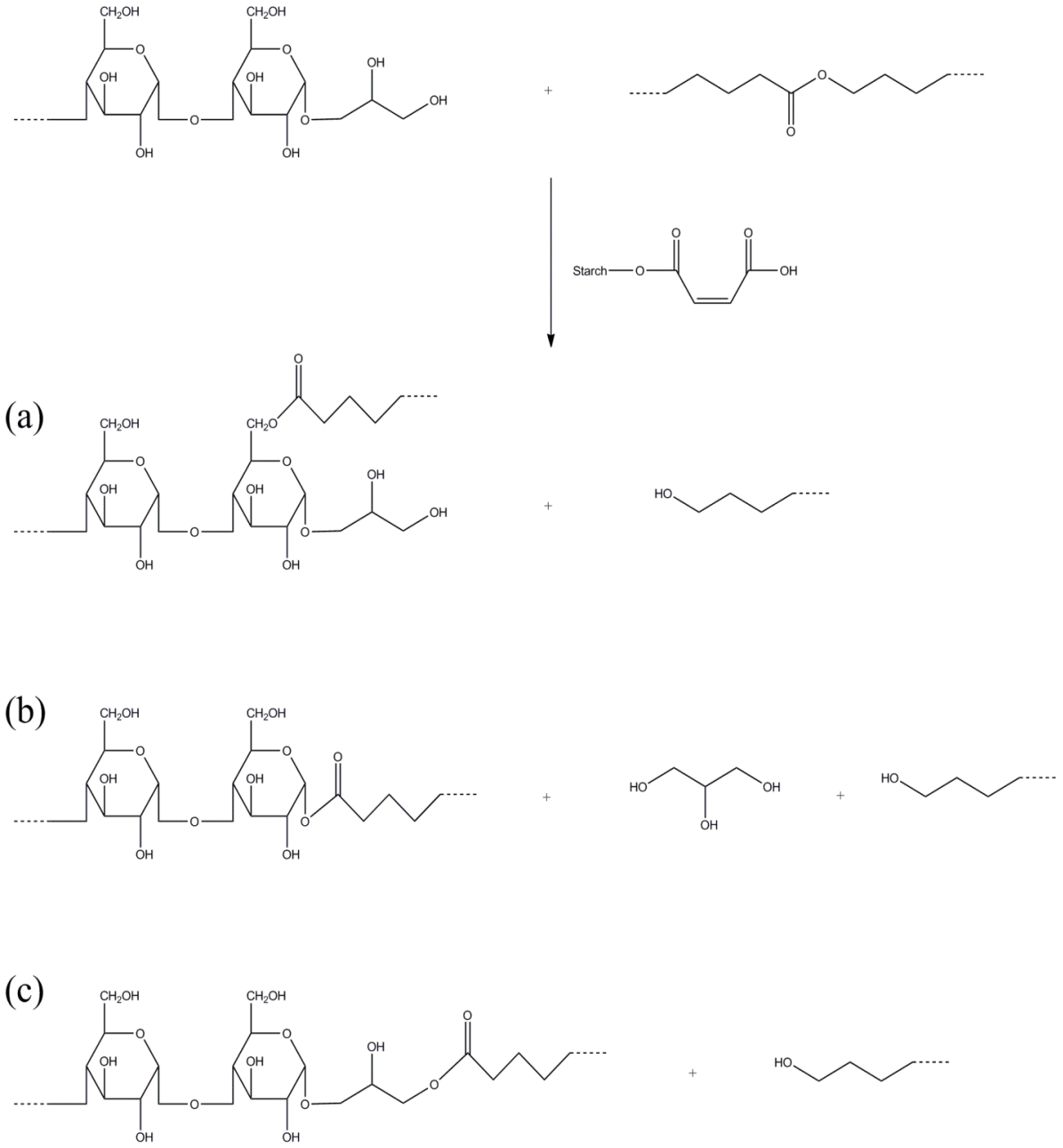

Figure 2.8 Proposed mechanism of transesterification reactions between thermoplastic starch and PBAT

2.5 Nanoparticles-Thermoplastic Starch Composites

Nano-size particles can be used to fill many types of thermoplastics in order to enhance their chemical, mechanical and even electromagnetic properties. Clay-based nanocomposites

have been extensively studied in the last decade and can now be applied commercially. They have shown many advantages over their conventionally filled micro-counterparts. Improved tensile properties, high modulus, increased strength and heat resistance, thermal stability, decreased gas permeability, and flammability are all advantages of the clay nanocomposites. Recently, clay-TPS composites were synthesized and their properties were reported [39].

The synthesis of carbon nanotube (CNT) is a relatively newly developed technology. CNTs have been prepared with a high aspect ratio. These cylindrical carbon-rich molecules have a wide range of applications in nanotechnology, including in composites, electronics, and optics. Despite inconsistencies in properties due to the CNTs synthesis, a wide range of aspect ratios, and difficulties in purification, CNT composites are extensively studied for many engineering applications. A few studies on CNT-TPS composites can be found in the literature. CNT showed a reinforcing effect while the CNT-TPS composites had improved water resistance and some electrical conductivity [40].

Another environmentally friendly option for TPS nanocomposites is using cellulose nanocrystal (CNC) which is further described in the next section.

2.6 Cellulose Nanocrystal (CNC)

In the area of nano-cellulosic materials, there are three major groups of materials. They are cellulose nanofibers (CNF), cellulose nanocrystals (CNC, also known as nanocrystalline cellulose NCC), and bacterial nanocellulose (BNC). CNF is produced by mechanical delamination of wood fibres using high-pressure, homogenizer equipments or super grinders. CNC can be obtained from native fibres by acid hydrolysis, giving rise to highly crystalline

and rigid nano particles which are shorter (100-1000 nm) than CNF obtained through the homogenization route. BNC is formed by several species of fermentation bacteria [41]. In this research, only CNC was considered and utilized.

CNC can increase the strength and stiffness of materials. Just a small amount can increase the resistance to stress, making it attractive as a high-performance reinforcing material. CNC can also alter the surface of materials like paper, changing its permeability, strength, flexibility and optical properties. Adding a little CNC to paper noticeably boosts its gloss. CNC can also improve tensile strength, stiffness and surface smoothness. These properties can provide new opportunities to develop advanced high-strength materials [42].

Another advantage of CNC is environmental friendliness. CNC is the product of renewable, recyclable natural resources (pulp is the main source material) and testing to date suggests that it is virtually non-toxic and its production poses no serious environmental risks.

The length and width of CNC depend on the nature of the cellulose source, as well as the extraction conditions. It is reported that CNC can have a diameter ranging from 5 to 20 nm and its length can be a few hundreds of nanometers. Literature reports that its Young modulus ranges from 130 to 250 GPa [43].

2.7 Potential Applications

2.7.1 Films for Packaging

Many paper-based packagings these days have implemented plastic coatings for various reasons. It gives a glossy look, better moisture resistance, improved mechanical properties, and sometimes works as an oxygen barrier in food packaging. In most of these cases,

conventional petroleum-based polyethylene is used. Regardless of these benefits, when it comes to disposal and recycling, polyethylene films attached to paper products exhibit limitations and cause environmental issues [44]. Hence consumers and government legislations are in opposition to this type of packaging. The demand for more environmentally friendly packaging materials is rising quickly. After imposing a surcharge on plastic and paper grocery bags, San Francisco, California became the first city in the United States that made an effort to reduce the amount of plastics used in packaging. Table 2.3 shows the status of legislations on plastic bags in the USA [45].

Table 2.3 Status of plastic legislation (reproduced from [45])

States	Plastic bag ban	Plastic bag fee	Discussion
Alaska	2009 (Bethel)		
Arizona	2013 (Bisbee)		
Arkansas			2013 (Little Rock)
California	2007 (San Francisco)		
Colorado	2010 (Telluride)		
Connecticut	2008 (Westport)		
Hawaii	2008 (Maui County)	2009 (Kauai County)	
Illinois	2014 (Chicago)		
Indiana			2012 (House Bill No. 1521, IN)
Iowa	2009 (Marshal County)		
Maine		2014 (Portland)	
Maryland	2012 (Chestertown)	2011 (Mongomery County)	
Massachusetts	2012 (Brookline)		
Nevada			2009 (Bill 397, NV)

New Mexico	2013 (Santa Fe)		
New York	2011 (East Hampton)		
North Carolina	2009 (Hyde, Currituck and Dare)		
Oregon	2010 (Portland)	2012 (Corvallis), 2013 (Eugene)	
Pennsylvania			2009 (Bill 864, Bill 609)
Rhode Island	2009 (Barrington)		
Texas	2010 (Fort Stockton)		
Vermont			2013 (Bill 262, Bill 33, VT)
Virginia			2009 (Bill 1814, VA)
Washington	2009 (Edmonds)		
West Virginia			2009 (House Bill 3058, WV)
Wisconsin			2009 (Assembly Bill 170, WI)
District of Columbia		2009 (Washington)	

Although there are many materials in the market that are compostable, their properties do not meet some standards. One of the most important factors to consider is the moisture barrier. Traditional thermoplastic starch, for example, has satisfactory mechanical properties; it comes from renewable sources and it is compostable. However, it is extremely susceptible to moisture which makes it unsuitable for many packaging applications. This is one of the motivations to study the new improved moisture resistant thermoplastic starch copolymer from PSI Inc.

2.7.2 Films for Agricultural Uses

In order to secure and increase produce outputs while enhancing crop quality, agricultural growers often apply plastic films as an aid (Figure 2.9). An estimated 98,000 tons of polyethylene plastic mulch is used in North American and 700,000 tons worldwide to improve crop yield, modify soil temperature, and conserve moisture [46]. However, this agricultural tool is very costly from both economic and environmental perspectives. The mulch is produced from non-renewable fossil fuels and is difficult to recycle after using it for one season due to pesticide and soil contamination. If not removed, the plastic film will stay in the soil for centuries [47].

Figure 2.9 Agricultural polyethylene mulch films

Alternative mulches have emerged since the late 20th century to resolve environmental concerns about conventional polyethylene uses. Films are produced from renewable, biodegradable polylactic acid (PLA) or polyhydroxyalkanoates (PHA). Bio-based films look similar to PE mulches and provide benefits, including increased moisture and soil temperature [48]. In contrast to PE mulch, bio-based films exhibit unfavourable mechanical properties such as lower tensile strength and resistance, resulting in a less durable product subject to uncontrolled degradation, and exhibit increased rips, tears, and holes, which can increase weed pressure [49].

2.8 Renewable Polyethylene

A commodity plastic, polyethylene (PE) is the most widely used plastic in the world. It is under the category of thermoplastic which can be easily processed and re-processed using high temperature. The chemical formula only contains carbon and hydrogen atoms. PE can be further categorized into different groups based on their density. High-density polyethylene (HDPE) has a density range between 0.940 and 0.965 g/cm^3, low-density polyethylene (LDPE) has a range between 0.915 and 0.942 g/cm^3, and there are other subcategories such as linear low-density polyethylene (LLDPE) [50]. The difference in density is determined by their degree of crystallinity which is determined by the amount of side chains (degree of branching). HDPE has long linear chains with a minimum number of side chains whereas LDPE contains a higher amount of side chains than HDPE. Due to its long chains with little branching, HDPE shows higher crystallinity than LDPE and, therefore, has higher density. Because of this, HDPE tends to have better chemical resistance and higher opacity than LDPE. Main applications for HDPE include household chemical containers, shampoo

bottles, cosmetic containers, pharmaceutical bottles, and other packaging applications. LDPE, on the other hand, shows other desirable properties including clarity, and flexibility; main applications are containers, shopping bags, agricultural films, and stretch-wraps.

The traditional way of manufacturing PE is based on non-renewable sources using ethylene feedstock-petrochemicals. Though it has been beneficial for consumers to have this material that has been used in everyday applications over a century, it is based on non-renewable resources. In many markets, the consumers have requested materials that are more environmentally friendly and have a reduced CO_2 footprint. Therefore, the major driving force for renewable thermoplastics is based on consumer demand.

A more environmentally friendly alternative was recently commercialized by a chemical company in Brazil (Braskem SA). Instead of collecting resources from petrochemicals, they harvested sugar cane and manufactured PE from it. Ethanol produced from sugarcane becomes the source of the monomer, ethylene. Then the ethylene is polymerized to produce PE (Figure 2.4) [51].

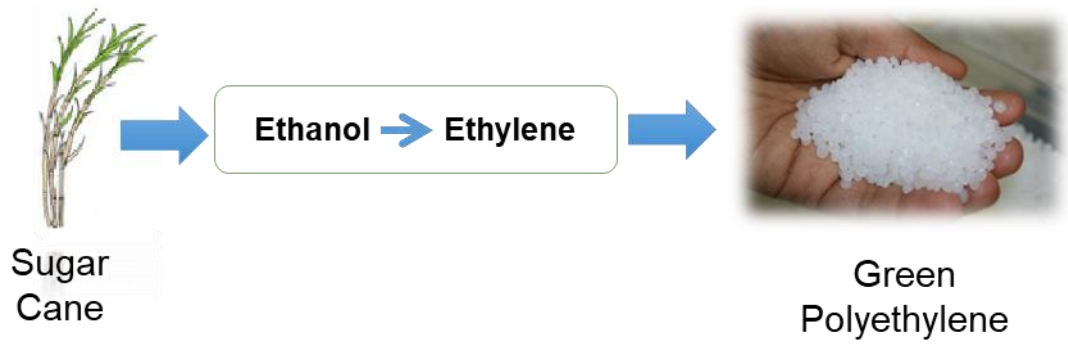

Figure 2.10 Process of manufacturing renewable polyethylene from sugar cane

The sugar cane production accounts for about 7.8 hectares and only about 1% of this land is used specifically for ethanol production. Therefore, it hardly competes against food sources. Also, this method represents a very sustainable way of manufacturing PE. It has significantly lower greenhouse gas emissions with nearly 100% made from renewable materials. The report for the carbon content analysis of this bio-based PE can be found in the Appendix section. The production captures about 2.5 kg of CO_2 per 1 kg of PE resin produced.

The PE produced via this environment friendly method is no different from the one derived from petrochemicals. Although there are limited numbers of grades present today, their properties are similar to the counterpart grades made from petrochemical sources. Braskem produces HDPE, LDPE, and LLDPE for specific applications. More recently, some companies including Proctor and Gamble started mass production of their consumer product using this renewable PE.

2.9 Properties of Interest

Characterization of starch-based materials can be done via both quantitative and qualitative investigations. There are standardized methods from the American Society for Testing and Materials (ASTM) and the International Organization for Standardization (ISO) that are available. Repeated trials are necessary for analysis.

Not only the material itself but also the processing environments and techniques can influence the properties. Even with the same plastic material, for example, if one was injection molded and the other was hot-pressed, they certainly will show different physical

properties. Furthermore, different processing conditions such as temperature and extrusion speed affect the properties of the materials as well.

Information about the properties of interest and analysis techniques are covered in this section. Thermal behaviour, rheological properties, chemical structure, morphological and mechanical properties are all included.

2.9.1 Thermal Behaviour

Thermogravimetric analysis (TGA) uses programmed heating in a chamber to measure the mass change as a function of temperature or time. The chamber can be fed with either air or nitrogen gas. TGA is a valuable tool to determine the onset of thermal degradation of the starch, polyester, CNC and other nano materials.

Differential scanning calorimetry (DSC) is another analytical tool to determine the thermal properties of different samples. It measures the difference in heat flow between the sample and a reference. DSC can identify the crystallization (T_c) and the glass transition (T_g) temperatures. The changes in these thermal properties can easily be characterized by studying the DSC curves.

2.9.2 Rheological Property

The melt flow index (MFI) measures the ease of flow of molten thermoplastics and is a very common parameter used in industry as an indirect measurement of molecular weight. MFI is defined as the mass of polymer flow, in grams, per ten minutes. ASTM D1238 describes the procedure for measuring the MFI of polymers. Initially, the MFI can be used to determine the processability of the polymer. Thermoplastic starch and its composites can

have a range of MFIs. In order to utilize a specific plastic processing technique, these materials have to be in a certain range of MFIs.

2.9.3 Chemical Structures

Fourier transform infrared (FTIR) is a relatively easy tool to determine the chemical structure of unknown substances. Depending on the source of starch, initial reactant composition, and type of nano materials, different FTIR spectra will be obtained. If any chemical modifications are done to the sample, FTIR can easily assess the degree of modification. In this research, both potassium bromide (KBr) pellets and hot-pressed films are analyzed. Either absorbance or transmittance is displayed with respect to wave numbers between 4000 and 400 cm^{-1}.

Similar to FTIR, nuclear magnetic resonance (NMR) also helps to determine the chemical structure of unknown substances. The resonance frequency of a particular sub-structure is directly proportional to the strength of the magnetic field applied. A structural parameter of interest in starch and modified starches is the degree of branching (DB). DB can be measured by hydrogen and carbon NMR for starch. NMR is a powerful and reliable characterization technique, but only when it is performed under conditions in which there is a complete and homogeneous dissolution of the sample. However, because of the presence of many different hydroxyl groups, the hydrogen NMR spectra of polysaccharides can sometimes be complicated to interpret.

2.9.4 Morphological Property

Scanning electron microscopy (SEM) is a powerful tool to investigate the surface morphology of materials. It yields high resolution images by utilizing a beam of electrons aimed at the surface of the samples. Depending on the microscope, SEM has the ability to image nano-sized structures.

Nevertheless, there is a disadvantage of using an electron beam over a light beam in visible optical microscopy. The surface of the material has to be conductive so that electrons can travel easily. Many plastic composites are non-conductive materials. Therefore, without any pre-treatment, they are challenging to visualize under the SEM. To overcome this disadvantage, the samples are coated with a thin layer of gold [52].

The electron gun shoots electrons towards the sample with a known voltage. Once the electrons reach the surface of the sample, they interact with the surface and scatter. Different detectors are mounted and detect the specific scattering of electrons [53].

There are a few valuable morphological properties that can be obtained when studying the starch-based composites and blends via SEM. The roughness of the surface, distribution of fillers in the matrix, fracture mechanisms and interaction between different phases are all important characteristics to investigate under the SEM.

2.9.5 Mechanical Properties

Both ASTM D790 and ISO 178 are three-point bending tests for flexural properties. Flexural strength measures the ability to resist against flexural deformation (bending). The modulus gives the ratio between the flexural stress and the strain [54]. The load cell measures

both displacement and force that are recorded in the computer. Then the following formulae calculate flexural strength, strain, and the modulus:

$$\sigma_f = \frac{3PL}{2bd^2}; \qquad \varepsilon_f = \frac{6Dd}{L^2}; \qquad \mathrm{E}_B = \frac{\sigma}{\varepsilon_f}$$

where:

σ_f = strength or stress in the outer surface at midpoint, MPa

P = load at given point, N

L = support span, mm

b = width of beam tested, mm

d = depth of beam tested, mm

ε_f = strain in the outer surface, mm/mm

D = maximum deflection on the centre of the beam, mm

E_B = modulus of elasticity in bending, MPa

Rigid fillers for plastic composites commonly increase the stiffness. However, they may have negative effects on the strain at failure. The strength of the material can also be reduced when there is not enough interfacial interaction between the fillers and the matrix. [55, 56] If the stress is not sufficiently transferred from one phase to the other, a reduction in mechanical properties may occur.

Tensile properties are also essential when analyzing plastic materials. The specimen undergoes uniaxial deformations and the load cell monitors stress that is recorded by the computer. This procedure can provide tensile strength, modulus, and elongation at break

[57]. Tensile strength and the percentage elongation at break were calculated via the following equations:

$$\text{Tensile Strength} = \frac{Maximum\ Force}{Unit\ Cross - Sectional\ Area}$$

$$\%\ \text{Elongation at Break} = \frac{final\ gage\ length - original\ gage\ length}{original\ gage\ length} \times 100\%$$

Typically, a specimen undergoes elastic deformation first which is reversible. Once, stresses reach the yield strength (elastic limit), the plastic deformation takes place. Plastic deformation is a permanent one where the material loses elasticity. Eventually, failure (rupture) occurs. Brittle materials rupture before plastic deformation can occur [58].

A stress-strain curve yields a number of parameters. The tensile strength can be calculated by dividing the maximum load by the average cross-sectional area. The percent elongation at break is obtained by dividing the length of extension by the original gauge length and multiplying by 100%. ASTM D1708 describes a standard method to determine the tensile properties of plastics by the use of micro-tensile specimens.

Impact behaviour is an essential aspect when characterizing polymer and composite materials. Impact tests are conducted in numerous ways and each has different advantages.

One standardized test, the IZOD impact test uses a pendulum with a known weight. A specimen is held as a cantilevered beam in the device. A notch is made prior to the test and the pendulum hits the top half of the notched specimen. The test yields the impact strength which is the amount of energy for crack propagation before failure. The value is reported in

J/m and J/m^2 in ASTM and ISO standards, respectively. ASTM D256 describes standard methods for the IZOD pendulum impact resistance of plastics [59].

Another useful type of standardized method is the Gardner impact test. It determines the relative ranking of materials according to the amount of energy required to crack or break a flat specimen. A weight falls in a vertical tube and hits the striker resting on top of a specimen. Repeated trials are to be conducted and the mean failure energy is reported. ASTM D5420 describes the standard methods of the Gardner impact test [60].

Chapter 3
Materials and Methods: Starch as Copolymer

3.1 Materials

The material containing 34 wt.% starch was manufactured by compounding corn starch and poly(butylene adipate-co-terephthalate) (PBAT) in a batch process by Polymer Specialties International Ltd. (Canada). This starch copolymer was provided in pellet form (Figure 3.1). The manufacturer has provided Fourier-transform infrared (FTIR) spectroscopy results (Figure 3.2). Details of this material preparation are provided in a patent that describes the process for making the starch-resin copolymer [14] and it was briefly described in the previous chapter. Dried regular corn starch (Tate and Lyle lot# DW2572B2, UK) was used for comparison as well. Cellulose nanocrystals (CNC) (200 to 400 nm in length and a few nm in thickness [61]) was provided by Celluforce (Canada).

In order to run the NMR analysis, lithium bromide (LiBr), deuterated dimethyl sulfoxide (DMSO-d^6), and deuterated trifluoroacetic acid (TFA-d^1) were purchased from Sigma-Aldrich (Canada).

For the extrusion process, PBAT (Ecoflex® F Blend C1200) was purchased from BASF (Canada). Organic peroxide, 2,5-dimethyl-2,5-di(tert-butylperoxy)hexane (Trigonox® 101)

was purchased from Akzonobel (Canada). Maleic anhydride was purchased from Fluka Analytical (Canada).

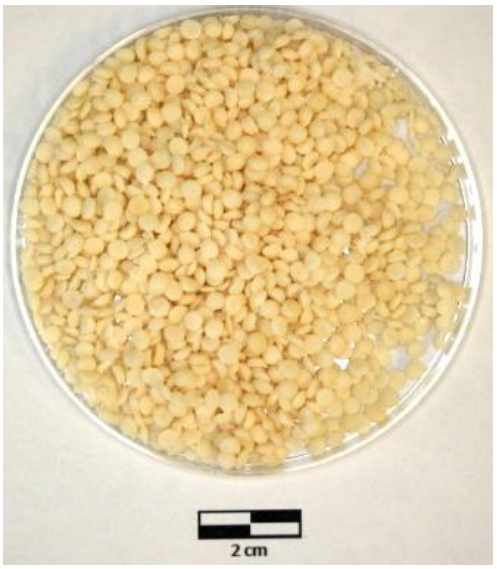

Figure 3.1 Starch resin copolymer manufactured by PSI

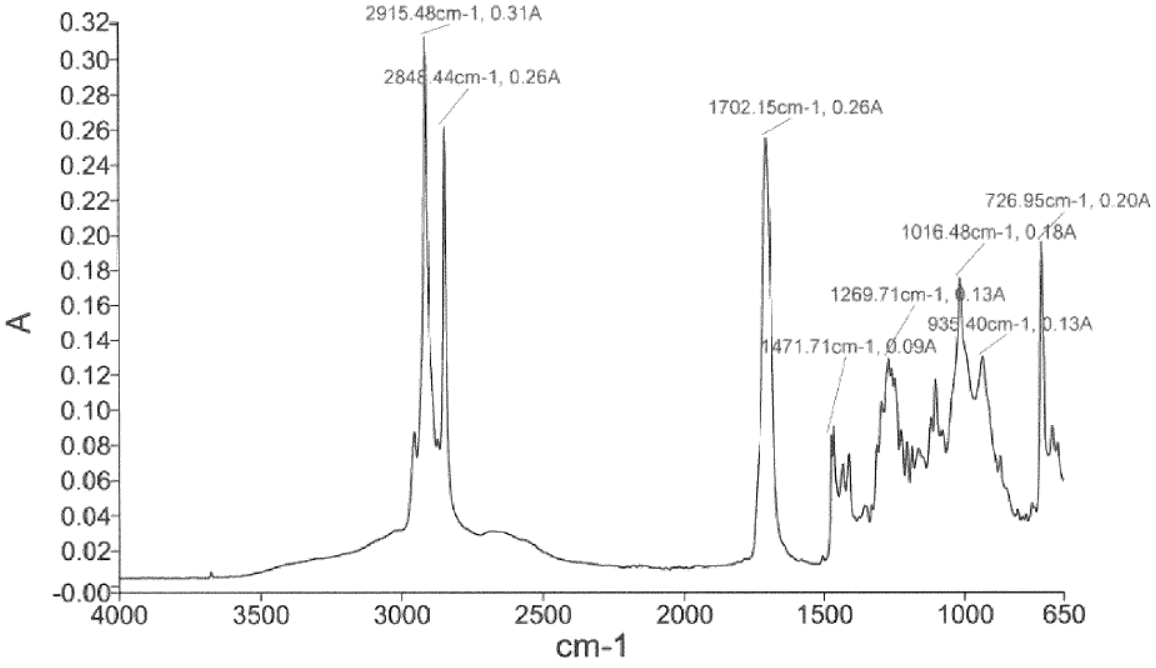

Figure 3.2 FTIR spectrum of starch resin copolymer manufactured by PSI [14]

3.2 Sample Preparation and Characterization

3.2.1 Chemical Composition Analysis

Regular starch and TPS-PBAT copolymer resins were analyzed using nuclear magnetic microscopy (NMR). Tizzotti et al. used an effective method to analyze starch by NMR [62]. With some modifications, the same method was implemented in this study. 0.05 g of LiBr was dissolved in 10 g of DMSO-d^6 and 10 mg of starch or TPS-PBAT copolymer was mixed with the LiBr – DMSO-d^6 solution. The mixture was heated at 70 °C and was constantly shaken for 20 hours. The samples were then transferred into NMR tubes and were delivered to Bruker-Spectrospin 500 Ultrashield for analysis and the proton NMR (^{1}H NMR) scans were done. A moderately high temperature of 70 °C was used to enhance the solubility of the starch samples and not to damage the polymer chain at the same time. 64 scans were acquired for chemical shifts ranging from -1 to 19 ppm. Spectra of raw corn starch were analyzed before and after adding TFA-d^1. Then the TPS-PBAT copolymer resins were studied with the pre-treatment of TFA-d^1. The spectra were Fourier transformed and the MestReNova (Mestrelab Research) software was used for the analysis. Baseline and phase corrections were done prior to peak assignments and quantitative analysis.

3.2.2 Sample Preparations and Mechanical Characterizations

Preparation of specimens for mechanical tests are described here. First, the TPS-PBAT copolymer resins were cryogenically ground. Pellets were submerged in liquid nitrogen and ground and a powder particle size of less than 0.1 mm was obtained. The ground powder was vacuum dried at 40 °C for 24 hours. The powdered samples were then injection molded (Injection Molding Apparatus, Ray-Ran). The processing temperature (barrel) was varied

from 150 to 175 °C. The mold temperature was set at 40 °C. The pressure of 690 kPa (100 psi) with 15 seconds of injection hold periods was applied.

There were three different geometric shapes for the specimens (Figure 3.3): plain rectangular bars, dumbbell shapes, and circular specimens. The plain bar-shaped specimens were used for flexural and notched IZOD impact strength tests, the dumbbell-shaped specimens were used for tensile tests, and the circular specimens were for the Gardner impact tests. The injection molded specimens went through a brief annealing procedure at 120 °C to erase thermal history. As a final step prior to testing and characterization, the specimens were placed in a conditioning chamber with a temperature of 23 ± 1 °C and a humidity of 50 ± 5 % for 48 hours. Specimens prepared for DMTA were conditioned at various humidities.

Figure 3.3 Flexural / IZOD impact (left, rectangular), tensile (centre, dumbbell) and Gardner impact (right, circular) specimens for mechanical characterizations

Flexural strength and modulus were obtained via a flexural test (ASTM D790). A Q Series Mechanical Test Machine (Test Resources Inc.) was used for 3-point bending system. Six

replicate tests were conducted for each sample and their average with standard deviation was reported. The values were calculated using the equations outlined in Chapter 2.

Tensile strength, modulus, and elongation at break were obtained via tensile tests (ASTM D1708). The same testing machine as the flexural test was utilized. A dumbbell shaped bar was placed between the upper and lower grips. The distance between the grips was 22 ± 0.5 mm after placing the bar. The tensile force was applied to pull the bar at a rate of 1.3 mm/min. Six replicate tests were carried out for each sample and their averages and standard deviation were reported. The reported values were calculated using the equations outlined in Chapter 2.

The impact strength was examined via IZOD impact test (ASTM D256). Test method A of the standard was used. A depth of 2.5 mm notch was creased before the test was conducted. The specimen was mounted vertically on a Monitor Impact Tester (Testing Machine Inc.) and hit by a 5 ft-lb swinging pendulum type hammer at 90°. The result was reported in joules per metre. Six replicate tests were done, and their averages with standard deviations were reported.

Another type of impact analysis was done via the Gardner impact test (ASTM D5420) to obtain the impact failure energy. An 8 lb weight was dropped through a guide tube and hit a striker resting on top of a supported circular specimen. The procedure determined the energy that caused 50% of the specimens tested to fail (mean failure energy). A failure was defined as complete cracking through the specimen. The weight was dropped from a height and if the sample failed, the drop height was reduced by half an inch. If the sample did not fail then the

height was increased by half an inch. Repeating this procedure more than 20 times, the average failure height was calculated as the ASTM standard indicates.

Dynamic mechanical thermal analysis (DMTA) was performed on samples exposed to different conditioning cycles. The first and second samples were conditioned at 30 and 50% relative humidity at 23 ± 1 °C for 24 hours. The third sample was exposed to DI water (23 ± 1 °C) for 24 hours. Dynamic mechanical thermal analyzer V (Rheometric Scientific) and the software TA Orchestrator (TA Instruments) were used for the analysis. The single cantilever clamp test method was applied on the injection molded samples. The specimen size was 25.0 × 12.5 × 3.0 mm^3. The temperature was raised from 35 to 115 °C with a rate of 3 °C/min. The frequency was 1 Hz and the strain was 0.1%.

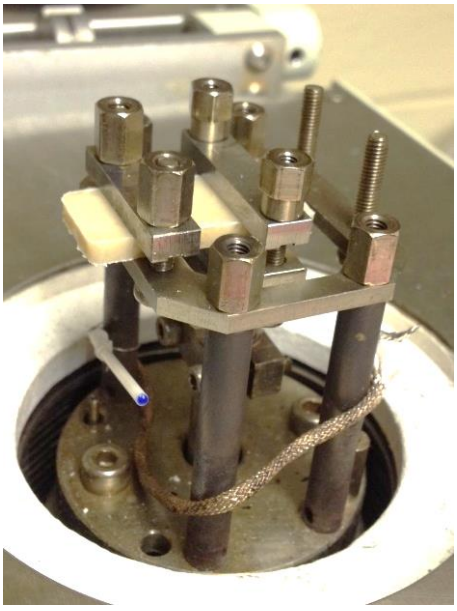

Figure 3.4 Single cantilever mounting in DMTA

3.2.3 Composite Preparation and Mechanical Characterization

The TPS-PBAT copolymer-CNC composites were prepared to study the effect of CNC on their mechanical properties. The CNC was vacuum dried at 40 °C for 24 hours. Powdered and dried TPS-PBAT copolymer resins with dried CNC mixtures were loaded into a co-rotating conical twin-screw extruder (Figure 3.5) (Haake MiniLab Micro-compounder, Thermo Electron Corporation) barrel using a hopper.

Figure 3.5 Co-rotating conical twin-screw extruder configuration

The CNC concentration was varied from 0 to 6 wt.% The samples were extruded at 140 °C with a rotational speed of 75 rpm. Then the compounded material was air-cooled and hand pelletized. The pellets were then injection molded in the same manner as the pure resins at 155 °C and 690 kPa (100 psi). Annealing at 120 °C was done in order to remove the thermal history and conditioning (23 ± 1 °C for 24 hours at 50% relative humidity) was done prior to mechanical testing. The prepared specimens went through flexural and tensile tests in the same manner as the aforementioned techniques.

3.2.4 Thermal Analysis and Stability

Thermal gravimetric analysis (TGA) was done before and after processing the material. The heating program increased the temperature from room temperature to 600 °C with a 10 °C/min rate. Samples processed at different temperatures ranging from 150 to 185 °C were analyzed. The 2 and 5% weight loss temperatures were compared with respect to the processing temperatures.

3.2.5 Melt Flow Analysis

In order to see the ease of flow at different processing temperatures, the mass flow index (MFI) of the sample was determined. Initially, the indexer was preheated to the temperatures of 140, 150, 160, 170 and 180 °C. A weight of 2.16 kg was used following a standard method, ASTM D1238. Depending on the speed of the flow, the samples were collected every 10 or 20 seconds. At every temperature, 5 samples were collected and their average and standard deviation were calculated.

3.2.6 Morphological Analysis

Scanned electron microscopic (SEM) analysis was done on TPS-PBAT copolymer-CNC composites for morphological comparison. Fractured surfaces of injection molded bar specimens were vacuum dried at 50 °C for 24 hours. The dry specimen was gold coated with a thickness of 10 nm to avoid electrical charging. FEI Quanta Feg 250 ESEM (Thermo Fisher Scientific) with an accelerating voltage of 15 kV was used.

3.3 Study on Maleation of Starch

3.3.1 Methods for Starch Maleation

The synthesis of the TPS copolymer by PSI was described in the previous chapter. The first stage was to react starch with maleic anhydride at moderately high temperature (90 °C) for 10 minutes in a batch system. The purpose of this section is to compare alternative methods of starch maleation and perform quantitative and qualitative evaluation. Three different approaches were taken: using a microwave reactor, a twin-screw extruder, and a rotary evaporator.

The first method was to use a microwave reactor. An Anton Parr Multiwave 3000 microwave reactor was used. The schematic diagram of the process is shown in Figure 3.6. Dry starch and freshly ground maleic anhydride powder (4:1 weight ratio) were mixed in acetone. Without any heat applied, the mixture was continuously stirred until acetone had completely evaporated. This was done to make sure to obtain a uniform mixture of starch and maleic anhydride, and to enhance the interaction between the two chemicals. Four different weights of mixture were prepared: 100, 150, 200, and 250 mg. They were put into separate microwave reactor tubes. Each sample was continuously stirred using magnetic stirrers fitting inside the tubes while the microwave reactor was running. A power of 750 W was applied for 15 minutes in the reactor.

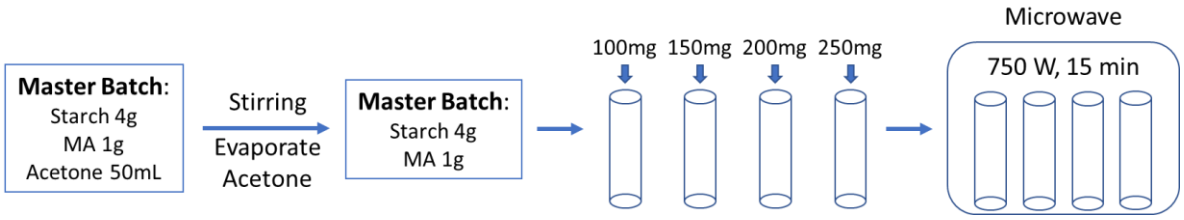

Figure 3.6 Schematic diagram of starch esterification via microwave reactor

The second approach was done on a continuous system using a twin-screw extruder. A 27 mm, 52 length per diameter (L/D) ratio, 13 elements, co-rotating twin-screw extruder (MIC 27, Leistritz Extrusion, USA) was utilized for the experiment. The rotation speed was 250 rpm, the output rate was 9 kg (20 pounds) per hour, and the extruder set-up with its temperature profile is shown in Figure 3.7.

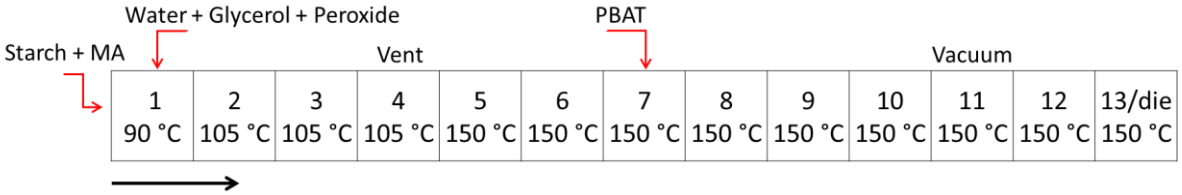

Figure 3.7 Twin screw extruder set-up and temperature profile

Starch and maleic anhydride (MA) went into the feeding zone with a ratio of 1:0.01 (weight ratio). Water, glycerol, and peroxide were fed in zone 1. The sample was collected at the vent (zone 4) before being exposed to a higher temperature (150 °C) starting from zone 5 and before the addition of PBAT in zone 7.

The third approach was done by using a vacuum rotary evaporator. Heidolph Collegiate Rotary Evaporator with Heidolph Eco Bath was used. The ratio between dry starch and maleic anhydride was 4:1 (weight ratio). The mixture was loaded into the rotating flask and a vacuum was applied. The water bath was kept at a moderate temperature, 60 °C for 8 hours.

This was a dry process where no solvent was used in the initial mixture. Finally, the sample was washed with acetone to remove any remaining free maleic anhydride that did not react with starch.

3.3.2 Maleated Starch Characterization

The first analysis was on the thermal degradation behaviour using the TGA technique (TGA Q500, TA Instruments, DE, USA). The heating program started from 30 to 600 °C at 10 °C/min rate. The change in weight (DTG) was obtained with respect to temperature. The results were compared with each other and with regular corn starch.

Differential scanning calorimetry (DSC) was performed to study the change in the gelatinization behaviour of maleated starch (DSC Q2000, TA Instruments, DE, USA). First, 2 mg of starch samples were suspended in 6 µL of distilled water for 1 hour prior to the experiment. The samples were transferred to the pans and sealed. The program monitored the heat flow with respect to temperature throughout the experiment. The heating sequence increased the temperature from 40 to 90 °C with a 5 °C/min rate. Again, regular corn starch was run alongside the maleated starch for comparison. An empty pan was used as a reference. The measurements were taken at least three times.

Fourier-transform infrared (FTIR) spectroscopy was used to characterize the chemical composition of the samples (FTIR – Tensor 27, Bruker Co., MA, USA). Potassium bromide (KBr) powder was dried prior to the preparation. The starch samples were ground with dry KBr and pellets were prepared. The spectra were obtained in the transmission mode through

the pellets. 128 scans were done on the specific wavenumber range of interest (2000 to 1500 cm^{-1}). The resolution was 1 cm^{-1} and the aperture setting was 1 mm.

The chemical composition of starch prepared by three different methods and regular corn starch was compared with the NMR analysis. Similar to the previous NMR procedure, 0.05 g of LiBr was dissolved in 10 g of DMSO-d^6 first. 10 mg of each sample was dissolved in a separate LiBr – DMSO-d^6 solution. The solution was heated for 20 hours at 70 °C and was transferred to NMR tubes. Bruker-Spectrospin 500 Ultrashield (Bruker Co., MA, USA) was used for the analysis at a constant temperature of 340 K (66.85 °C). ^{1}H NMR scans were done from 0 to 12 ppm and each sample went through 256 scans. All four samples reacted with TFA-d^1 prior to the scans. The spectra were Fourier transformed and MestReNova (Mestrelab Research, S.L., CA, USA) software was used for the analysis. Baseline and phase corrections were done prior to peak assignments and quantitative analysis.

Chapter 4
Results and Discussions: Starch as Copolymer

The driving force for this research comes from customers requiring products with a lower environmental impact or from legislation. This driving force leads to several research problems that include i) lack of understanding on the preparation of thermoplastic starch copolymers, and ii) lack of understanding on the effect of nanocellulose to improve the properties of thermoplastic starches.

The goal of this chapter is to evaluate the thermoplastic starch copolymer produced from PSI through collaboration with our research group. The detailed characterization of such material is not reported elsewhere yet. Furthermore, this research will extend the understanding of possibilities for starch modification by evaluating the effect of nanocellulose on the physical properties and the mechanism of starch maleation. These are two strategies that could be implemented in the manufacturing process conceived by PSI.

4.1 Chemical Composition of Starch Copolymer: ^{1}H NMR analysis

High temperature (70 °C) ^{1}H NMR analysis was performed to study the chemical composition and the structure of the material. Peak assignment and quantitative analysis of the degree of branching were done.

Figure 4.1 shows the ^{1}H NMR results of (a) regular starch, (b) regular starch with an addition of TFA-d[1], and (c) TPS-PBAT copolymer also with an addition of TFA-d[1]. All the essential peaks were assigned to the protons in the structure. The ^{1}H NMR spectrum of regular corn starch exhibits all the characteristic peaks. As it is well described by Tizzotti et al., the peaks of the hydroxyl hydrogens overlap with the 1 and 1' anomeric protons (5.11 and 4.75 ppm) [62]. However, with the addition of a small amount of TFA-d[1], the hydroxyl protons and TFA undergo rapid exchange, giving rise to only a single peak at a higher chemical shift (> 6 ppm). Typically, the higher the amount of TFA is added, and the higher the chemical shift is expected. Other protons present in the region of 3.21-3.89 ppm were not affected by the addition of TFA-d[1].

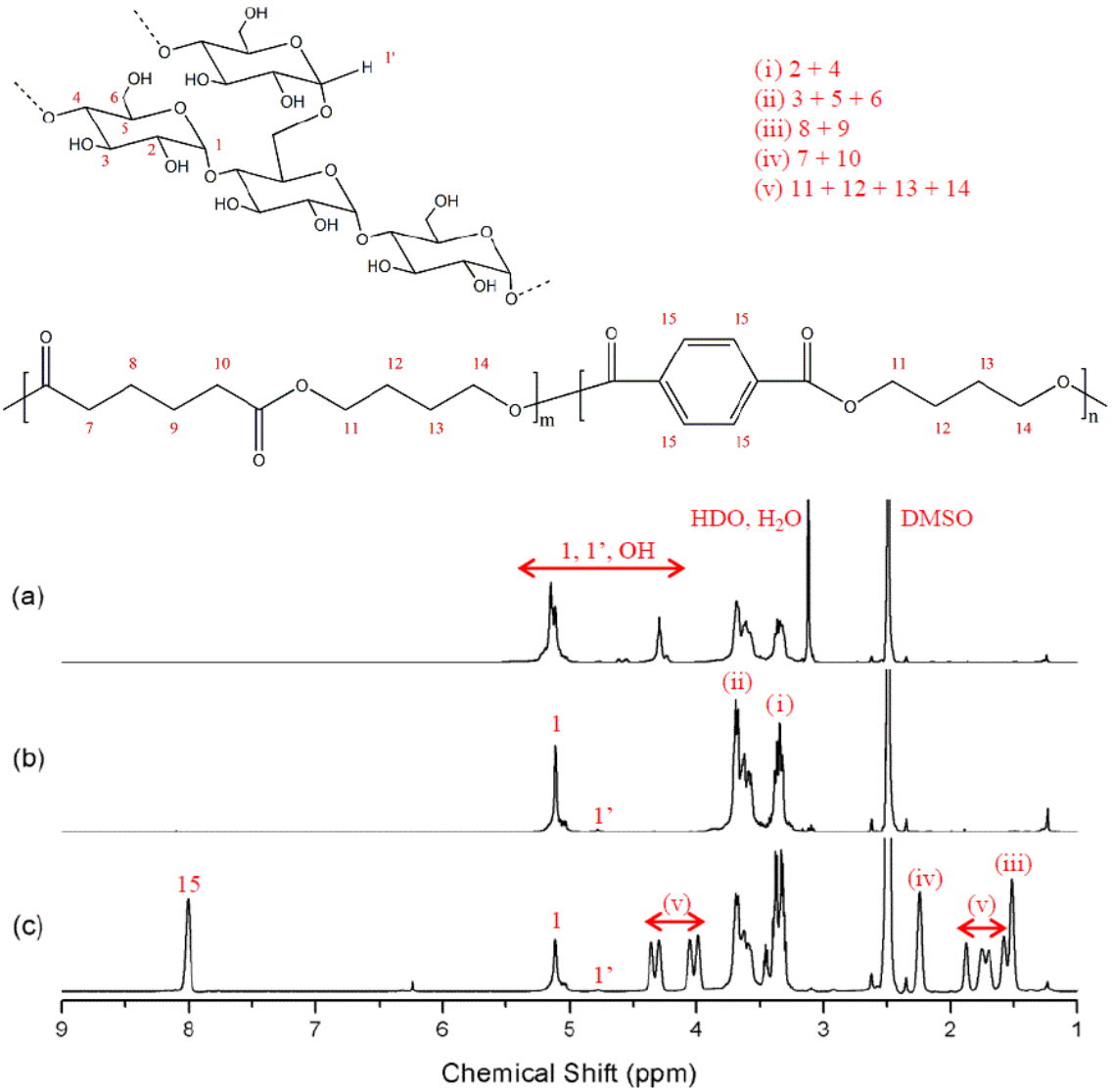

Figure 4.1 ^{1}H NMR results of (a) regular starch, (b) regular starch with an addition of TFA-d^{1}, and (c) TPS-PBAT copolymer with an addition of TFA-d^{1}

Since starch is a polymeric molecule with the presence of branching points, the degree of branching (DB) can affect the physical and chemical properties of TPS. The DB can be calculated for the starch molecule using the ^{1}H NMR spectrum and Equation 4.1 [62]:

$$\mathrm{DB}\ (\%) = 100\frac{I_{\alpha-1,6}}{I_{\alpha-1,6}+I_{\alpha-1,4}} \qquad (4.1)$$

Here, $I_{\alpha\text{-}1,6}$ and $I_{\alpha\text{-}1,4}$ are the ^{1}H NMR integrals of internal branching α-1,6 and linear α-1,4 linkages represented by the integral of the signal corresponding to the 1 and 1' protons in the spectra, respectively. Since α-1,6 linkage is the branching point, DB is a ratio between the amount of α-1,6 linkage and the total amount of linkages. The calculated values of the regular corn starch used in this study is DB = 3.8% and the TPS-PBAT copolymer's DB is 3.1%. Nilsson et al. investigated the DB in different types of commercially available starches via ^{1}H NMR analysis. The DB generally lies between 1 and 5% depending on the source of starch and genetic differences which alter the amylose/amylopectin ratio [63]. However, they also provided a cautionary comment that longer-term studies might be necessary. This was because starch from different ages have been reported to have different molecular structures [64]. For example, the ripening of potato leads to higher amylose content and elongation of both amylose and amylopectin chains.

After analyzing the pure starch, the TPS-PBAT resin was investigated. TFA-d[1] was also added prior to the analysis. The result is shown in Figure 4.1 (c). Peaks numbered 1 to 6 are the signature peaks of the starch molecule whereas peaks numbered 7 to 15 are the signature peaks of PBAT. The protons from the grafted ring-opened maleic anhydride peak are formed at 6.22 ppm. Maleic anhydride may work as a coupling agent between hydrophilic starch and hydrophobic PBAT.

Additional ^{1}H-NMR analysis was done on samples collected throughout the batch process at PSI. 3 samples prior to the addition of PBAT and the final products were analyzed (Figure 4.2). The purpose of this analysis was to understand the change in chemical structures during the process of manufacturing and the results showed a reduction in DB from 3.8 to 3.1%. The

top spectrum (a) was collected after the addition of peroxide, water, and glycerol to the dry starch-maleic anhydride mixture. The spectrum (b) was collected after 10 minutes had elapsed and (c) was collected prior to the addition of PBAT. Spectrum (d) was collected from the final product. The first three samples showed all the signature peaks of starch (5.11, 4.75, 3.3-4.7 ppm) and grafted maleic anhydride (6.2 ppm) as expected. The final product had additional peaks that correspond to protons in the PBAT molecule. Although the time elapsed in the batch process (spectra (a) through (c)), there was no significant difference observed. In order to study the esterification reaction by maleic anhydride in-depth, a further investigation was necessary and executed. This study is presented in a later sub-section (4.8).

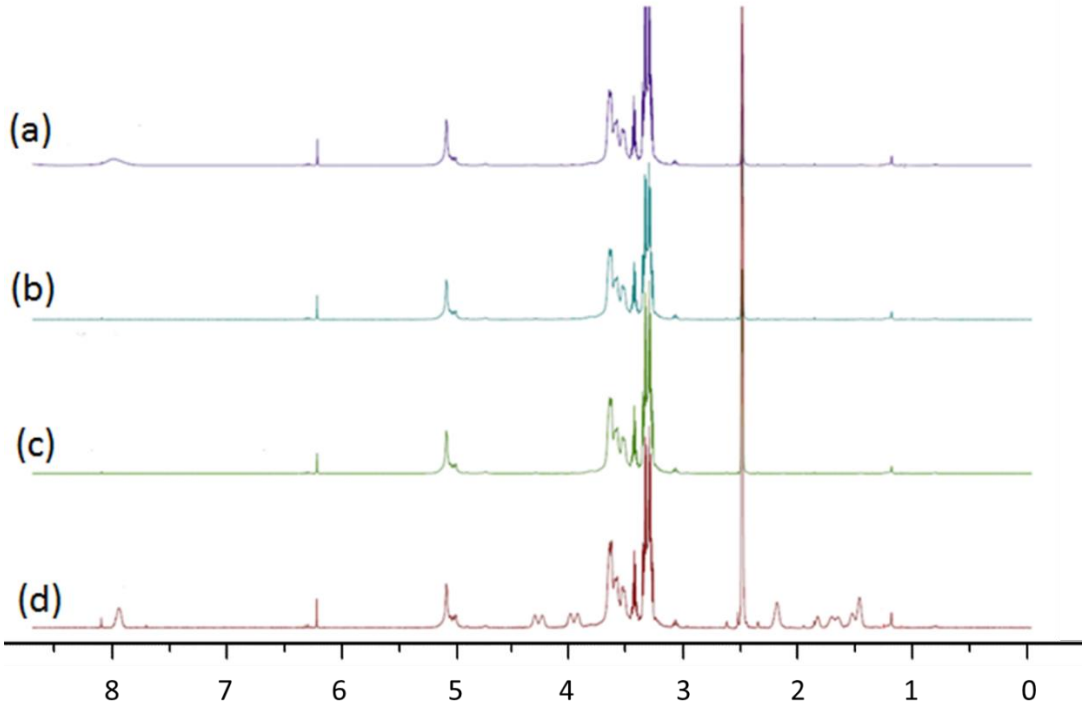

Figure 4.2 ^{1}H NMR results on samples collected throughout processing: (a) collected after addition of peroxide, water and glycerol to starch; (b) collected after mixing 10 minutes; (c) collected prior to addition of PBAT; (d) final product

4.2 Thermal Analysis

Figure 4.3 shows TGA results from a 35 to 600 °C sweep under nitrogen gas environment. The major vertical axis (left, green) shows weight percentage and the minor vertical axis (right) shows the derivative of the weight changes in %/°C. The first major decrease in weight started at around 220 °C and the decrease slowed down at around 320 °C. The second weight drop happens at around 350 °C until 450 °C. The first drop corresponds to the degradation of amylose and amylopectin [65] whereas the second drop corresponds to the weight decrease of polyester [65, 66]. TGA is an excellent tool to evaluate the stability of starch and its blends because of its simplicity and effective information provided. Many studies employed the technique to analyze starch in the past. Aggarwal et al. and Teramoto et al. used the TGA method to investigate the thermal stability of the main starch components and found that there was a difference in thermal resistance between amylose and amylopectin in corn starch [67, 68]. Because of the difference in thermal resistance, the TGA technique could be employed to estimate the contents of amylose and amylopectin in starch. Furthermore, the TGA can be employed to investigate the thermal degradation and stability of starch and starch-based materials under different processing conditions [69].

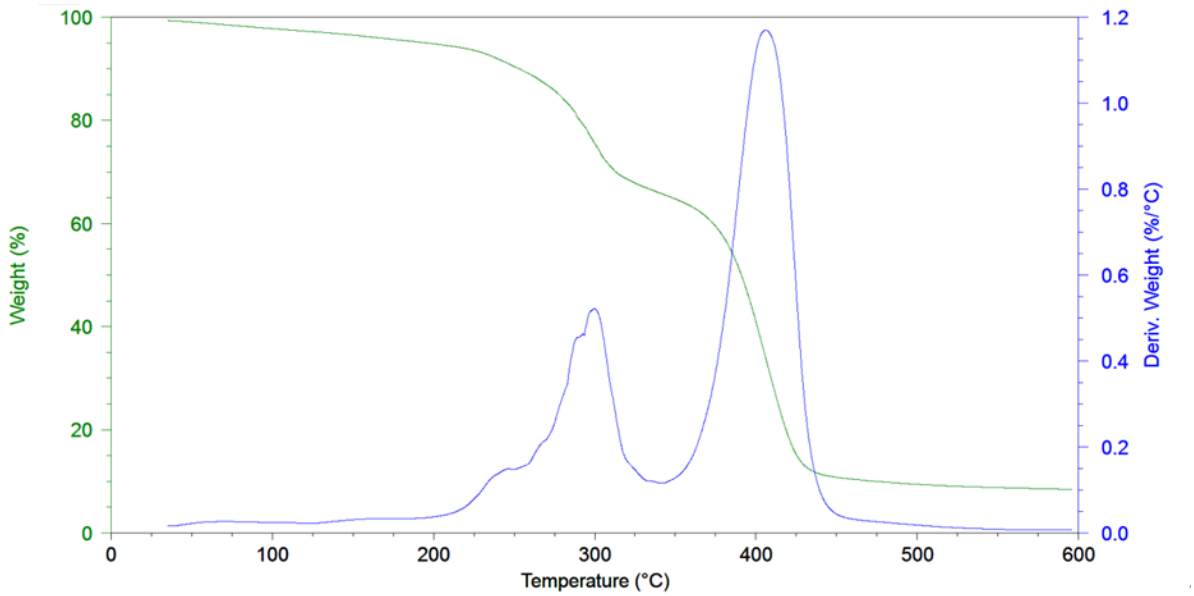

Figure 4.3 Thermal gravimetric analysis on TPS copolymer resin

In order to study the effect of processing temperature, further experiments were done using TGA on the samples that went through different processing (extrusion and injection molding) at temperatures ranging from 150 to 185 °C. 2 and 5% weight loss temperature have been recorded after water evaporation. These temperatures were compared with the 2 and 5% weight loss temperature of the pre-processed sample (Figure 4.4). This was done to visualize the amount of sample loss due to high temperature and shear during extrusion and injection molding. The increase in weight loss temperature indicates the increase in sample loss during the high temperature processing.

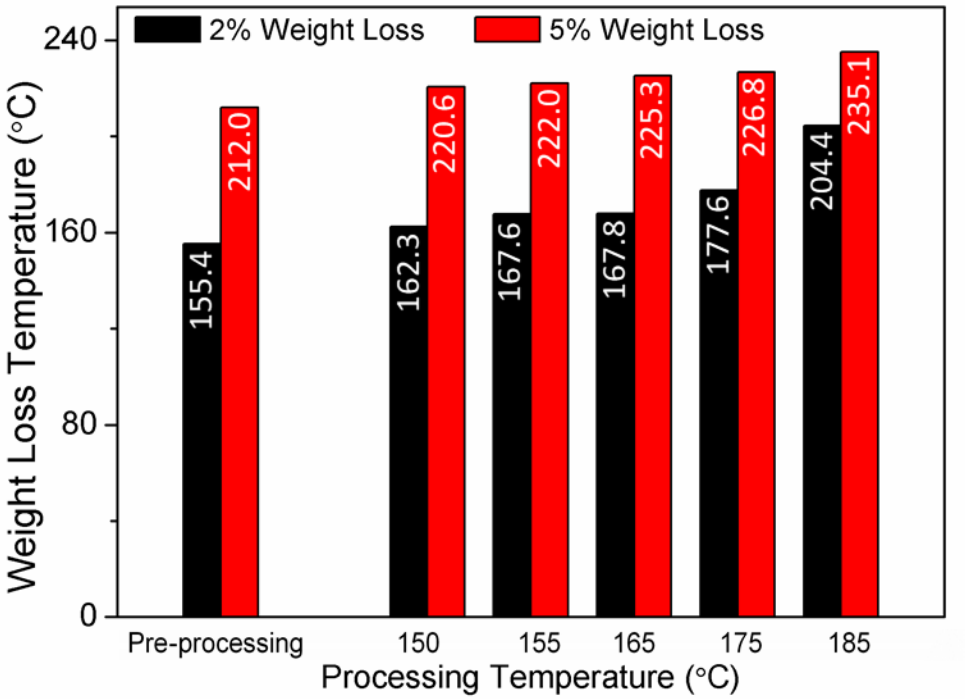

Figure 4.4 TGA results of pre- and post-processed samples

As expected, both 2 and 5% weight loss temperatures have increased as the processing temperature has increased. When comparing the 2% weight loss temperature, the pre-processed sample was at 155.4 °C whereas the 185 °C-processed sample was at 204.4 °C. This is a 31.5 % increase. The same pattern was observed with the 5% weight loss temperature as well. TGA is one of the most commonly used techniques to characterize the thermal stability of materials. There have been a few studies that have emphasized the importance of the thermal stability and degradation of starch [70-72]. Considering that common industrial starch materials go through a series of thermal treatments and processing stages, it is a vital step to conduct an in-depth analysis on their thermal stability. The result indicates that there was a significant effect of processing temperature on the sample and it is crucial to control the thermal stability during extrusion and injection molding. However, it is

also important to reach sufficiently high temperature to achieve good mixing and flow of the molten polymer.

The thermal decomposition and stability of starch depend on its composition such as its amylose and amylopectin contents. Its molecular weight also alters the property. Processing conditions such as high temperature and shear stress affect thermal stability as well. Liu et al. have investigated the thermal decomposition of starch extensively [69]. According to their report, there are three stages of the thermal decomposition mechanism. The first stage is physical dehydration when adsorbed water evaporates. The second stage is chemical dehydration and thermal decomposition. Thermal reactions start at around 300°C with thermal condensation between the hydroxyl groups of starch chains. This reaction forms ether segments and yields water molecules with other small molecular species. This second stage of the mechanism was clearly observed in this thesis as well (Figure 4.3, peak at ~300 °C). The last stage is carbonization reactions at temperatures above 500 °C. Although the main chemical dehydration and thermal decomposition take place at higher temperatures (~300 °C), exposure to high shear along with relatively higher processing temperature may have caused the degradation at an earlier stage.

4.3 Mass Flow Index Analysis

In order to further investigate the effect of processing temperature, the melt flow index (MFI) was also measured at different temperatures. Typically, plastics suitable for injection molding have MFI values ranging from 3 to 10 grams/10 min using a 2.16 kg weight. An MFI value lower than this range may not be suitable for injection molding applications. Figure 4.5 summarizes the MFI values obtained at different temperatures. The MFI values

measured at 140, 150 and 160 °C are 4.04, 6.84 and 9.68 grams/10 mins, respectively. These three values are in the suitable MFI range for injection molding. At 170 °C and above, the MFI has increased significantly and all readings were above the target range (>10 grams/10 min). The experiment above 170 °C even exhibited some evidence of oxidation of the sample (burning), such as caramelization (darkening of colour) and unpleasant burning odour.

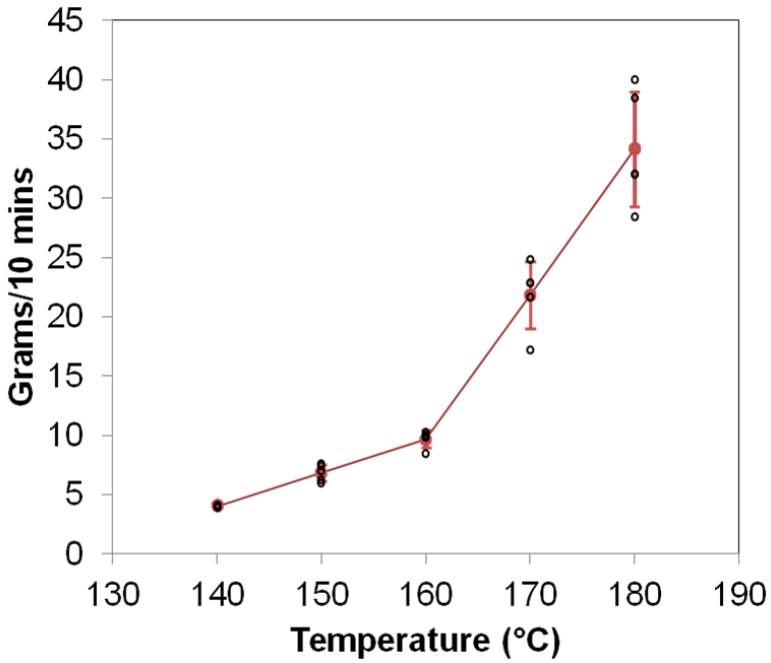

Figure 4.5 MFI of thermoplastic starch copolymer at different temperatures

Both TGA and MFI experiments demonstrated the effect of the processing temperature. Although the residence time in the processing equipment (extruder and injection molder) is also important, in order to minimize the sample loss and burning while maintaining a good flow of the molten polymer, it is necessary to control the processing temperature. The temperature above 170 °C showed clear evidence of caramelization and burning with

significant losses (Figure 4.6). Therefore, it was concluded that the processing temperature must not exceed 170 °C.

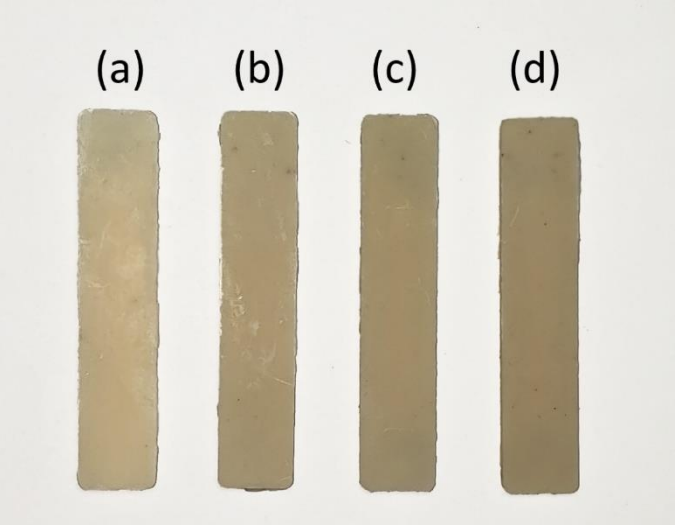

Figure 4.6 Flexural bars injection molded at (a) 150 °C, (b) 155 °C, (C) 165 °C, and (d) 175 °C

4.4 Effects of Processing Temperature on Mechanical Properties

As the previous sub-section has demonstrated, the temperature window for processing TPS is rather narrow. It needs an optimum combination of thermal input and high shear to fully plasticize. However, this point is easily surpassed by slight variations, which leads to degradation and caramelization of the material (Figure 4.6). In order to understand the effect of processing temperature on the TPS-PBAT copolymer, mechanical analysis including flexural, tensile and impact tests were performed. The processing temperatures were varied once again from 150 to 175 °C. The result under 150 °C is not reported here since the temperature was too low to evaluate sufficient polymer flow to extrude and injection mold the test specimens.

Figure 4.7 shows the flexural test results. Both flexural strength and modulus are reported here. It was found that both flexural strength and flexural modulus decreased as the processing temperature increased. A noticeable drop was recorded when the processing temperature reached 175 °C. Thermograms of PBAT found in the literature show the stability of PBAT chains well above 300 °C [73]. Therefore, the burning, oxidation, and shortening of starch chains are responsible for the significant decrease in properties.

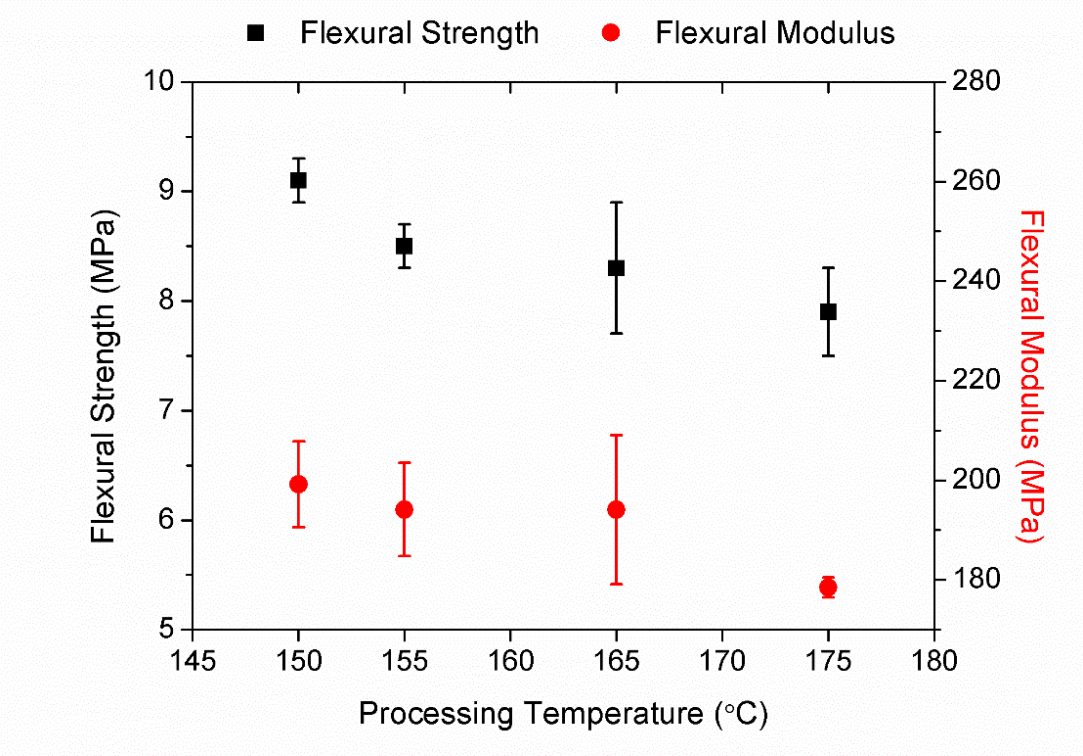

Figure 4.7 Flexural strength and modulus with respect to processing temperature

Tensile properties were measured with respect to the processing temperature as well. The tensile strength, Young modulus, and percentage elongation at break results are summarized in Figure 4.8. Both tensile strength and percentage elongation at break decreased significantly as the processing temperature increased from 150 to 175 °C. Although Young

Modulus had a slight increase from 150 to 155 °C, it reached a plateau in the higher temperature range. This overall decrease in tensile property is associated with oxidation and shortening of polymer chains in the higher processing temperature range. Also, the increase in thermal stress may have caused the decrease in properties. A recent study by Lekube et al. demonstrated the tensile behaviour of a TPS-PBAT blend (50 wt.% TPS) [74]. Specimens were prepared via extrusion and blown film processes and the processing temperatures were varied. Tensile properties and tear resistance were measured at three different extruder temperature profiles. Through the first decrease in temperature (-5 °C), tensile strength and modulus increased, whereas tear resistance showed no changes. However, a further reduction (-10 °C) caused a drop of tensile strength. At the temperature lower than the critical point, higher shear and friction in the material have caused poor physical properties. This study exhibits a good example of the narrow temperature window for processing TPS materials.

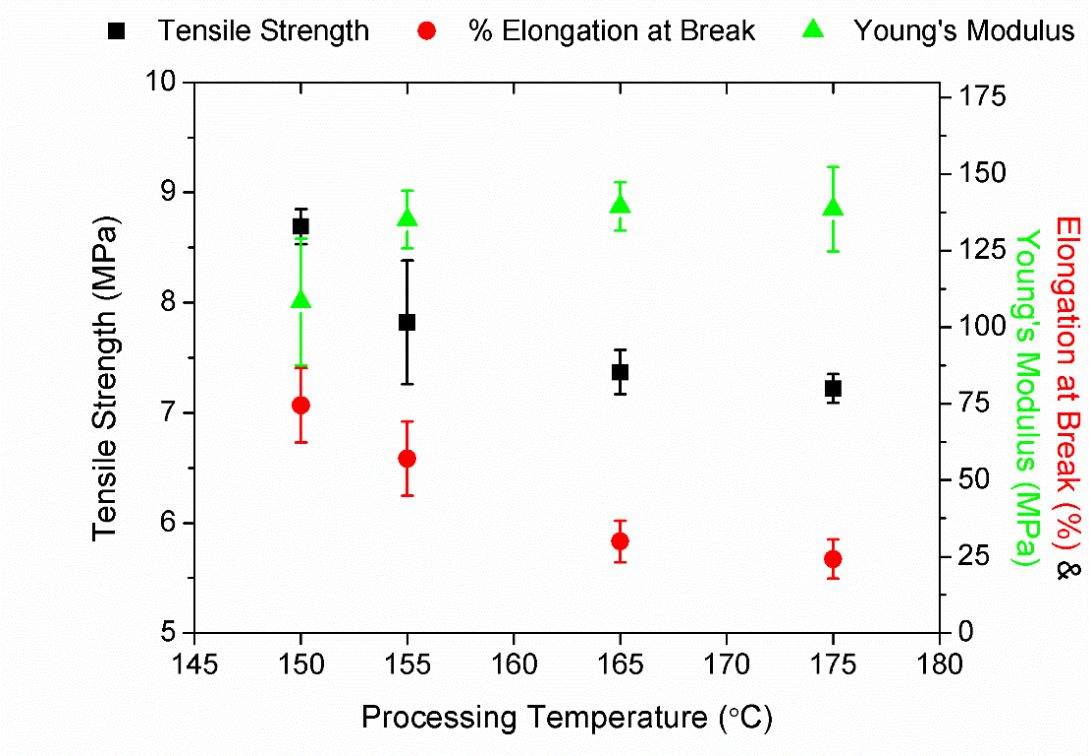

Figure 4.8 Tensile strength, Young's modulus, and % elongation at break with respect to processing temperature

Finally, two types of impact test results were monitored on the samples processed at different temperatures. Gardner impact test gave combined information of crack initiation and propagation while notched IZOD impact test gave crack propagation information. Figure 4.9 shows the results of these tests. Both impact properties did not show any significant changes while varying the processing temperature.

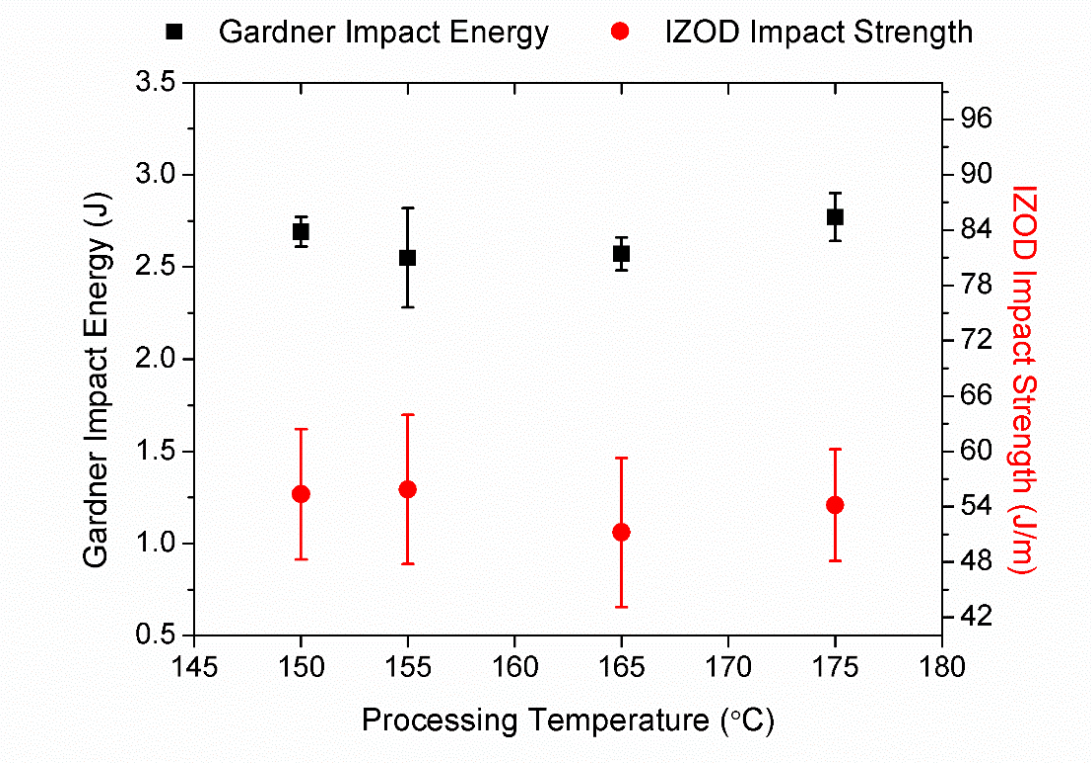

Figure 4.9 Gardner impact energy and IZOD impact strength with respect to processing temperature

4.5 Dynamic Mechanical Thermal Analysis

DMTA often provides critical information on the viscoelastic performances of polymers of various temperatures. A single cantilever bending DMTA test was done to study the behaviour under periodical stress throughout the temperature range of interest. Figure 4.10 shows the storage modulus (E'), and the ratio between E' and loss modulus (E"), represented as tan(δ). TPS copolymers conditioned at 30 and 50 % relative humidity are shown as solid and dashed lines, respectively. The short-dotted line represents the sample merged in water for 24 hours. The three samples conditioned differently showed a definite reduction in E' values as the temperature increased. It was found that specimens exposed to water had significantly lower E' values throughout the test. Being hydrophilic, TPS is susceptible to

moisture attack during storage and service. The increase in moisture content decreases the glass transition temperature (T_g) of TPS and subsequently affects its mechanical properties [75]. All three samples analyzed in this work did not show clear T_g although the first two conditioned at 30 and 50 % relative humidity exhibited rather smooth tan(δ) peaks at 70 and 65 °C, respectively (Figure 4.10). The submerged TPS copolymer did not show any peak in the measured range. PBAT is known to degrade in an aqueous environment over time, depending on the average chain length of the aromatic blocks [76]. A prolonged exposure of moisture would definitely decrease the property of the TPS-PBAT resin.

A study by Mitrus provided an in-depth analysis of the change in T_g of thermoplastic starch [77]. Potato based thermoplastic starch was produced by using glycerol and a single-screw extruder. The T_g was measured while conditions were varied. It was found the changes in the T_g of thermoplastic starch were only minimally affected by the moisture content. It was also shown that repeated extrusion up to three times did not affect the T_g significantly either. However, with a varied amount of plasticizer (glycerol) in the extrusion process, the T_g was significantly affected. When the glycerol content increased from 15 to 30%, the glass transition temperature decreased more than 100 °C, from 132 to 18 °C. Another study by De Graaf et al. have also shown that the difference in T_g of thermoplastic starch causes the changes in mechanical properties [78]. The T_g measured by DMTA was compared with the tensile properties. Lowering T_g has caused a decrease in modulus, tensile strength, and elongation. These studies found in the literature have indicated that T_g of thermoplastic starch is affected significantly by many environmental conditions and it is directly related to the physical properties. The result of mechanical analysis and DMTA experiment in this thesis

have also shown the sensitivity of TPS to the change in environmental and processing conditions.

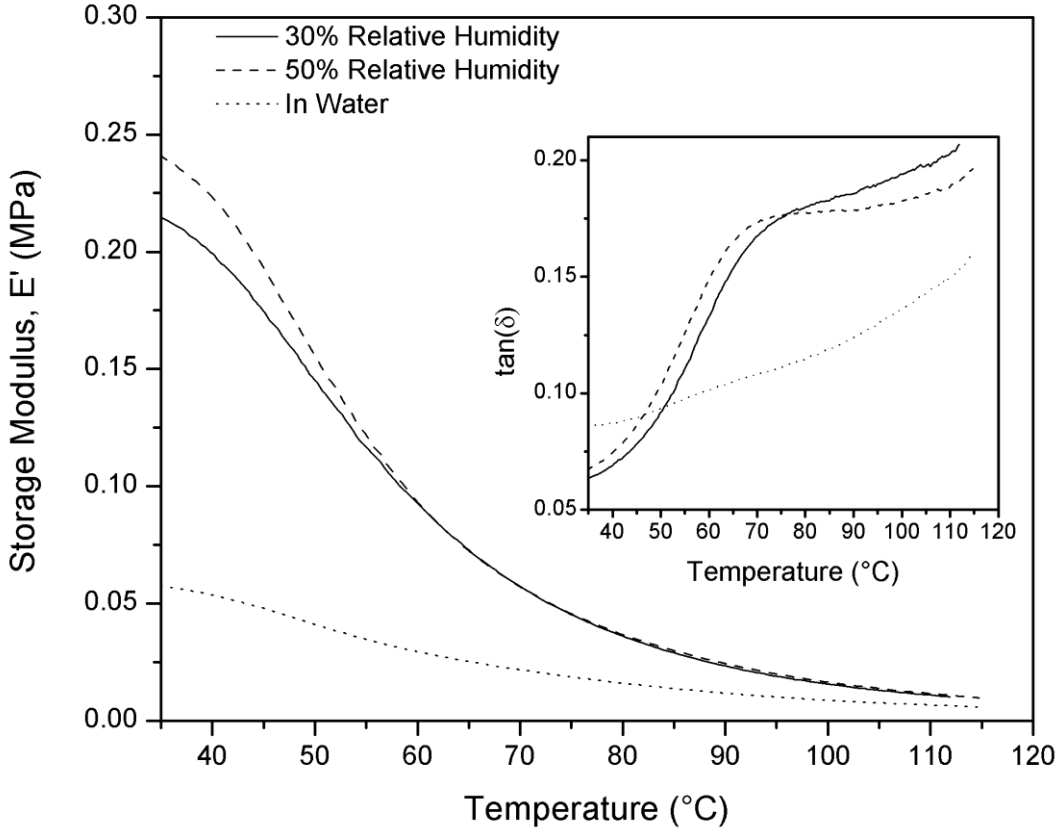

Figure 4.10 Storage modulus (E') and tan(δ) (insert) of samples exposed to various environment

4.6 Effect of CNC Filler on Mechanical Properties

A new set of mechanical tests was conducted on TPS-PBAT copolymer-CNC composites while varying the CNC concentration from 0 to 6 %. Flexural strength and modulus with respect to CNC concentration are shown in Figure 4.11. Overall, both properties increased as the CNC concentration increased. Flexural strength was improved by 24 %, reaching 11

MPa, and the modulus was improved by 34 %, reaching 292 MPa as the CNC content was increased from 0 to 6 %.

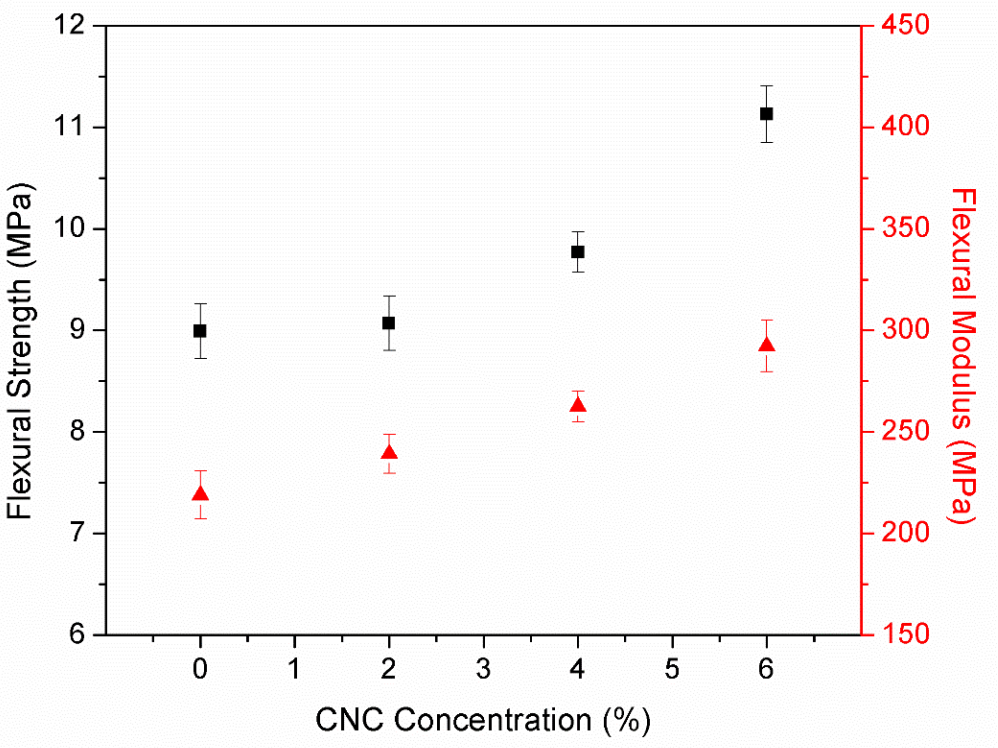

Figure 4.11 Flexural strength and modulus with respect to CNC concentration

Figure 4.12 displays the tensile properties of the composites, including the tensile strength, Young modulus, and elongation at break with respect to CNC concentration. Unlike the flexural properties, only tensile strength was improved by 7% while the Young modulus did not change significantly and elongation at break slightly decreased as the CNC concentration was increased. Although this may be an evidence of weak adhesion between CNC and the matrix's interface, significant improvements in other mechanical properties are indirect indications of uniform dispersions and good interfacial adhesions. In particular, the nanoscale dimension, the high aspect ratio, and the orientation of CNC are important characteristics to

enhance polymer properties. However, poor orientation of crystals cannot directly be translated to poor mechanical properties. According to literature, a lower degree of CNC orientation may induce high toughness of composites while tensile properties may decrease at the same time [79]. Therefore, variations of CNC orientation may change the path of energy dissipation and increase toughness.

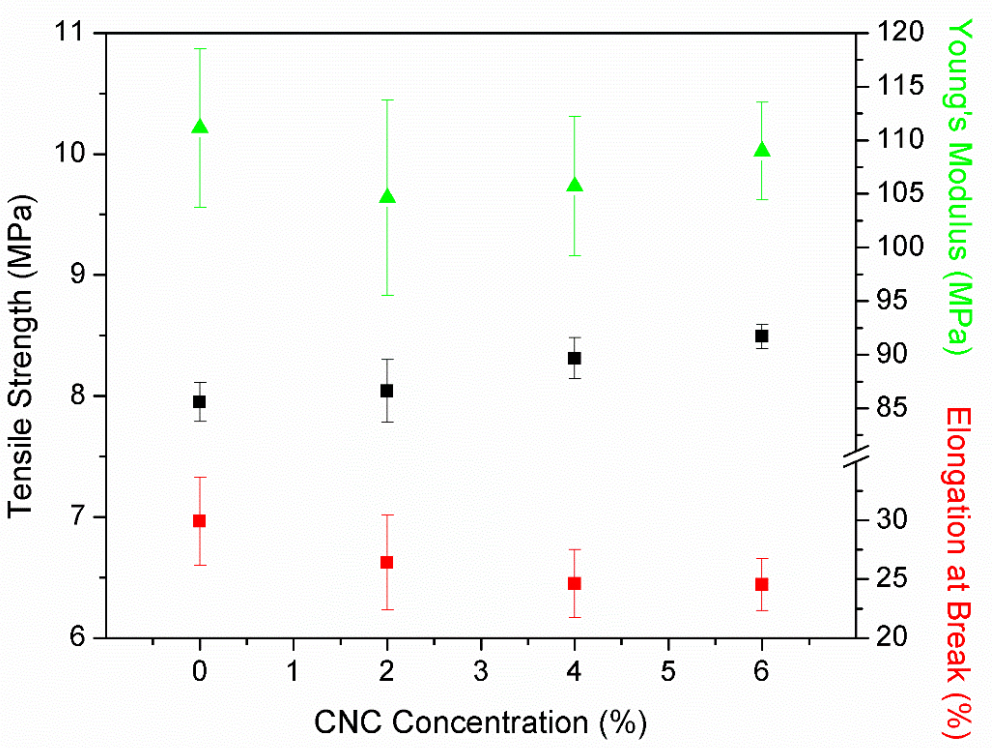

Figure 4.12 Tensile strength, Young's modulus, and % elongation at break with respect to CNC concentration

Table 4.1 Mechanical properties of starch copolymer resin-CNC composites

CNC (%)	Flexural Strength (MPa)	Flexural Modulus (MPa)	Tensile Strength (MPa)	Young's Modulus (MPa)	Elongation at Break (%)
0	9.0 ± 0.3	219 ± 12	8.0 ± 0.2	111 ± 7	30 ± 4
2	9.1 ± 0.3	239 ± 10	8.0 ± 0.3	105 ± 9	26 ± 4

4	9.8 ± 0.2	262 ± 8	8.3 ± 0.2	106 ± 7	25 ± 3
6	11.1 ± 0.3	292 ± 13	8.5 ± 0.1	109 ± 5	25 ± 2

The reinforcing effect of the CNC on polymer matrix could be attributed to the presence of hydroxyl groups on both starch and CNC. Strong hydrogen bonds could be formed that could enhance the reinforcement. Also, this strong interfacial adhesion between the two materials could have worked as a stress transfer agent or a binder [80].

Literature on CNC indicates that its strengths and stiffness equal 7.6 GPa and 160 GPa, respectively [81]. With such a magnitude of strength and stiffness, a minimal addition of CNC to the polymer matrix greatly enhances the mechanical properties. Uniform dispersion of CNC, the orientation with respect to the direction of stress applied, and good interfacial adhesion between the filler and the matrix are all essential factors to maximize mechanical properties.

Table 4.1 summarizes all the mechanical test results of starch copolymer resin-CNC composites.

4.7 Morphological Analysis

An attempt was made to prepare samples for transmission electron microscopy (TEM) observation in order to visualize CNC in the matrix. Unfortunately, due to the softness of the material, the use of neither glass nor diamond knife in a microtome provided desirable smoothness and thickness at room or cryogenic temperature. Instead, scanning electron microscopy (SEM) analysis was performed on the material with various CNC contents. This

analysis was done to visualize micrometer size CNC aggregates, if any, in the matrix. Even at very high magnification, identifying individual CNC fiber in the polymer matrix is challenging from SEM images. However, when present, aggregates are visible even at low magnification and they are easy to identify [82].

The four SEM images in Figure 4.13 show fractured surfaces of the 0, 2, 4 and 6 % CNC composites. Even with the highest CNC content (6 %), there was no visible aggregates found in the image. Although flexural properties have improved with increasing CNC concentration, the SEM images did not exhibit any significant difference.

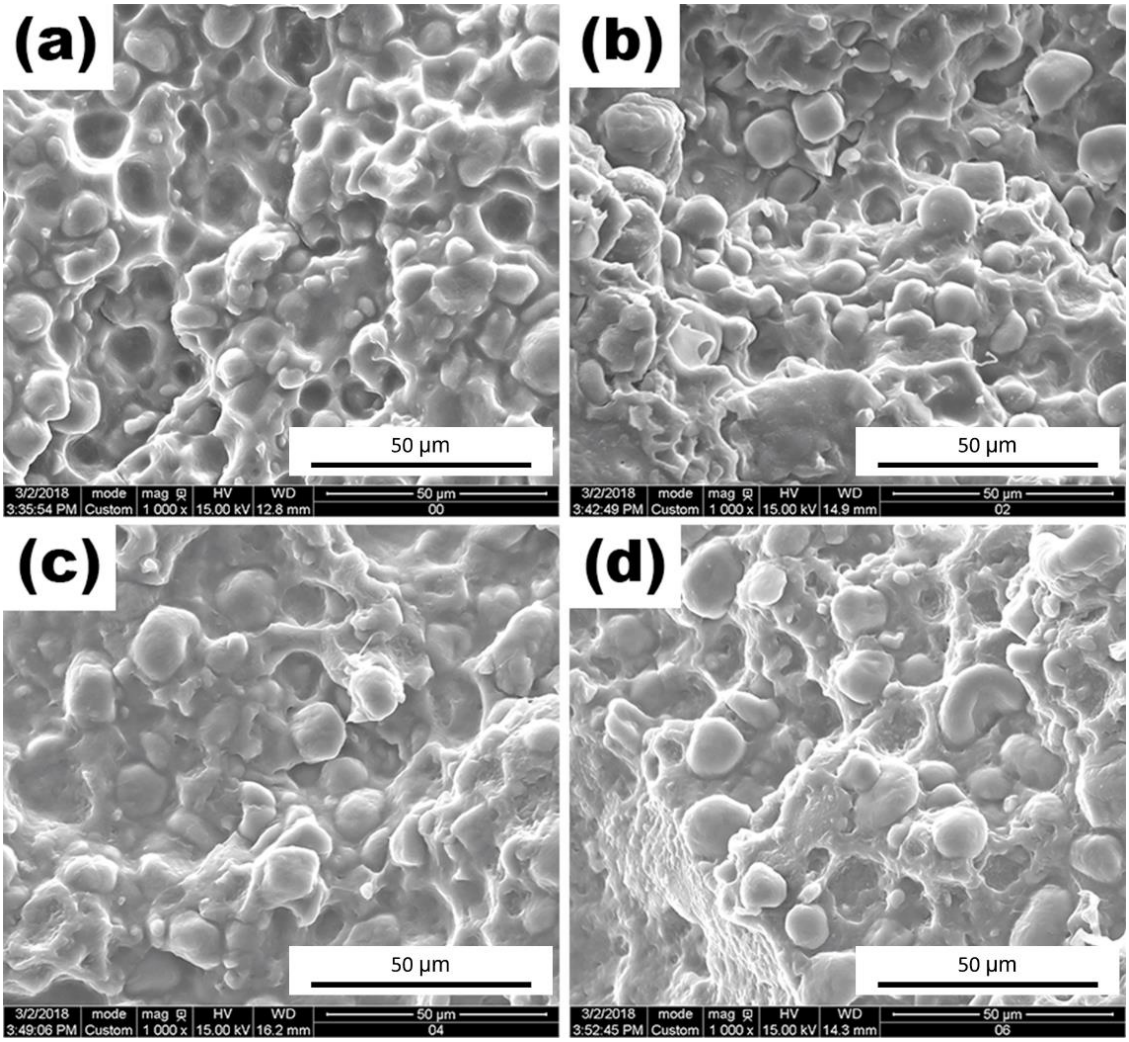

Figure 4.13 SEM images of fractured surface of (a) 0 %, (b) 2 %, (c) 4 %, and (d) 6 % CNC

4.8 Study on Maleation of Starch

4.8.1 Thermal Degradation Behaviour of Maleated and Unmodified Starches

TGA analysis was performed to study the thermal degradation behaviour of maleated starch and the results were compared with the unmodified starch. The TGA curves are shown in Figure 4.14.

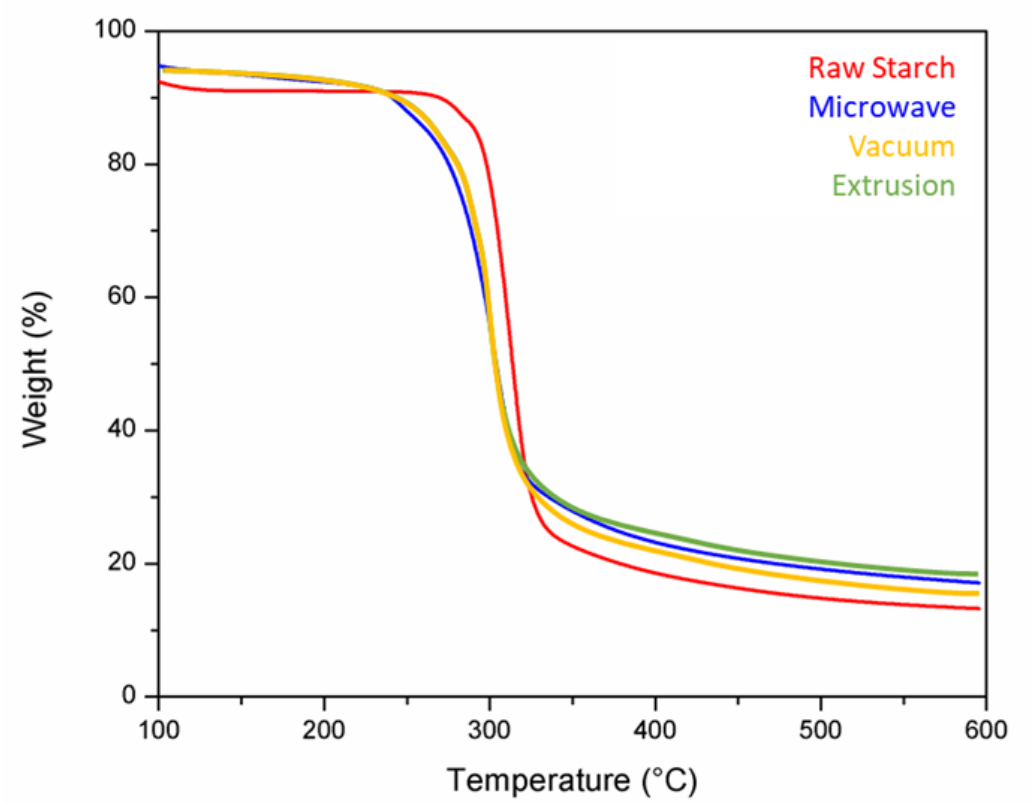

Figure 4.14 TGA on maleated (microwave, vacuum rotary evaporator, and extrusion) and unmodified (raw) starch

It is clearly seen that modified starches have greater heat loss rates than the unmodified (raw) starch. The esterification destroyed the starch crystalline domains and therefore, the density degree has decreased. This led to the conclusion that modified (esterified) starch would decompose more easily than native raw starch at a lower temperature. The DTG curve shown in Figure 4.15 confirms the weight loss which starts at a lower temperature than unmodified starch. The peak temperature of maleated starch was 303.0 °C and that of native starch was 312.7 °C. This could be evidence that starch was successfully esterified by maleic anhydride. Zuo et al. have demonstrated via DSC and X-ray diffraction (XRD) that esterification of starch induced weakening intensity of diffraction peaks and a significant

decrease in the degree of crystallinity [13]. This suggests that the reaction has destroyed the crystalline structure of starch to some extent.

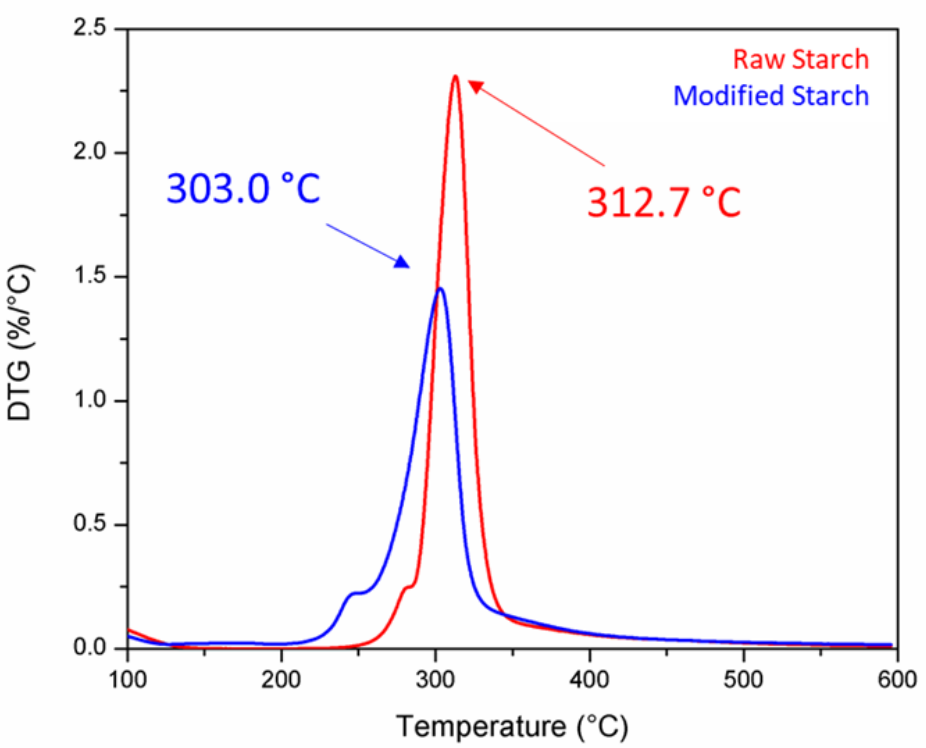

Figure 4.15 DTG curves of unmodified (raw) starch and modified (microwave method) starch

4.8.2 Gelatinization Properties of Maleated and Unmodified Starches

Gelatinization properties of starches were compared by DSC and the curves are shown in Figure 4.16. Both onset and peak temperatures were determined and the heats of gelatinization were calculated based on the results (Table 4.2). This analysis is a good measure to determine changes in the crystalline structure of starch after its modification.

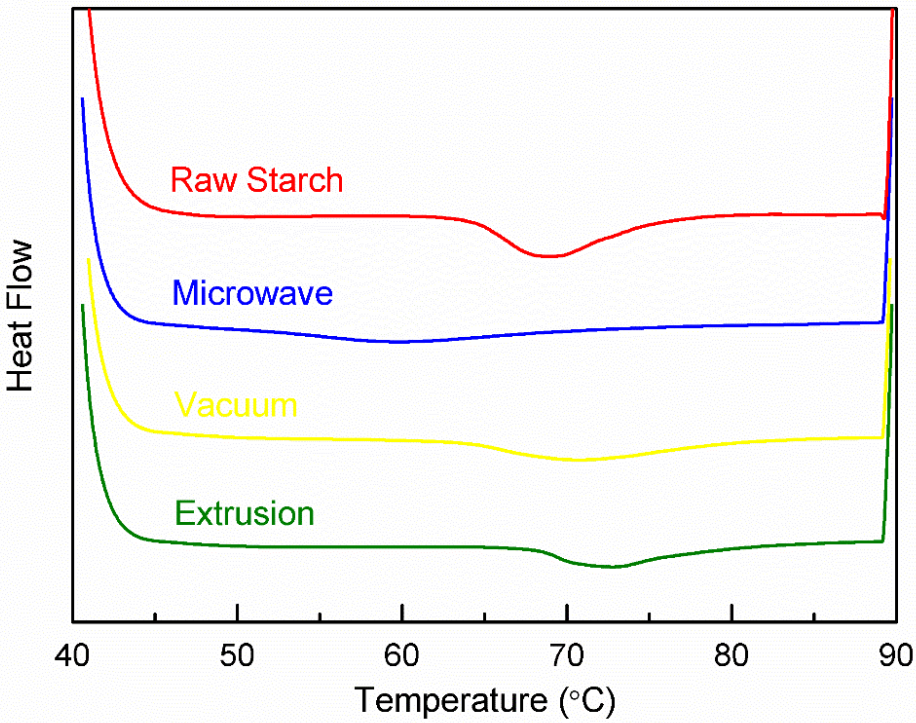

Figure 4.16 DSC curves of unmodified (raw) and maleated (microwave, vacuum rotary evaporator, and extrusion) starches

Table 4.2 Thermal properties of unmodified raw starch and maleated starches

Sample	Onset (°C)	Peak (°C)	Heat of Gelatinization (J/g)
Raw Starch	64.2 ± 0.1	68.8 ± 0.3	11.7 ± 0.4
Microwave	N/A	N/A	N/A
Vacuum	62.8 ± 1.0	69.8 ± 1.1	9.0 ± 0.5
Extrusion	67.9 ± 0.3	72.7 ± 0.2	8.3 ± 0.6

With the exception of the starches modified by the microwave method, the onset and peak temperatures were not significantly altered by the esterification. On the other hand, the heat of gelatinization showed significant reduction when modified with the vacuum rotary

evaporator or the extruder. This could be another evidence that the crystalline domains of starch were altered after the esterification. The intermolecular bonding of starch molecules was weakened by the modifications and it was clearly shown when comparing the heat of gelatinization. Since the unmodified raw starch had stronger intermolecular bonds than the modified starches, it required a higher amount of energy to break the bonds. The microwave-modified starch did not show a clear peak of gelatinization which would suggest that very little energy was required for this specific sample. This DSC result agrees with the conclusion made after the TGA analysis of thermal degradation.

In order to further investigate the esterified starch, FTIR analysis was performed and the spectra are shown in Figure 4.17. Both native and modified (microwave method) starches were studied.

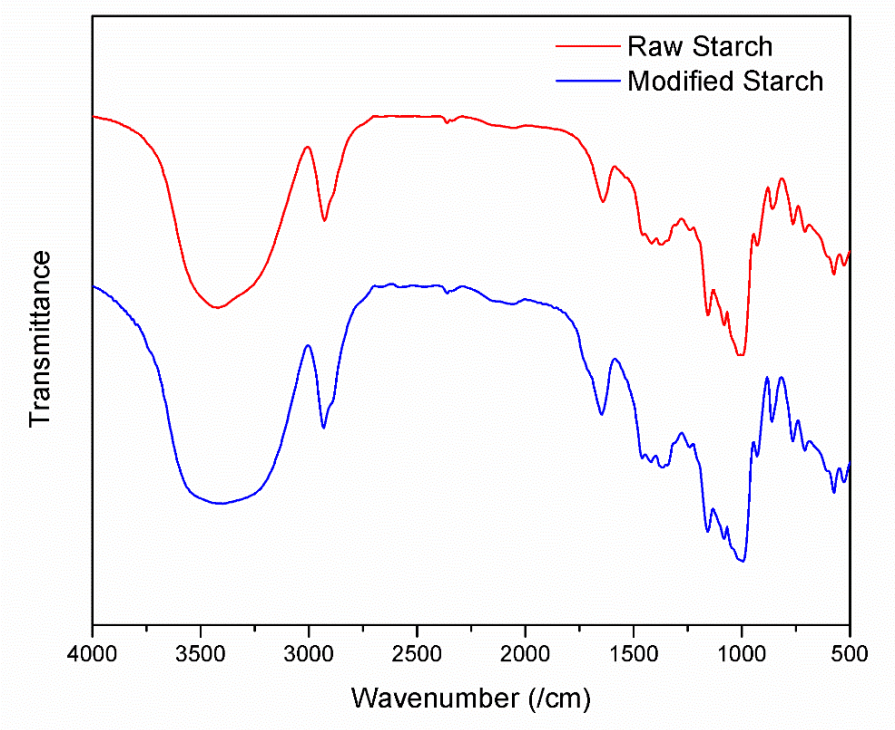

Figure 4.17 FTIR spectra of raw (native) starch and modified (microwave method) starch with 8 cm^{-1} resolution

An FTIR spectrum of starch typically shows bands at 2900-3000 cm^{-1} for C-H stretching, 1100-1150 cm^{-1} for C-O, C-C, and C-O-H stretching, and 1100-900 cm^{-1} for C-O-H bending. The native starch contains all of the above characteristic peaks. It is difficult to assign the bands in the spectra unambiguously as the bands overlap. Even with high resolution, it is not possible to individually assign each band [83]. However, there are bands distinguishable between the two spectra.

The spectrum of modified starch should show the absorption of the carbonyls at 1720 cm^{-1} (red circles in Figure 4.18). Although the modified starch spectrum in Figure 4.17 does not show a clear peak at 1720 cm^{-1}, a distinguishable shoulder is present. Because the samples

were treated by acetone, any unreacted maleic anhydride had been removed. This confirms the presence of carbonyls from maleated starch.

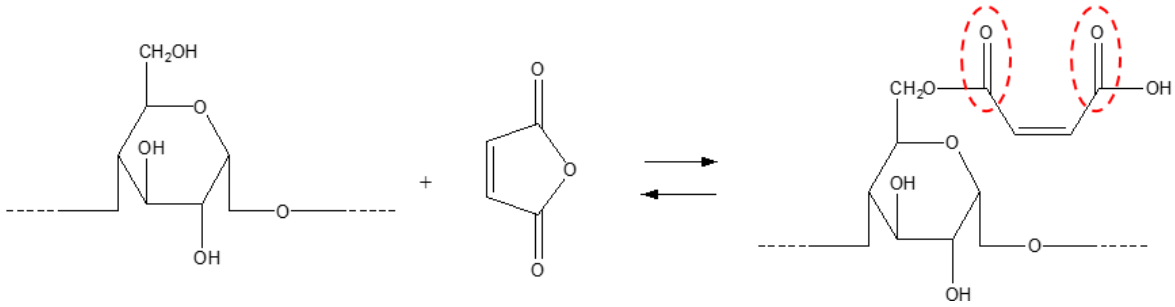

Figure 4.18 Esterification of starch by maleic anhydride

A higher resolution (1 cm^{-1}) FTIR spectra of the targeted region between 2000 and 1500 cm^{-1} is presented in Figure 4.19. Here, the carbonyl absorption shoulder is clearly present in the modified starch's spectrum at 1720 cm^{-1}. The FTIR experiment demonstrated that there was a successful esterification reaction of starch by maleic anhydride. Parts of the hydroxyl groups in the starch molecules were replaced by ester bonds.

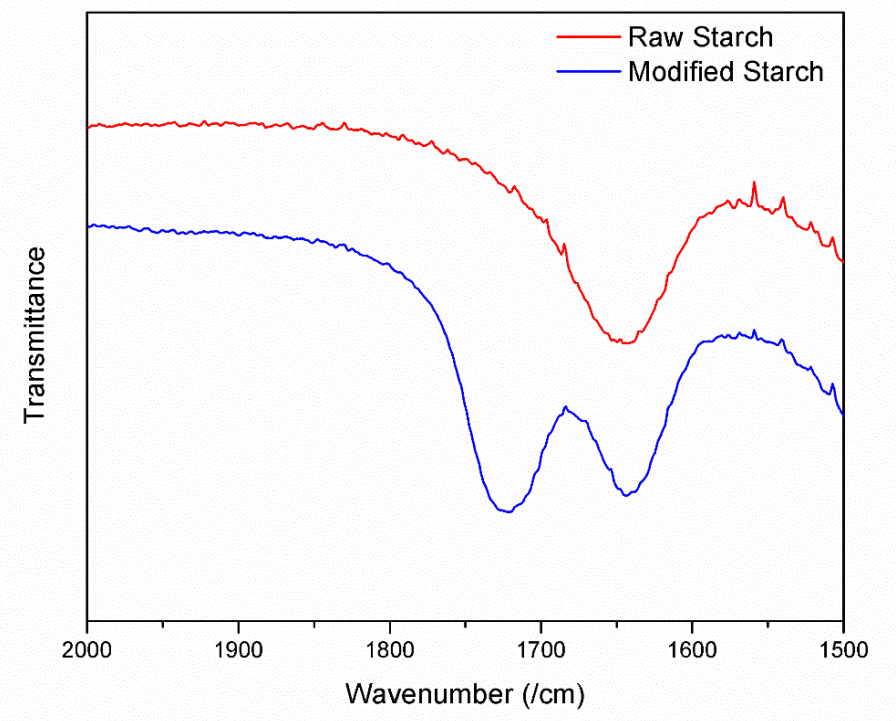

Figure 4.19 FTIR spectra of raw (native) starch and modified (microwave method) starch with high resolution (1 cm^{-1}) from 2000 to 1500 cm^{-1}

As it was mentioned earlier, the bands present in the FTIR spectra are difficult to assign because they overlap. For the quantitative study, it was necessary to use another analytical technique to compare one sample to another. ^{1}H NMR was performed on the native starch and the three modified starches (Figure 4.20).

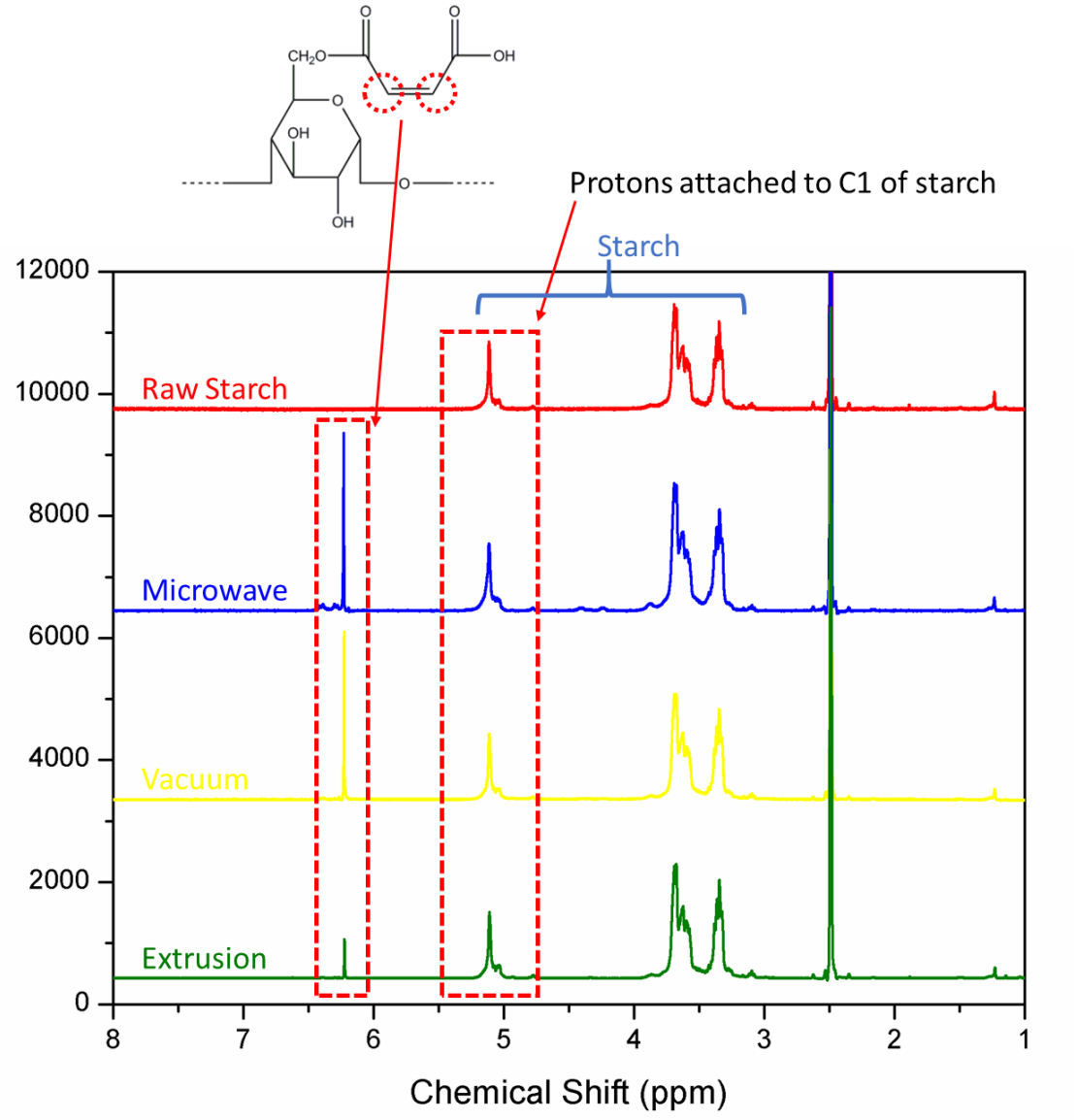

Figure 4.20 ^{1}H NMR Spectra of unmodified (raw) and maleated (microwave, vacuum rotary evaporator, and extrusion) starches

The peak assignment was already done on the starch molecule in the previous section. It was only necessary to identify new peaks generated by the chemical modification. The peaks from the hydroxyl groups had been shifted to higher ppm by adding TFA-d[1] so that they would not interfere with the others. This would leave only the two protons from the ring-

opened maleic anhydride. This vinyl double bond is shown in the chemical structure on top of Figure 4.20.

The anomeric proton from starch at 5.11 ppm is present as expected. Other protons in starch from the C2 to C6 carbons are also present in the region of 3.21-3.89 ppm. The large peak at 2.49 ppm represents the solvent, DMSO. The newly emerged peak at 6.23 ppm is from the vinyl double bond of maleic anhydride. These results are supported by several NMR studies [15, 29, 62].

The C1 proton was used as a reference to calculate the ratio with the new peak at 6.23 ppm. This yielded the degree of substitution (DS) of such modified starches. The DS can be obtained by Equation 4.2:

$$\mathrm{DS} = \frac{I_{6.23} \,/\, 2}{I_{\alpha-1,6} + I_{\alpha-1,4}} \qquad (4.2)$$

$I_{6.23}$ is the ^{1}H NMR integral of the signal from the two vinyl protons of maleic anhydride grafted to starch. $I_{\alpha\text{-}1,6}$ and $I_{\alpha\text{-}1,4}$ are the ^{1}H NMR integrals of internal branching α-1,6 and linear α-1,4 linkages, respectively. Since there are two protons from each vinyl group of open maleic anhydride, the $I_{6.23}$ values are divided by 2. The calculated DS values of the modified starches are shown in Table 4.3.

Table 4.3 Degree of substitutions of maleated starches

Sample	Starch : MA	$I_{\alpha\text{-}1,6} + I_{\alpha\text{-}1,4}$	$I_{6.23}$	DS / Maleation
Raw Starch	-	1	-	-
Microwave	4:1	1	0.37	0.19
Vacuum	4:1	1	0.40	0.20

Extrusion	100:1	1	0.09	0.05

As the NMR spectra have revealed, the two methods, microwave and vacuum rotary evaporator, show about four times greater degree of substitutions than the extrusion methods. However, considering the extrusion method had significantly less amount of maleic anhydride (0.01 wt% of starch) and short reaction time compared to the other two, the extrusion method was highly efficient to substitute starch.

Chapter 5
Materials and Methods: Starch as Nano-Filler

This chapter describes the materials and methods of compounding starch nano-particle powder with green linear low-density polyethylene to achieve well-dispersed nano-size filler composites. Additives such as compatibilizers and plasticizers were considered while different processing conditions were tested. Various analytical techniques were considered to characterize the newly developed materials.

5.1 Materials

Linear low-density polyethylene (LLDPE) SLL318 (MFR = 2.7 g/10min) from Braskem (Brazil) was used as a base polymer. This polymer is a new grade offered by Braskem being made by renewable carbon. Ethanol extracted from sugar cane was the source of ethylene, and the ethylene was polymerized to produce polyethylene. Information on this LLDPE material was covered in detail in the literature review section (Chapter 2).

Different grades of starch nanoparticles (SNP) (Ecosphere®) were produced from EcoSynthetix (Burlington, ON, Canada). Each SNP was prepared through reactive extrusion processes by the manufacturer through collaboration with our research group (Figure 5.1). The process uses a twin-screw extruder with starch, water and various amounts of glycerol (0, 9, 17, and 24 wt.%) for plasticization and glyoxal for crosslinking. Although the size of

each SNP ranges between 10 to 50 nm, it forms micro-sized aggregates in air, but forms a latex in water.

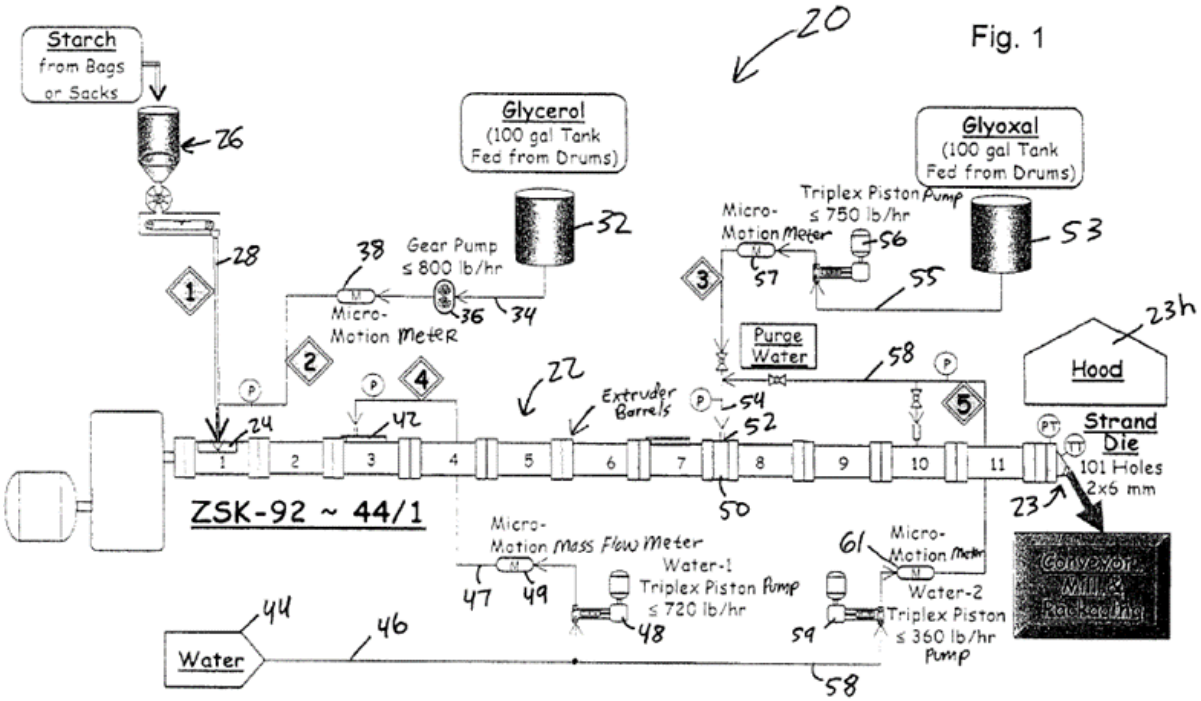

Figure 5.1 Production apparatus of starch nano-particle (SNP, Ecosphere®) [84]

Two types of plasticizers, glycerol (Sigma-Aldrich, Canada) and D-sorbitol (Sigma-Aldrich, Canada) were used. Licocene®, polyethylene grafted maleic anhydride 4221 fine grade (Clariant, Canada) was used as a compatibilizer. Lithium bromide (LiBr), deuterated acetone (acetone-d^6), deuterated trifluoroacetic acid (TFA-d^1) and toluene were purchased from Sigma-Aldrich (Canada) for nuclear magnetic analysis.

5.2 Sample Preparations and Characterizations

5.2.1 Chemical Composition Analysis: Free Glycerol

A schematic diagram of the sample preparation for NMR analysis is shown in Figure 5.2. The SNP samples went through a series of steps to quantify the amount of free glycerol using NMR. 0.05 g of LiBr was dissolved in 10 g of acetone-d^6 and 10 mg of SNP was mixed with the LiBr–acetone-d^6 solution. The mixture was constantly shaken and ultra-sonicated for 24 hours. An adequate amount of toluene was added as an internal standard for quantitative analysis. After another ultra-sonication, the liquid phase of the sample was then transferred into NMR tubes that were introduced into a Bruker-Spectrospin 500 Ultrashield (500 MHz) for spectrometer analysis and the proton NMR (^{1}H NMR) scans were run. A constant temperature of 298 K was maintained while scanning NMR spectra with chemical shifts from -1 to 10 ppm with 32 scans. Spectra of four different SNPs and glycerol were collected, and their remaining free glycerol contents were calculated.

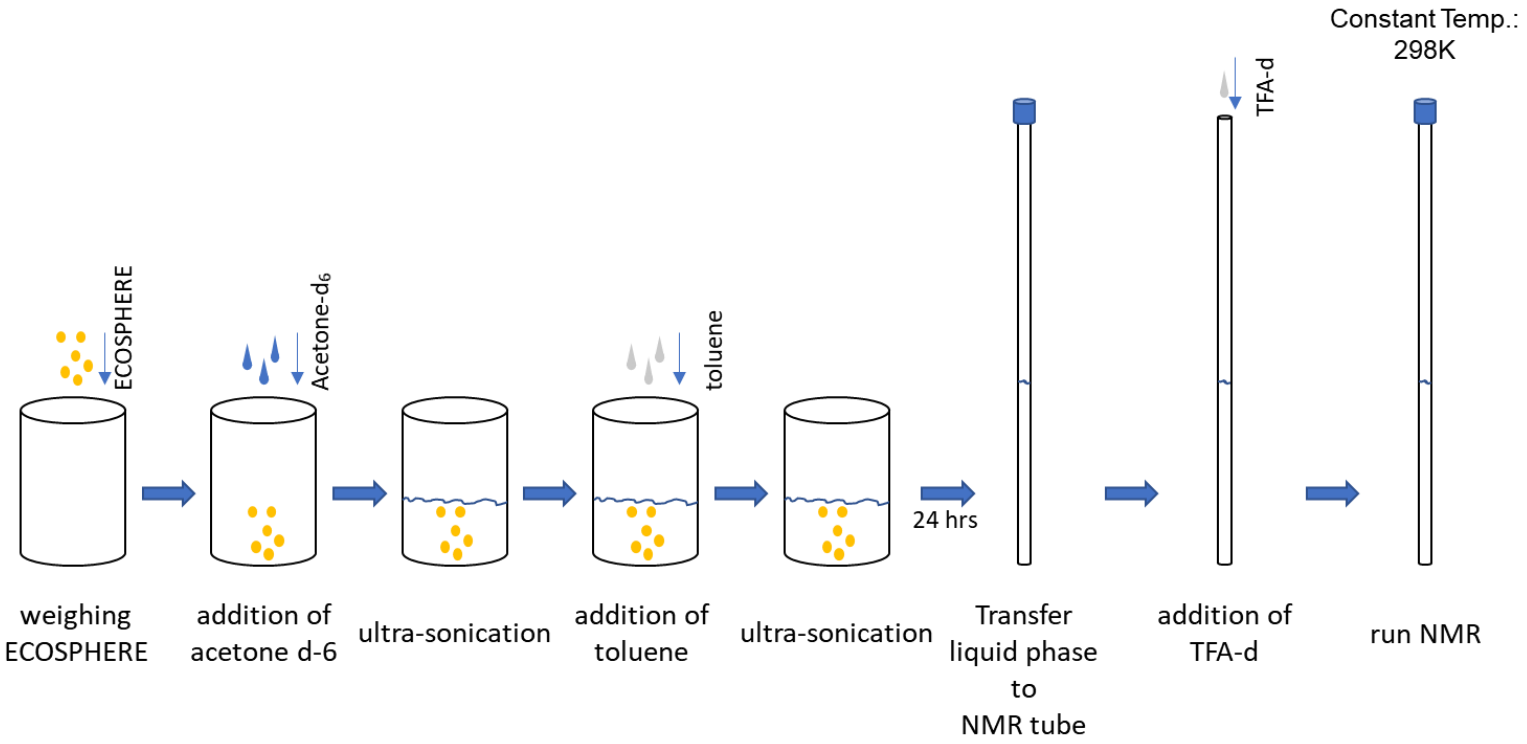

Figure 5.2 Schematic diagram of NMR sample preparation

Table 5.1 List of samples for ^{1}H-NMR analysis

Tube #	Sample	Solvent
1	11.5µL Toluene	1mL Acetone-d^6
2	4mg Glycerol	1mL Acetone-d^6
3	11.5µL Toluene + 4mg Glycerol	1mL Acetone-d^6
4	SNP #1 (0% glycerol) + 11.5µL Toluene	1mL Acetone-d^6
5	SNP #2 (10% glycerol) + 11.5µL Toluene	1mL Acetone-d^6
6	SNP #3 (17% glycerol) + 11.5µL Toluene	1mL Acetone-d^6
7	SNP #4 (24% glycerol) + 11.5µL Toluene	1mL Acetone-d^6
8	11.5µL Toluene + 4mg Glycerol + TFA-d	1mL Acetone-d^6
9	SNP #1 (0% glycerol) + 11.5µL Toluene + TFA-d	1mL Acetone-d^6
10	SNP #2 (10% glycerol) + 11.5µL Toluene + TFA-d	1mL Acetone-d^6
11	SNP #3 (17% glycerol) + 11.5µL Toluene + TFA-d	1mL Acetone-d^6
12	SNP #4 (24% glycerol) + 11.5µL Toluene + TFA-d	1mL Acetone-d^6

5.2.2 Experimental Design

A systematic approach was applied for the experiments. Table 5.2 presents a list of samples with the amount of each component added and the processing conditions for extrusion. A 2^4 factorial design was implemented. The concentration of SNP and PE-g-MA remained constant at 20% and 2%, respectively, throughout the experiments. Two plasticizers were added to the mixtures: glycerol and sorbitol, and each of them had two levels of concentrations (3 and 7%). The processing temperature (150 and 170 °C) and screw rpm (75 and 150 rpm) had two levels each. These four factors were carefully chosen based on previous research work reported in Khan's thesis [85].

5.2.3 Sample Processing

The sample preparation started with extrusion. The SNPs were dried at 40 °C for 12 hours prior to compounding. Each pre-mixed mixture (Table 5.2) was loaded into a co-rotating conical twin-screw extruder (Haake MiniLab Micro-compounder, Thermo Electron Corporation) barrel using a hopper. The processing conditions (temperature and screw speed) were varied accordingly. Extrudates were pelletized, dried and injection molded (Injection Molding Apparatus, Ray-Ran). Simple rectangular bar specimens were prepared. The injection molding temperature (barrel) was varied from 150 to 175 °C. The mold temperature was set at 40 °C. A pressure of 690 kPa (100 psi) with 15 seconds of injection hold periods was applied. The injection molded specimens went through a brief annealing procedure at 120 °C to erase the thermal history.

Table 5.2 List of samples with percentage of added components and processing conditions for the experiment

Sample Code	PE (%)	Dry SNP (%)	Moisture (%)	Glycerol (%)	Sorbitol (%)	PE-g-MA (%)	Plasticizing Ratio (%)	Temp. (°C)	RPM
EG09	70.55	20	0.45	7	0	2	35	150	75
EG10	70.42	20	0.58	7	0	2	35	150	150
EG11	70.55	20	0.45	7	0	2	35	170	75
EG12	70.55	20	0.45	7	0	2	35	170	150
EG13	74.48	20	0.52	3	0	2	15	150	75
EG14	74.48	20	0.52	3	0	2	15	150	150
EG15	74.42	20	0.58	3	0	2	15	170	75
EG16	74.42	20	0.58	3	0	2	15	170	150
ES06	70.48	20	0.52	0	7	2	35	150	75
ES07	70.48	20	0.52	0	7	2	35	150	150
ES08	70.48	20	0.52	0	7	2	35	170	75
ES09	70.42	20	0.58	0	7	2	35	170	150
ES10	74.42	20	0.58	0	3	2	15	150	75
ES11	74.42	20	0.58	0	3	2	15	150	150
ES12	74.42	20	0.58	0	3	2	15	170	75
ES13	74.42	20	0.58	0	3	2	15	170	150

5.3 Morphological analysis and Image Processing Method

In order to determine morphological characteristics including distribution, dispersion and particle size of fillers, scanning electron microscopy (SEM) on individual samples was performed.

The injection molded bars were cryo-fractured in liquid nitrogen and underwent extraction (Figure 5.3) in water at 50 °C for 4 hours. The sample submerged in water was continuously stirred using magnetic stirrers so that the starch particles could migrate away from the surface. This process ensured the contrast in the images between the surfaces of polyethylene and voids that SNPs left (Figure 5.4 (a)). Although the equipment was capable of environmental scanning microscopy, the sample surfaces were sputter coated with 10 nm of gold for better resolution and contrast. FEI Quanta Feg 250 ESEM (Thermo Fisher Scientific) with an accelerating voltage of 15 kV was used. For each sample at least two specimens were examined.

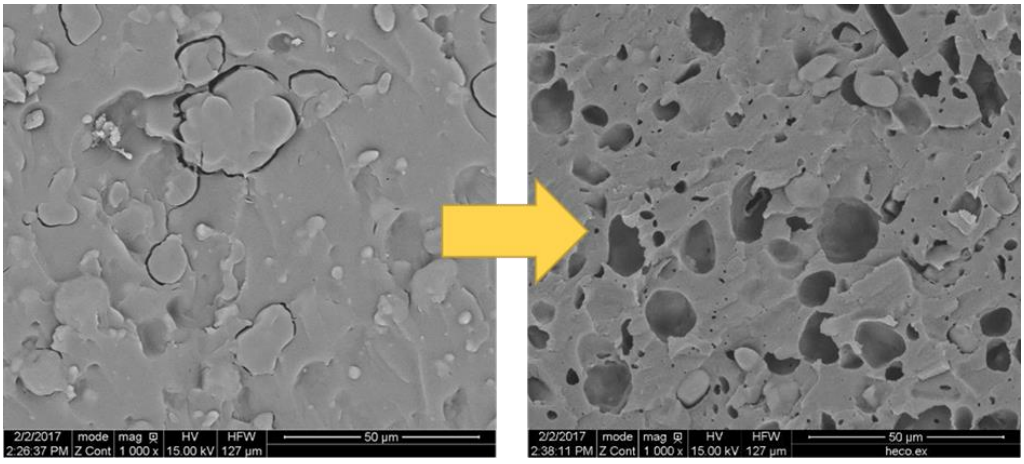

Figure 5.3 Extraction of SNP from surface

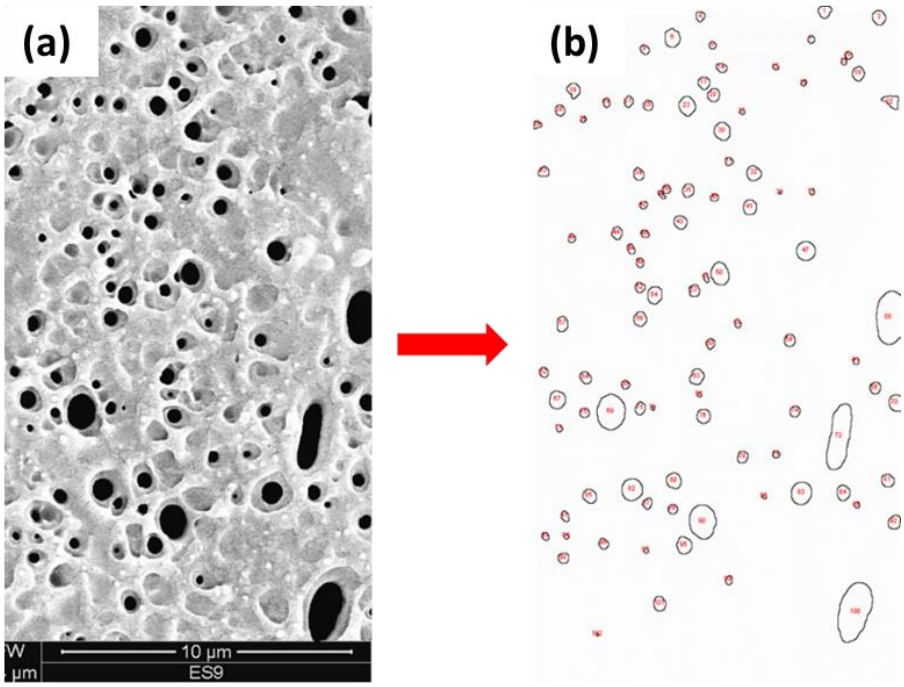

Figure 5.4 SEM image and image processing technique using Image J

Using an image processing and analysis software (Image J, National Institute of Health), all the SEM images were processed. Figure 5.4 illustrates an example of an SEM image before (a) and after (b) the processing. After this transformation was finished, the software found voids in the image and automatically calculated their areas. Assuming all voids are spheres, the software calculated the equivalent diameter of each void based on the area. Depending on the compositions, 100 to 300 voids were used to calculate the averages. Number average (d_n), area weighted average (d_A), and volume weighted average (d_V) diameters were calculated using Equations 5.1, 5.2 and 5.3.

$$d_n = \left(\sum_{i=1}^{n} d_i\right) / n \tag{5.1}$$

$$d_A = \sum_{i=1}^{n} \left(d_i \cdot \frac{A_i}{\sum_{i=1}^{n} A_i}\right) \tag{5.2}$$

$$d_V = \sum_{i=1}^{n}(d_i \cdot \frac{V_i}{\sum_{i=1}^{n} V_i}) \quad (5.3)$$

where:

d_i = ith diameter

n = total number of diameters counted

A_i = area calculated by using ith diameter

V_i = volume calculated by using ith diameter

The average diameters and size distributions were compared to analyze the effects of glycerol/sorbitol contents, PE-g-MA contents, and processing conditions on SNP filler particle sizes and dispersion.

Chapter 6
Results and Discussions: Starch as Nano-Filler

Dispersing hydrophilic starch in a hydrophobic polymer matrix such as polyethylene can be very challenging. There have been a few studies in the literature where a compatibilizer such as PE-g-MA and poly(ethylene-co-vinyl alcohol) played a crucial role in starch-plastic composites [86-88]. Yatigala et al. have shown that just 2 to 3 % of maleic anhydride reduced the melt flow index (MFI) by 10 to 16 %. This implied that the crosslinking of the polymer occurred resulting in improved mechanical properties. Another study presented an attempt to disperse starch in a high-density polyethylene (HDPE) matrix. They have successfully reduced the starch droplet size near 1 μm by using high concentration (up to 20 wt.%) of compatibilizer. When considering scaling up to mass production, this is unfavorable because of economic reasons. It would be beneficial to minimize the use of additives while delivering the same or even better processability and properties of the material.

In this thesis, the focus was to control and minimize the starch filler size in a linear-low density polyethylene (LLDPE) matrix. This is a crucial factor when considering the composite material for film applications. Because typical mulch film thickness ranges up to 60 μm, film processability becomes an issue if the filler particle size is not small enough which prevents blown film extrusion or sheet casting.

The rate of degradation is another issue. If the processing window only allows producing thick films due to the particle size within the composites, it has a detrimental influence against the environment. [89]. It is certain that the smaller starch particle size within the polyethylene matrix have a larger surface area to volume ratio, and provide higher accessibility to microorganisms [89]. Therefore, with the same amount of starch used, the smaller filler particle size gives a better environmental advantage. These issues are discussed in this chapter.

This chapter reports the results obtained through the steps described in the previous chapter. The goal of this work was to produce a uniform nano-sized dispersion of starch nanoparticles in a linear-low density polyethylene matrix by minimum use of additives and by comparing various processing conditions.

The goals of this research were i) to determine the free glycerol contents in the SNPs and ii) to study the effect of additives and processing conditions on the filler particle size in the matrix.

6.1 Analysis of glycerol contents in starch nano-particles

There were four starch nanoparticles (SNPs) that went through reactive extrusion with various amounts of glycerol. Finding out the remaining free glycerol contents in the sample was necessary and proton nuclear magnetic resonance analysis (^{1}H NMR) was performed. As outlined in the previous chapter, the sample preparation ensured that only the substances soluble in acetone were seen in the NMR spectra. Removing the starch (and modified starch) from the sample was a critical process because they overlapped with the region where the

glycerol peaks appear in the spectra, and this makes it difficult to perform quantitative analysis. The known amount of toluene in the mixture was also necessary to calculate the amount of remaining free glycerol. The addition of deuterated trifluoroacetic acid (TFA-d) was also necessary for the quantitative analysis. Figure 6.1 shows a ^{1}H NMR spectrum of glycerol with toluene as an internal marker. Although this would give adequate information to identify the chemical compositions, with the addition of TFA-d (Figure 6.2), peaks from the hydroxyl protons disappeared from the region of interest (3.5 to 3.8 ppm). This made it convenient for the peak assignment and quantitative analysis. Figure 6.3 shows the spectrum after the addition of TFA-d. Here, it is clearer to identify the peaks from glycerol and quantitatively calculate the exact amount of glycerol in the sample.

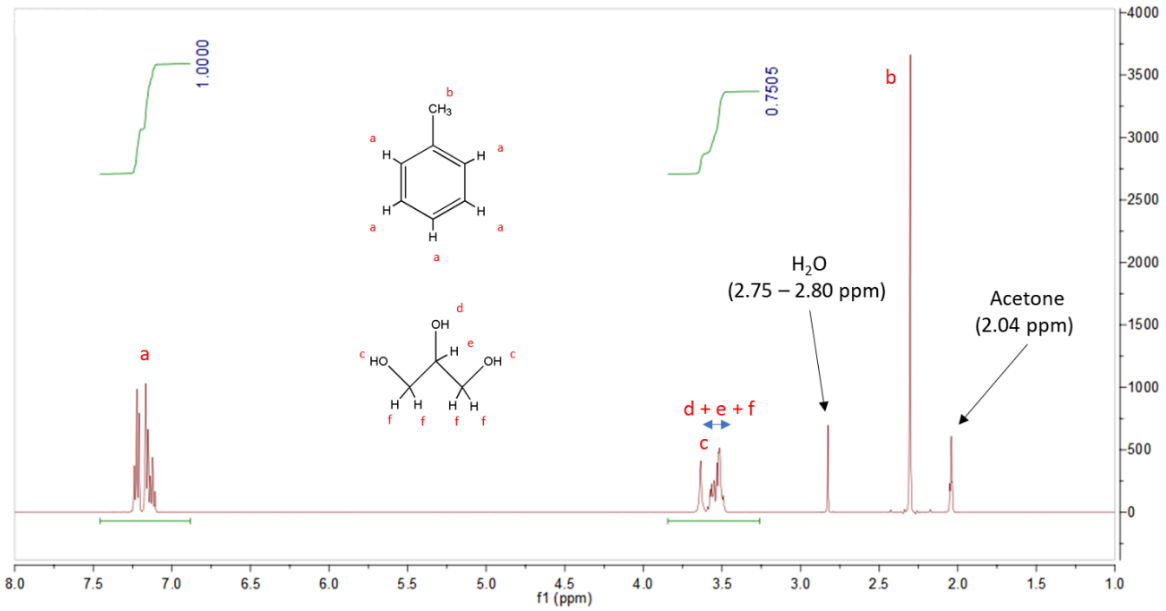

Figure 6.1 ^{1}H NMR spectrum of glycerol in acetone with toluene as internal marker

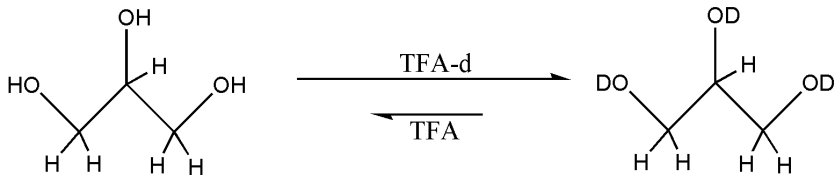

Figure 6.2 Glycerol to tri-deuterated glycerol by addition of TFA-d

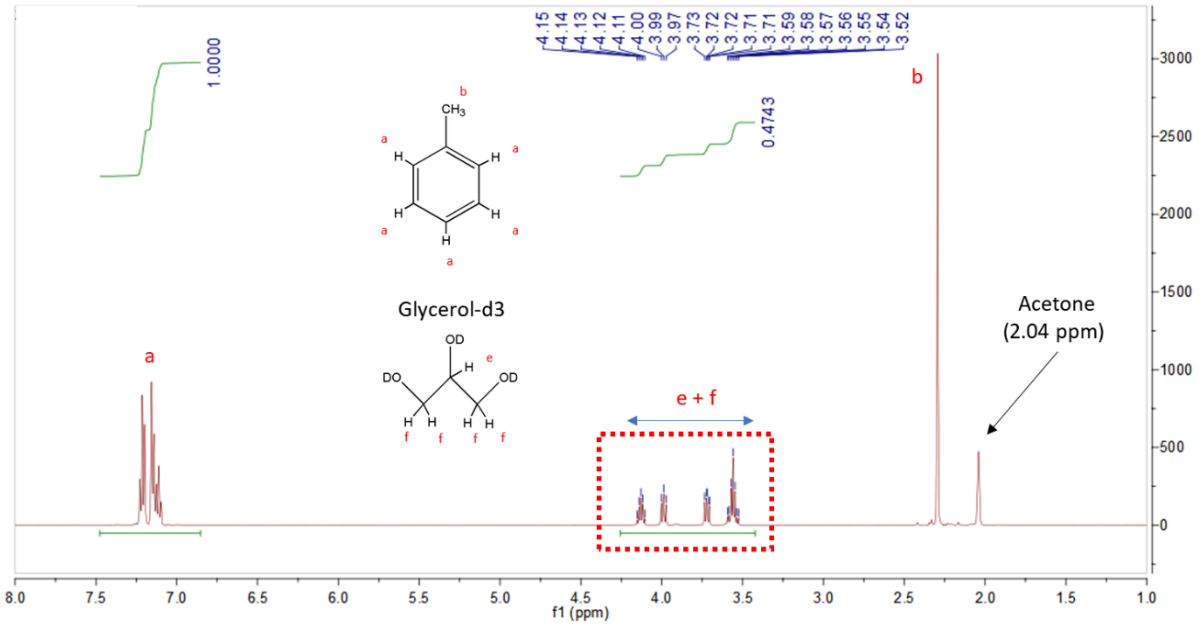

Figure 6.3 ^{1}H NMR spectrum of tri-deuterated glycerol in acetone with toluene as an internal marker and addition of TFA-d

The spectra are shown in Figure 6.4. The stacked spectra at the bottom show the region where the glycerol peaks are present. The ^{1}H NMR spectra of SNP with no glycerol treatment are not shown because of the absence of glycerol. Some of the spectra were amplified in order to easily identify the peaks. With the glycerol as a reference, it was easy to recognize that there was free glycerol present in two samples. The SNP with 17 % glycerol added in the extrusion process showed a very minimal amount of free glycerol whereas the 24 % one certainly contained more. The one with 9 % glycerol did not show evidence of free glycerol.

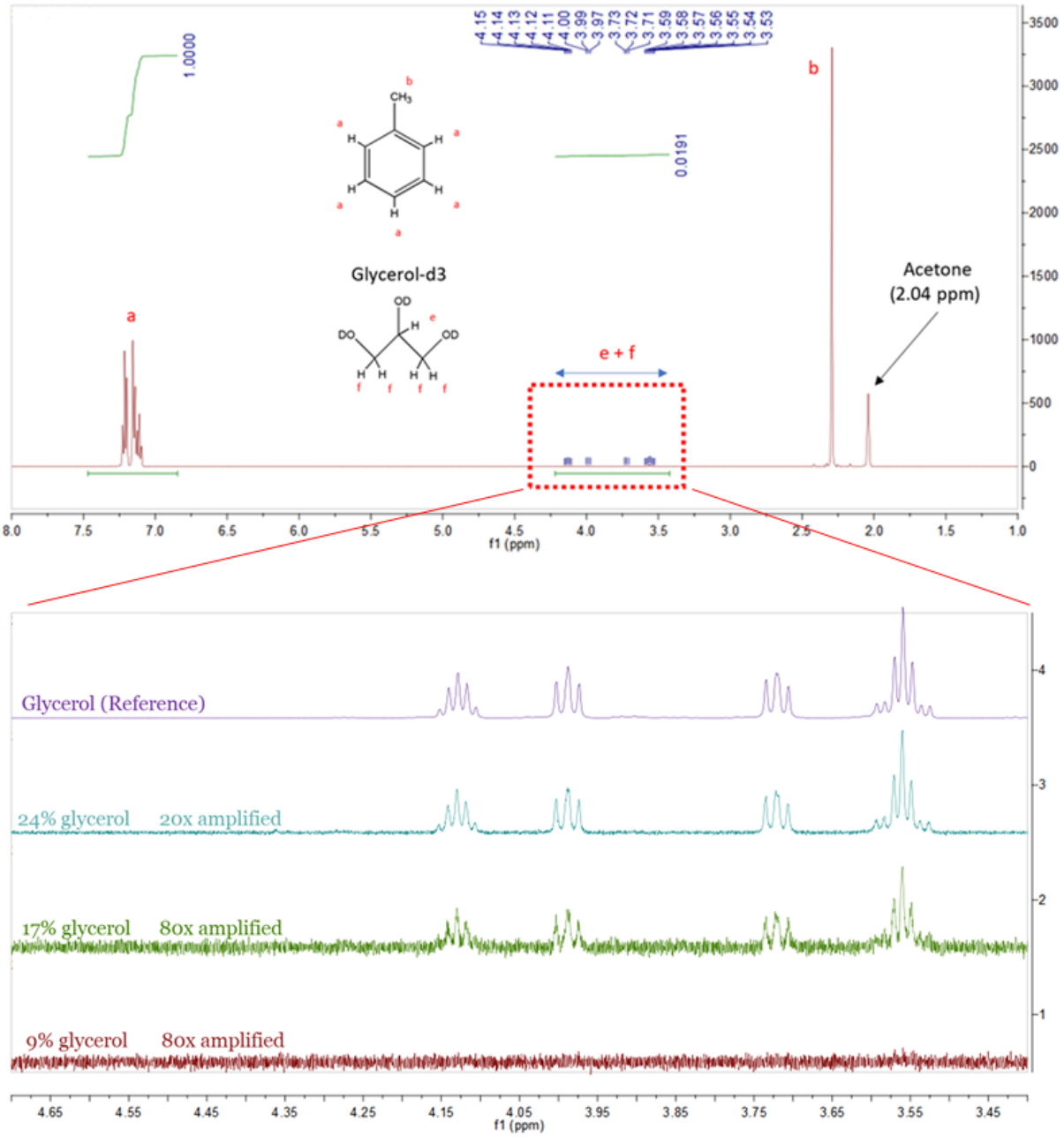

Figure 6.4 ^{1}H spectra of SNPs extruded with various amount of glycerol by manufacturer

In order to perform an accurate quantitative analysis, peak assignment was done first (Figure 6.4 and Figure 6.5). The quintet with 1:4:6:4:1 ratio at 4.15, 4.14, 4.13, 4.12 and 4.11 ppm belong to the C3 proton (middle) in the tri-deuterated glycerol structure. The two triplets

with 1:2:1 ratio from 4.00 to 3.97 ppm and 3.73 to 3.71, and the septet with 1:6:15:20:15:6:1 at 3.59 to 3.53 ppm belong to the protons attached to the two terminal carbons in the tri-deuterated glycerol structure. The peaks present at 7.25 to 7.10 ppm belong to the five aromatic protons of toluene. The sharp peak at 2.3 ppm belongs to the three protons from the methyl group attached to the aromatic ring. The solvent peak (acetone) is also present at 2.04 ppm.

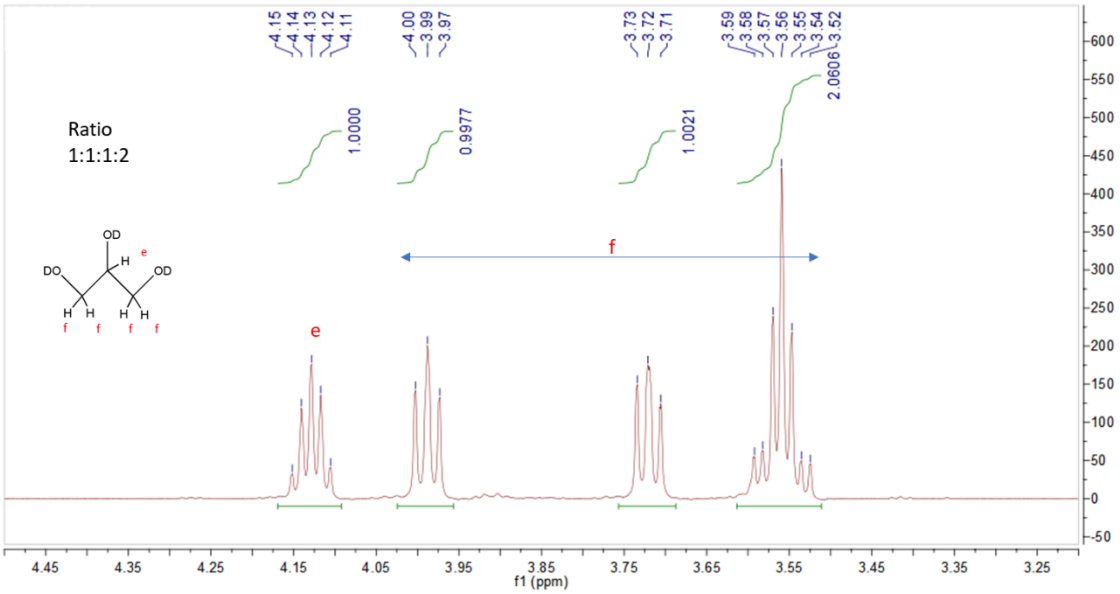

Figure 6.5 ^{1}H NMR spectrum of tri-deuterated glycerol in acetone: peak assignment and integral ratio

Using the toluene as the reference, the amount of tri-deuterated glycerol in each sample was calculated. The 9 % sample did not show any evidence of free glycerol. This suggests that all the glycerol has been cross-linked with glyoxal during the SNP production. The SNP extruded with 17 % glycerol showed a 1:0.0036 ratio between a (from toluene) and e + f (from tri-deuterated glycerol). With a further calculation, approximately 36 mg of free glycerol was present in every 10 g of this SNP. Following the same procedure, the SNP

extruded with 24 % glycerol contained approximately 190 mg of free glycerol in every 10 g of SNP. Although these SNPs contained free glycerol, it is difficult to conclude these amounts are significant considering that the plasticizing ratio of the later experiments go up to 35 % (plasticizer to SNP ratio). The next step was to compound these SNPs with LLDPE and perform a comparison study to analyze the effect of different amounts of glycerol.

6.2 Effect of glycerol contents on filler particle size and distribution in LLDPE matrix

The four SNPs prepared by the manufacturer were compounded with 0 to 10 wt.% extra glycerol, 2 wt.% PE-g-MA (compatibilizer), and LLDPE (Matrix). Each sample was analyzed under the SEM and their average particle diameter sizes were compared. Table 6.1 shows the results of the SNP filler particle size analysis. The two digits after "G" refer to the amount of original glycerol content added by the manufacturer, and the last two digits after "X" refer to the amount of glycerol added while compounding in Waterloo.

Table 6.1 Average filler particle size

Sample Code	Glycerol (SNP production) (%)	Extra Glycerol (compounded with LLDPE) (%)	Avg. Size (µm)
G00X00	0	0	7.95
G00X01		1	4.72
G00X03		3	1.50
G00X07		7	0.77
G00X10		10	0.92
G09X00	9	0	5.47
G09X01		1	5.09
G09X03		3	1.37
G09X07		7	1.00

G17X00	17	0	6.18
G17X01		1	4.01
G17X03		3	0.83
G17X07		7	0.97
G24X00	24	0	6.10
G24X01		1	4.71
G24X03		3	0.84
G24X07		7	33.26

With exceptions of the SNP's extruded with 0 wt.% during the SNP production (G00), the addition of 10 wt.% extra glycerol in the composites was too much and not suitable for the extrusion (too much glycerol migrating to the surface of extrudate). Also, the SNP-LLDPE composite with 24 wt.% original glycerol content with 7 wt.% extra glycerol (G24X07) showed extensive amounts of glycerol migrating to the surface after compounding. Furthermore, when analyzed under the SEM, this sample showed significantly larger particle size (33.26 μm) compared to others. Therefore, it was concluded that this was not suitable for processing either.

Without any extra glycerol added (G00X00, G09X00. G17X00 and G24X00), all four SNP-LLDPE composites appeared to have relatively larger diameters (5.4 to 7.6 μm) after compounding with LLDPE (Figure 6.6). There was not enough lubricating effect in these cases and most of the aggregates did not achieve nano-size. It is interesting to see that the average size got significantly reduced once the extra glycerol was added. Although the size still remained in the micrometer range, even the addition of as low as 1 % glycerol made a

significant difference. The G00 and G09 compositions showed the smallest average diameter when 7 % extra glycerol was added whereas the G17 and G24 compositions exhibited the smallest average diameter when only 3 % extra glycerol was used.

A general trend was observed that as the extra glycerol concentration increased, the filler particle size decreased. Figure 6.7 shows SEM images of the composites with 3 % extra glycerol added while compounding (G00X03, G09X03, G17X03, and G24X03). These images clearly show another trend that the particle size decreased as the amount of glycerol added during the SNP production increased. Both G17X03 and G24X03 showed nano sized uniform distributions with average diameters of less than 1 μm.

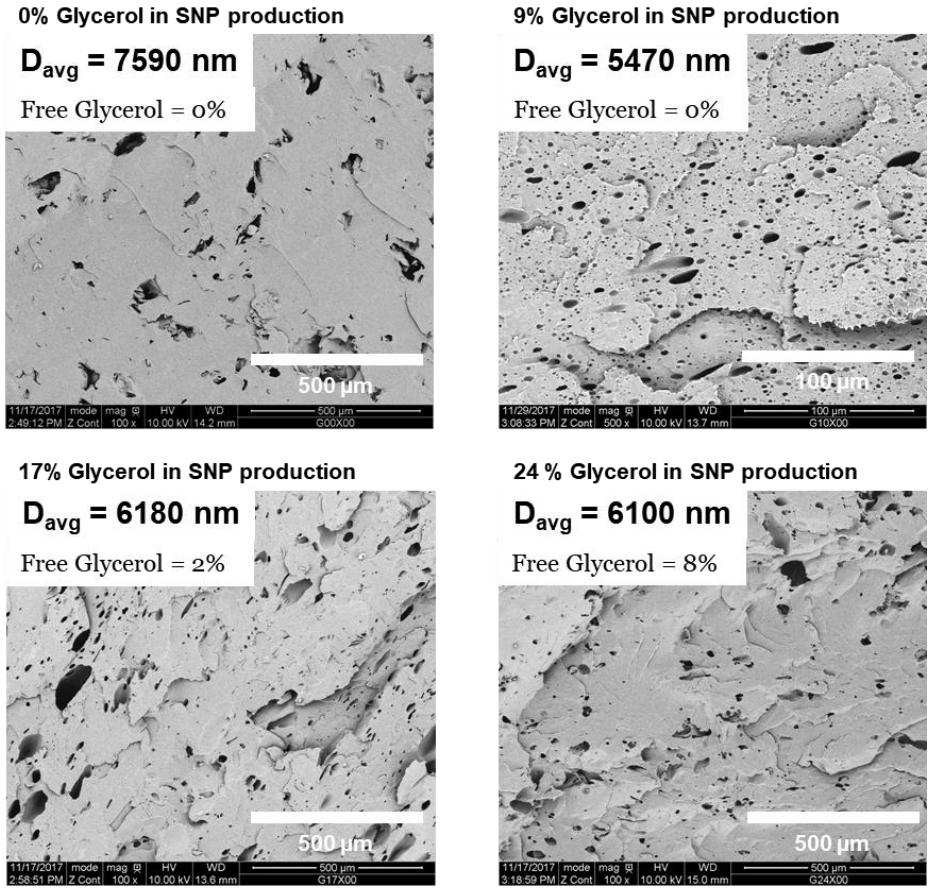

Figure 6.6 SEM images of SNP-LLDPE composites with various original glycerol concentration added in SNP

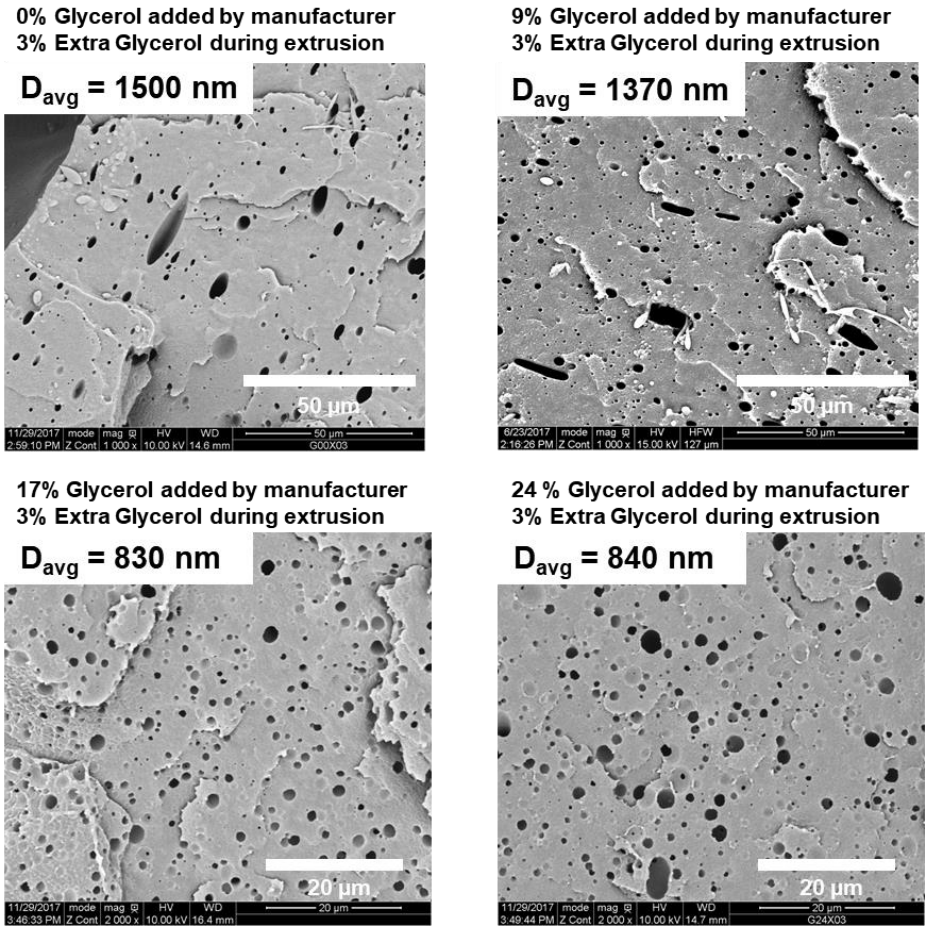

Figure 6.7 SEM images of SNP-LLDPE composites with various original glycerol concentration added in SNP with 3 % extra glycerol

Figure 6.8 illustrates the particle size distributions of SNP-LLDPE composites with no extra glycerol added (G00X00 to G24X00). The frequency of the volume fraction of each bin is also shown in orange. The volume fraction distribution is a good representation of how much space is occupied by these large aggregates in the composite. The horizontal axis represents the diameter in µm and the vertical axis represents the frequency. (a) G00X00 had the largest number average diameter (d_n = 7.95 µm) and the largest volume weighted average (d_V = 50.84 µm). Although (b) G09X00, (c) G17X00 and (d) G24X00 yielded d_n values close to that of (a) G00X00, the d_V values deviate from that of G00X00. Although a significant

amount was broken into smaller pieces during extrusion, there still were SNP aggregates large in size present within the matrix. It is quite clear that without any addition of glycerol during the process, most SNP aggregates tend to be in the micrometer range. This result also agrees with the SEM observations shown earlier.

Similarly, Figure 6.9 illustrates the particle size distributions of SNP-LLDPE composites with 3% glycerol added during extrusion (G00X03 to G24X03). The frequency of the volume fraction of each bin is shown in orange as well. By the addition of as small as 3% extra glycerol, the SNP aggregate size was reduced significantly. In all four composites, more than 90 % of aggregates were less than 1000 nm. Furthermore, the two compositions, (c) G17X03 and (d) G24X03 exhibit uniform distributions with d_n's lower than 1 μm. The volume fraction distributions of (c) and (d) are bell-shaped with peaks at 1.2 and 1.6 μm bins.

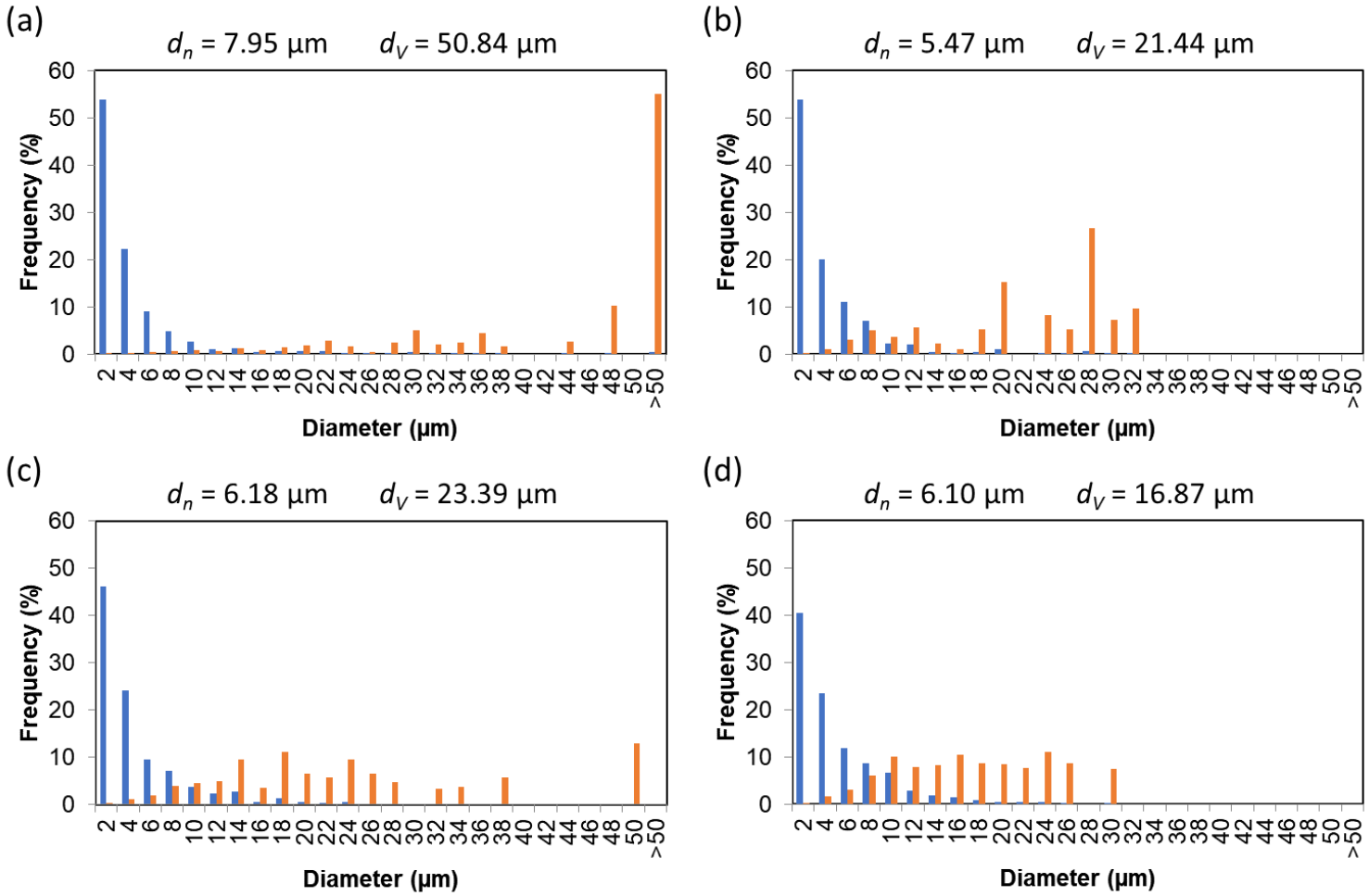

Figure 6.8 Particle size distribution (blue) and volume fraction of each bin (orange) of (a) G00X00, (b) G09X00, (c) G17X00 and (d) G24X00

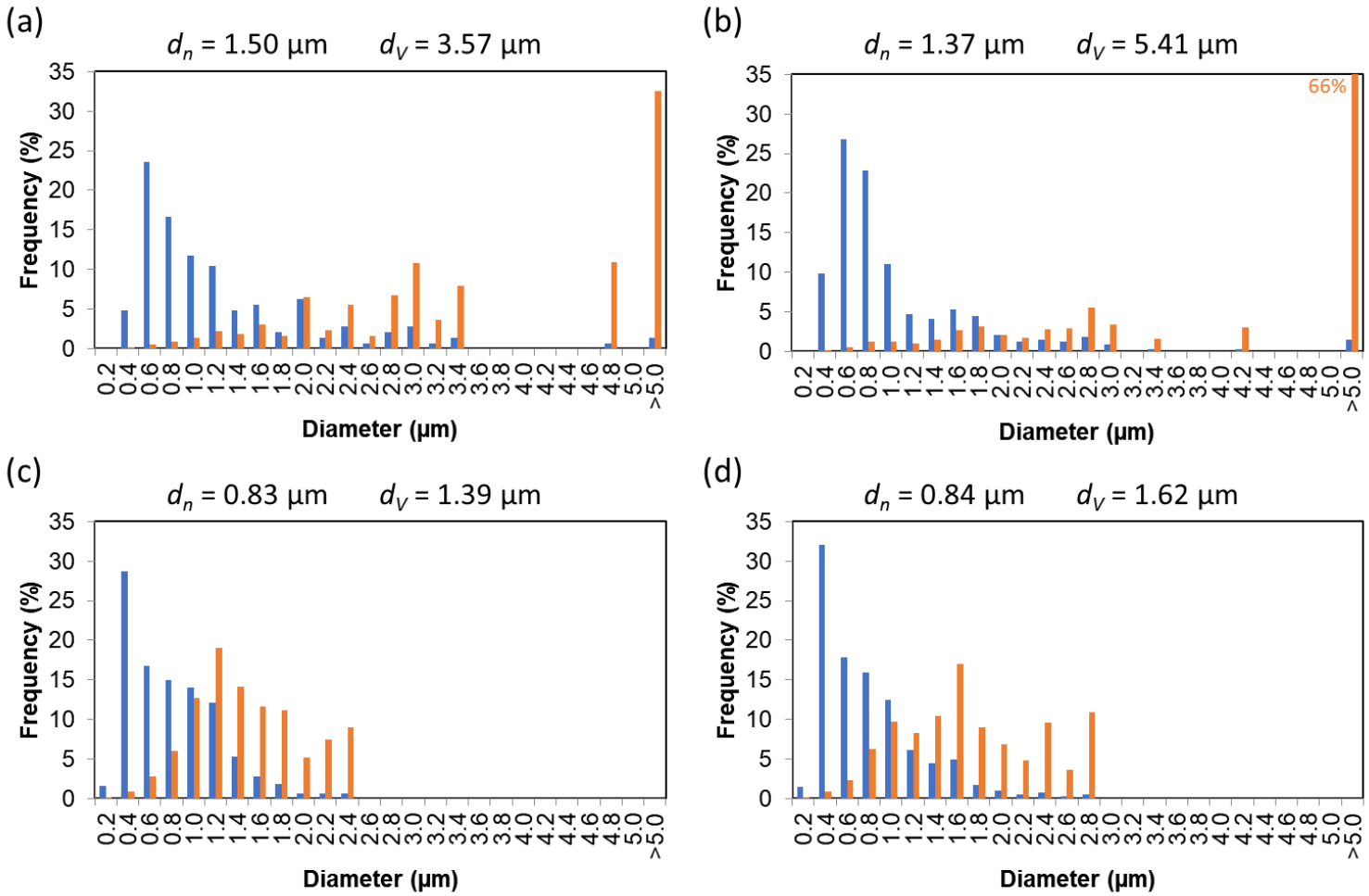

Figure 6.9 Particle size distribution (blue) and volume fraction of each bin (orange) of (a) G00X03, (b) G09X03, (c) G17X03 and (d) G24X03

A recent study from our research group conducted an analysis of the SNP manufactured by Ecosynthetix [85]. The goal of this study was to utilize the SNP as a compatibilizer to achieve a uniform distribution of cellulosic pulp in thermoplastic such as polypropylene and polyethylene. A basic morphological analysis was conducted on the SNP material. This was done by analyzing SEM images of the SNP powder and by calculating aggregate diameters based on the area of each particle shown in the image. The aggregates had an average size of 10 μm. The size distribution showed there were aggregates even larger than 90 μm with irregular and non-homogeneous morphology. It was evident that the material stays in micrometer size aggregates in the powder form. It was clear that the large aggregates were needed to be broken into smaller aggregates in order to achieve a nano size distribution. The study also demonstrated the results of extrusion and injection molding. The cryo-fractured surfaces were analyzed under the SEM. Although it was not able to achieve a full nano-scale size in average, the shear, high temperature, and more importantly, the use of glycerol significantly reduced the size of aggregates.

It was important to note the role of glycerol in this thesis as well. The addition of glycerol was a significant factor to control the SNP aggregate particle size. It was crucial to carefully plan the amount of glycerol in both the SNP production stage and the compounding with LLDPE. An adequate amount of glycerol worked well as lubricant and plasticizer in extrusion processes, and yielded uniform distribution of nano-sized particles. Because the SNP with 17 wt.% glycerol added by the manufacturer showed the most consistent results, the next sets of experiments were performed by using only this type.

6.3 Effect of processing conditions on starch particle size and distribution

In this sub-section, the experimental design (Table 5.2) outlined in the previous chapter was executed. The average particle diameter size with plasticizing ratio and processing conditions (temperature and screw speed) are shown in Table 6.2**Error! Reference source not found.**. Three types of averages were calculated. d_n is a simple arithmetic number average, d_A is a weighted average based on the area, and d_V is another weighted average based on the volume. The number average diameter is an indication of the size of the smallest droplets in a polydisperse system and the weighted average diameters are more sensitive to the contribution of the largest droplets in the system. Therefore, the large values of d_A and d_V indicate the co-existence of very small aggregates with very large ones.

An estimate of the mean diameter for spherical or sub-spherical particles is not a simple process. In this thesis, apparent particle sizes were obtained based on 2D sections from the SEM images. Although there are a few methods found in the literature, they were not implemented due to their complexity. For example, Cuzzi et al. have shown an algorithm using a computational binning system [86]. Each bin is comprised of a set of diameter bins with boundary conditions. However, in order to obtain unbiased results, each sample requires more than 100 measurements. They made an assumption that all the particles are spheres. The complexity of the method did not allow an elementary implementation of the dataset and it was not adopted in this thesis.

Table 6.2 Average filler particle size

Sample	Glycerol (%)	Sorbitol (%)	Plasticizing Ratio (%)	Temp. (°C)	RPM	Average Diameter		
						d_n (μm)	d_A (μm)	d_V (μm)
EG09	7	0	35	150	75	2.60	3.74	5.98
EG10	7	0	35	150	150	1.44	2.39	4.65
EG11	7	0	35	170	75	1.00	1.73	3.54
EG12	7	0	35	170	150	0.85	1.16	1.81
EG13	3	0	15	150	75	3.15	5.56	12.27
EG14	3	0	15	150	150	1.98	4.10	8.45
EG15	3	0	15	170	75	0.80	1.24	2.25
EG16	3	0	15	170	150	0.72	1.08	1.76
ES06	0	7	35	150	75	0.46	0.93	1.87
ES07	0	7	35	150	150	0.54	1.04	1.89
ES08	0	7	35	170	75	0.58	0.79	2.58
ES09	0	7	35	170	150	0.43	0.64	1.29
ES10	0	3	15	150	75	0.70	1.04	2.02
ES11	0	3	15	150	150	0.66	1.00	1.52
ES12	0	3	15	170	75	0.48	0.63	0.85
ES13	0	3	15	170	150	0.61	0.87	1.29

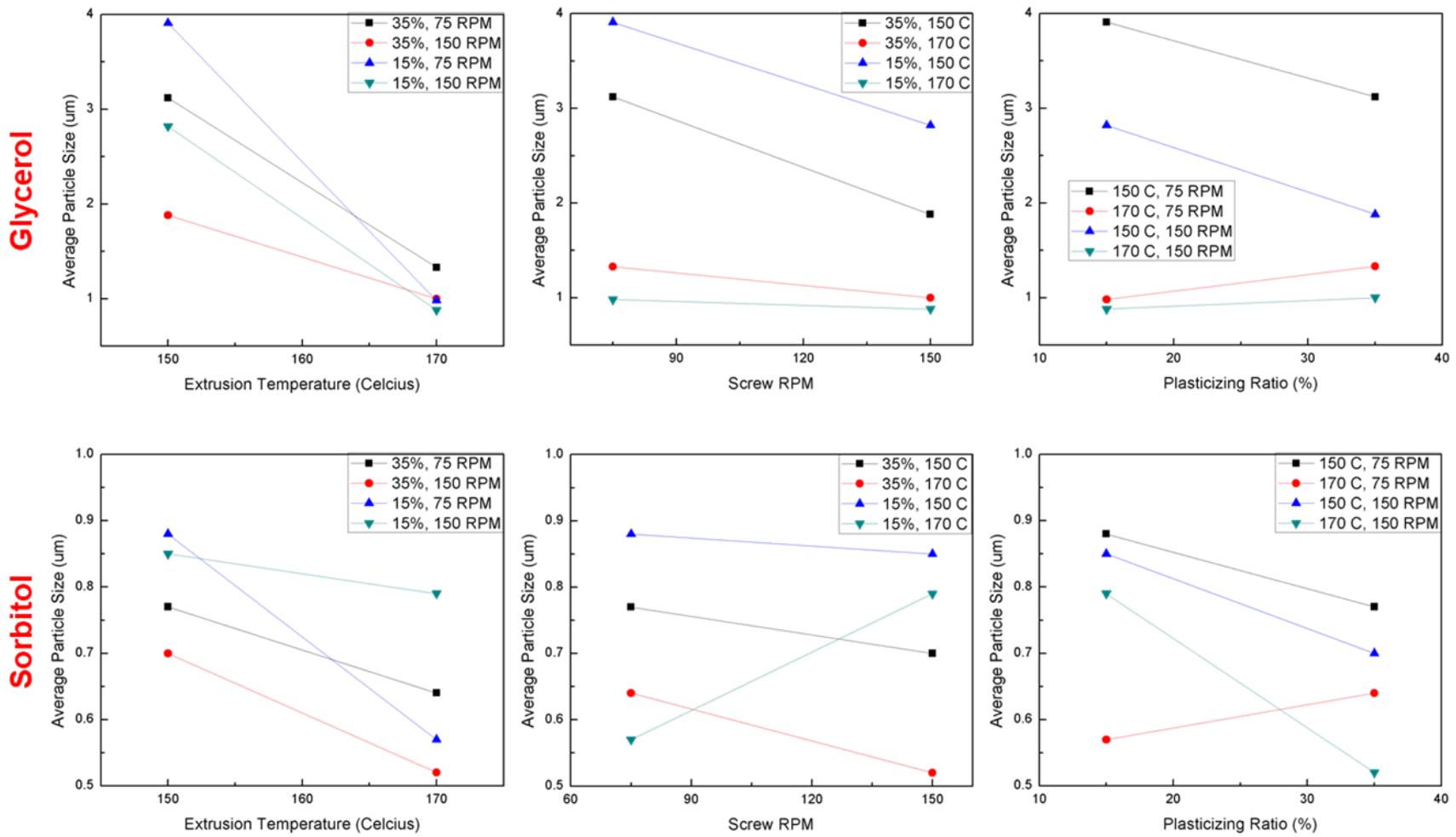

Figure 6.10 Average particle size with respect to plasticizing ratio and processing conditions

The smallest d_n (430 nm) was achieved by using sorbitol (7 wt.%) as a plasticizer, with the extrusion temperature of 170 °C, and the screw speed of 150 rpm (ES09). Based on the results, the samples that used glycerol as plasticizer were more sensitive to the change in processing conditions than the ones that used sorbitol. All samples that used sorbitol achieved nano-size average diameter (430 to 700 nm), whereas only three samples (EG12, EG15, and EG16) that used glycerol achieved nano-size average diameter (850, 800 and 720 nm). d_A, on the other hand, exhibited nano-size only in the ES group. This was due to the higher polydispersity in the EG than the ES group. Large aggregates were present in the compositions where the higher d_A values were observed. d_V values exhibited similar patterns with a range from 12.27 μm to 850 nm. The differences are more apparent when comparing the d_V's that none of the EG specimens had nano size average diameter.

The results (d_n) from Table 6.2**Error! Reference source not found.** were visualized and shown in Figure 6.10**Error! Reference source not found.**. Both EG and ES were plotted with respect to three factors (processing temperature, extrusion speed, and plasticizing ratio). The results have shown a couple of general trends. With few exceptions, the higher extrusion temperature (170 °C) and the higher extruder speed (150 rpm) displayed smaller average SNP filler sizes. The processing temperature, among all the factors, was the most effective way to reduce the SNP filler particle size in the LLDPE matrix. In the case of using sorbitol, when the particle size reached a certain nano-scale level (500 ~ 900 nm), change in extruder speed did not induce significant improvement. Figure 6.11**Error! Reference source not found.** displays some of the SEM images of the composite with various processing conditions.

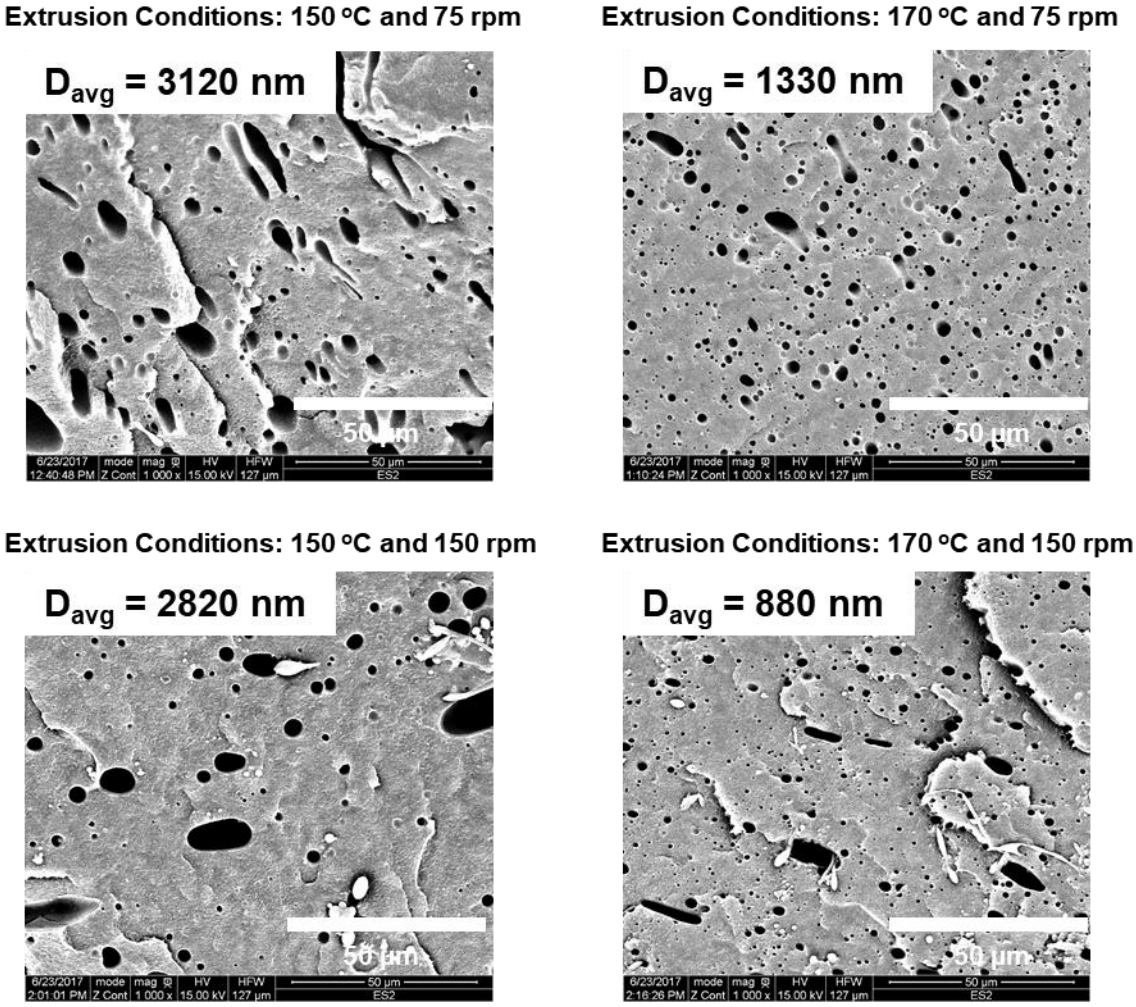

Figure 6.11 SEM images of SNP-LLDPE composites with various processing conditions

Along with water, polyols such as glycerol and sorbitol are often used as plasticizer when processing starch materials. However, these materials can act as another role within the extruder barrel. By adding these polyols, the molten mixture can achieve lower viscosity because they can act as lubricants. Glycerol is in the viscous liquid phase at room temperature with a melting point of 17.8 °C. On the other hand, having three extra carbons, sorbitol has a melting point of 95 °C and is solid at room temperature. In order to achieve a

good mixing and dispersion of nanoparticles inside a twin-screw extruder, an adequate shear is necessary. Because glycerol in liquid form should lower the viscosity more than sorbitol, the composites with glycerol may not have enough shear stress to achieve good dispersions.

6.4 Effect of compatibilizer on starch particle size and distribution

The effect of compatibilizer namely, polyethylene graft maleic anhydride (PE-g-MA), was studied by varying the amount from 0 to 4 %. Figure 6.12**Error! Reference source not found.** displays SEM images of SNP-LLDPE composites with various amounts of PE-g-MA. The materials were compounded with either glycerol or sorbitol. In both cases, a clear trend was observed. As the amount of PE-g-MA increased, the average filler size decreased. The smallest average size (310 nm) was achieved by using 4 % PE-g-MA and sorbitol as lubricant/plasticizer. This behaviour (reduction in average size) was attributed by other authors as a demonstration of typical emulsification effect of PE-g-MA in starch-PE blends [90]. The starch-PE blend showed a high interfacial tension and the PE-g-MA reduced the interfacial tension between the phases. Thus, it led to a reduction in the phase size until interfacial saturation of copolymer was reached. The compatibilization via PE-g-MA in the case of starch-PE blend is believed to be through the formation of an ester bond between maleic anhydride in the PE-g-MA with the hydroxyl groups of the starch phase [91].

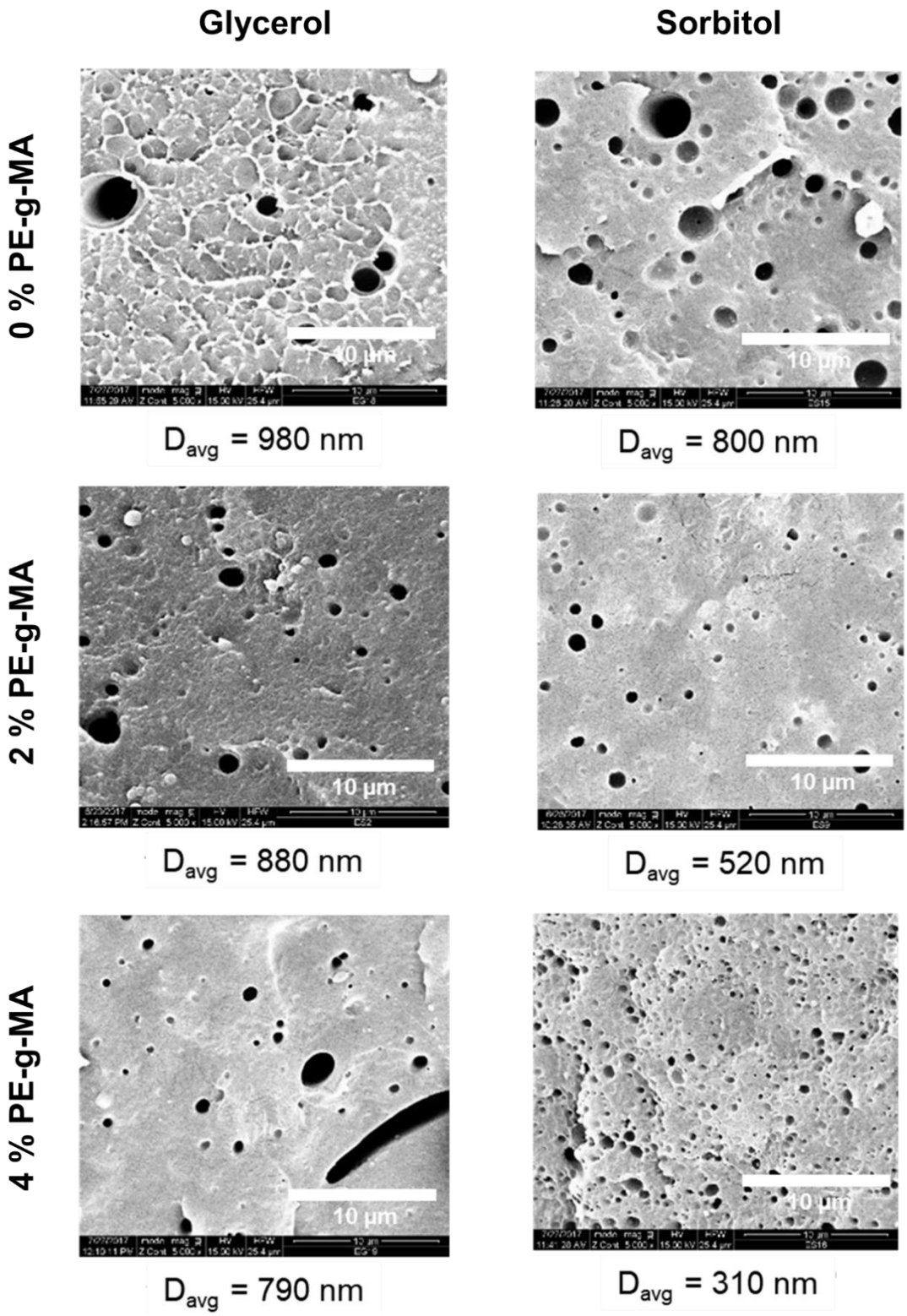

Figure 6.12 SEM images of SNP-LLDPE composites with 0, 2, and 4 % PE-g-MA

A study reported by Taghizadeh et al. in 2013 prepared TPS-PE composites by using different types of plasticizers (glycerol, sorbitol, diglycerol, and polyglycerol) [92]. TPS formulations were blended with HDPE at a concentration of 20 TPS/80 HDPE wt.% and interfacial modifiers contents in the extrusion process. Only a single processing condition, one temperature (160 °C) and one screw speed (100 rpm), was adopted throughout the process. All of the compositions had 36 wt.% plasticizing ratios. Among several plasticizers, glycerol (20 %) yielded the smallest starch size in the PE matrix. However, in order to reach nano-scale uniform distribution, a relatively large amount of PE-g-MA (9 to 20 %) was necessary. Their study reported an average (d_n) of 800 nm as the best result. This has been the smallest average size reported in the literature that incorporated starch in PE matrix so far. In this thesis, the author was able to reduce the starch filler size by more than half of the smallest size reported in the literature.

The work reported in this thesis has demonstrated the ability to engineer the SNP aggregate size in the LLDPE matrix with a minimum use of the compatibilizer (PE-g-MA). This was possible by considering various processing conditions and plasticizing ratios. Figure 6.13**Error! Reference source not found.**(a) compares the particle size distributions between one of the first trials (red bars) and the one that achieved the smallest SNP filler size within the LLDPE matrix (blue bars). Similarly, Figure 6.13(b) compares the frequency of volume fraction of the two samples. The author believes that this achievement could provide economic and environmental benefits, and thus create new opportunities.

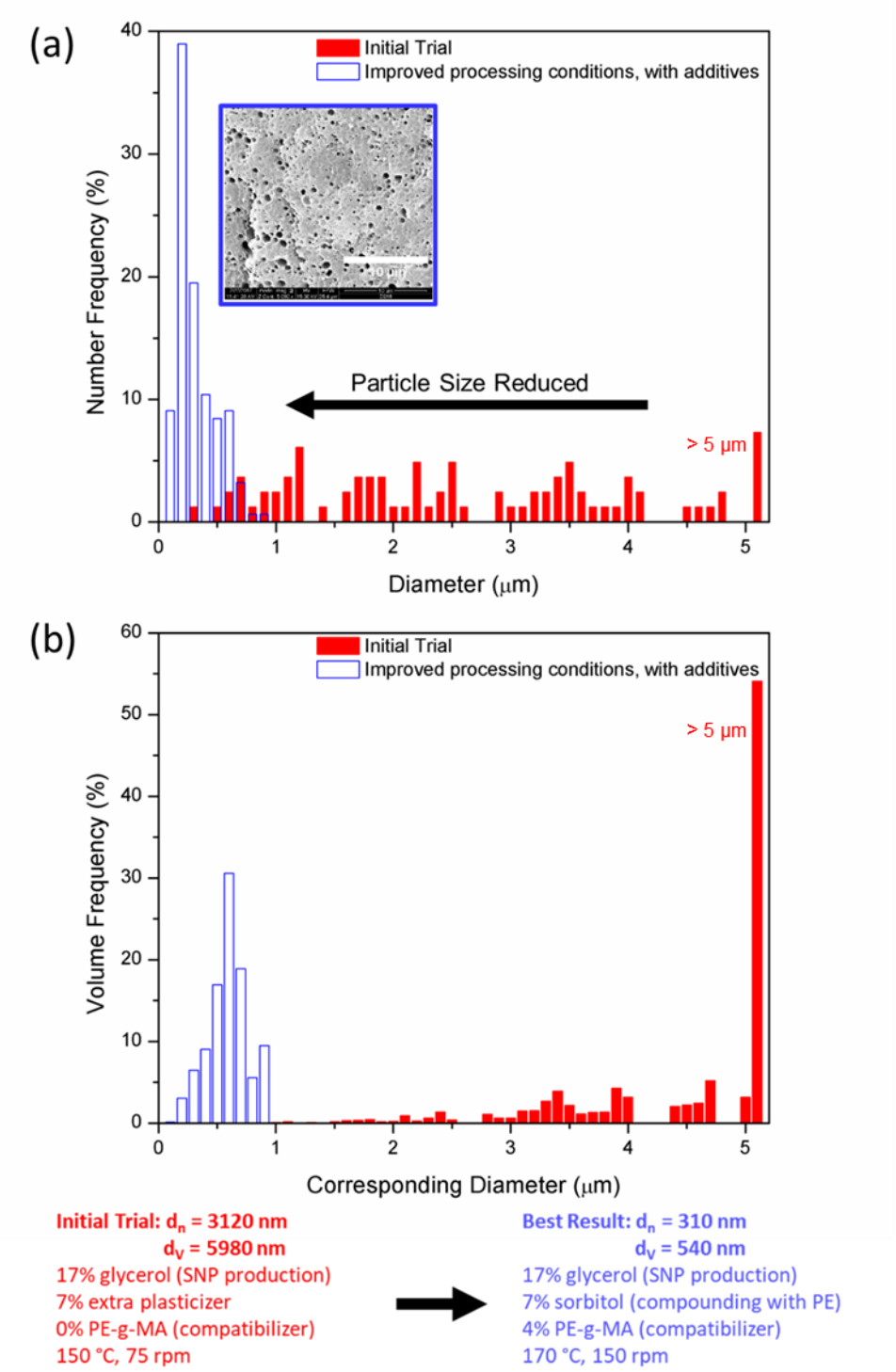

Figure 6.13 SNP filler particle size: (a) number distribution and (b) volume distribution

Chapter 7
Conclusions and Recommendations

7.1 Contributions and Summary

The objectives of this study were to investigate starch in two aspects: developing and processing environmentally friendly materials using starch as i) copolymer and ii) nano-filler. The newly developed thermoplastic starch copolymer resin by Polymer Specialties International is in the research and development stage and is not commercialized yet. This thesis represents the first study of this material. Another Canadian company, Ecosynthetix, has commercialized starch nano-particles for other applications (paper coating) but it has not been used as filler in polyethylene yet. This is also the first investigation where SNPs are used to produce a composite material.

This work addressed the lack of understanding on the preparation of thermoplastic starch copolymer to obtain competitive properties. A systematical approach was employed to reduce the starch filler particle size within a green polyethylene matrix, and nano-sized diameter with uniform distribution was achieved. The valuable accomplishment in this work would extend the range of properties of starch materials while maintaining environmental benefits and competitive physical properties for applications such as packaging and agriculture uses.

Chapter 2 reviewed background information along with relevant literature. The key role of this chapter was to help readers to understand basic concepts of renewable materials, starch, thermoplastic starch, chemical modifications and applications of these materials.

Chapter 3 described the materials and the methodology on processing and characterization of starch copolymer resin in detail. It also demonstrated the methods on esterification of starch and its characterization techniques.

Chapter 4 presented the results and discussion. It demonstrated the physical and chemical properties of starch copolymer resin. A comparison study on different starch esterification methods was presented as well.

Chapter 5 outlined materials and methods for the study of starch as nano-filler in the green LLDPE matrix. Preparation steps and characterization techniques were covered in this chapter.

Chapter 6 consisted of results and discussion on the study of LLDPE-starch nano-particle composites. The filler particle size and distribution were extensively studied using electron microscopy.

7.2 Main Conclusions

The first part of the research focused on characterizing a new thermoplastic starch (TPS) copolymer resin. The chemical composition of the material was determined via proton NMR. Information such as degree of branching was calculated based on the NMR spectra. The thermal gravimetric analysis revealed the thermal behaviour of the materials before and after processing. The effects of processing temperature on the material were also investigated.

Mechanical analysis including flexural, tensile and impact tests helped to define better processing conditions. Viscoelastic properties were also studied for the samples exposed to moisture and water. The resins were compounded with crystalline nanocellulose (CNC) via extrusion and injection molding, and their mechanical properties were compared. Overall, the composites' properties improved as the CNC loading increased due to the reinforcement effect.

After basic characterizations, a further investigation was executed to study the esterification of starch by maleic anhydride. This was an important step to understand the maleation process during the preparation of the material. The maleation process was done through three different systems: a reactive microwave reactor, a vacuum rotary evaporator, and a twin-screw extruder. In order to gain evidence for maleation, a series of analyses were conducted. Thermal degradation behaviour was monitored and compared with native starch and the results showed that the modified starches exhibited greater heat loss rates than the native one. The results from the gelatinization experiment indicated evidence of the weakening of intermolecular forces after the modification. FTIR and NMR analysis confirmed the maleated starch structure, and degrees of substitutions were calculated based on quantitative analysis of the spectroscopic data.

The second section of this work demonstrated the application of starch as nano-filler. Four starch nanoparticle (SNP) samples were analyzed by NMR to quantify the free glycerol content. These SNPs were compounded with green linear low-density polyethylene (LLDPE) and additives by using a twin-screw extruder. Although glycerol took a crucial role on reducing the particle size within the matrix, there was a critical point where the uniform

dispersion failed due to excessive glycerol content. A systematical approach was taken to study the effect of processing conditions and type of plasticizer/lubricant on the filler particle size. Furthermore, the effect of compatibilizer was investigated and a significant reduction in filler particle size was observed with a small increase of compatibilizer concentration. These experiments achieved an average SNP size as small as 310 nm within the LLDPE matrix. Finally, the author believes this research could be scaled up to the next level with economic and environmentally friendly aspects.

7.3 Recommendations

Based on the studies conducted in this thesis, a few recommendations for future investigations can be drawn.

Despite the results obtained via successful processing and characterization techniques, it would be beneficial to study a long-term ageing effect on properties. The thermal properties, structure, hydrophilicity and mechanical characteristics will change as starch ages and degrades over time. Since plausible applications utilizing starch materials will require certain lifetimes, monitoring long-term ageing, degradation and stability should provide valuable information. Ageing of starch-based materials can have different causes. Prolonged exposures to ultraviolet, high temperature, and different types of chemicals should be considered. An accelerated weathering test can be advantageous when designing the materials.

One of the target applications of the materials studied in this work was packaging films. Scaling up is an essential step to reach the product development for film applications. Studies

and efforts towards designing starch-based plastic materials should continue to pilot trials in order to meet manufacturing requirements. Considering there have been numerous research reported, there are very few studies found in the literature on pilot scale analysis and trials on starch-based plastic materials [93-95]. This will definitely bring the research one step closer to manufacturing valuable final products.

Bibliography

1. Mekonnen, T., et al., *Progress in bio-based plastics and plasticizing modifications.* Journal of Materials Chemistry A, 2013. **1**(43): p. 13379-13398.
2. Gourmelon, G., *Global Plastic Production Rises, Recycling Lags*. 2015, Worldwatch Institute.
3. Geyer, R., J.R. Jambeck, and K.L. Law, *Production, use, and fate of all plastics ever made.* Science Advances, 2017. **3**(7).
4. Reddy, M.M., M. Misra, and A.K. Mohanty, *Bio-based materials in the new bio-economy.* Chemical Engineering Progress, 2012. **108**(5): p. 37-42.
5. Wang, M., et al., *Progress in Toughening Poly(Lactic Acid) with Renewable Polymers.* Polymer Reviews, 2017. **57**(4): p. 557-593.
6. De Carvalho, A.J.F., A.A.S. Curvelo, and J.A.M. Agnelli, *A first insight on composites of thermoplastic starch and kaolin.* Carbohydrate Polymers, 2001. **45**(2): p. 189-194.
7. Huang, M.-F., J.-G. Yu, and X.-F. Ma, *Studies on the properties of Montmorillonite-reinforced thermoplastic starch composites.* Polymer, 2004. **45**(20): p. 7017-7023.
8. Sabetzadeh, M., R. Bagheri, and M. Masoomi, *Morphology and rheological properties of compatibilized low-density polyethylene/linear low-density polyethylene/thermoplastic starch blends.* Journal of Applied Polymer Science, 2017. **134**(16).
9. Gray, N., et al., *Influence of cellulose nanocrystal on strength and properties of low density polyethylene and thermoplastic starch composites.* Industrial Crops and Products, 2018. **115**: p. 298-305.
10. Raee, E. and B. Kaffashi, *Biodegradable polypropylene/thermoplastic starch nanocomposites incorporating halloysite nanotubes.* Journal of Applied Polymer Science, 2018. **135**(4).
11. Gáspár, M., et al., *Reducing water absorption in compostable starch-based plastics.* Polymer Degradation and Stability, 2005. **90**(3): p. 563-569.
12. Hablot, E., et al., *Reactive extrusion of glycerylated starch and starch–polyester graft copolymers.* European Polymer Journal, 2013. **49**(4): p. 873-881.
13. Zuo, Y., et al., *Study on the preparation of maleated thermoplastic starch by reactive extrusion.* Journal of Thermoplastic Composite Materials, 2014. **29**(3): p. 397-409.
14. Wolff, B. and G.M. Chapman, *Process for making starch-resin copolymer*, WIPO, Editor. 2013.
15. Gidley, M.J., *Quantification of the structural features of starch polysaccharides by n.m.r. spectroscopy.* Carbohydrate Research, 1985. **139**(C): p. 85-93.
16. Imberty, A., et al., *Recent Advances in Knowledge of Starch Structure.* Starch - Stärke, 1991. **43**(10): p. 375-384.
17. Jenkins, P.J. and A.M. Donald, *The influence of amylose on starch granule structure.* International Journal of Biological Macromolecules, 1995. **17**(6): p. 315-321.
18. Leloup, V.M., P. Colonna, and S.G. Ring, *Studies on Probe Diffusion and Accessibility in Amylose Gels.* Macromolecules, 1990. **23**(3): p. 862-866.

19. Fannon, J.E., R.J. Hauber, and J.N. BeMiller, *Surface pores of starch granules.* Cereal Chemistry, 1992. **69**(3): p. 284-288.
20. Da Róz, A.L., et al., *The effect of plasticizers on thermoplastic starch compositions obtained by melt processing.* Carbohydrate Polymers, 2006. **63**(3): p. 417-424.
21. Vergnes, B. and F. Berzin, *Modelling of flow and chemistry in twin screw extruders.* Plastics, Rubber and Composites, 2004. **33**(9-10): p. 409-415.
22. Kalambur, S. and S.S.H. Rizvi, *An overview of starch-based plastic blends from reactive extrusion.* Journal of Plastic Film and Sheeting, 2006. **22**(1): p. 39-58.
23. Xie, F., et al., *Starch modification using reactive extrusion.* Starch/Staerke, 2006. **58**(3-4): p. 131-139.
24. Chinnaswamy, R. and M.A. Hanna, *Extrusion-Grafting Starch Onto Vinylic Polymers.* Starch - Stärke, 1991. **43**(10): p. 396-402.
25. Camire, M.E., *Chemical changes during extrusion cooking: Recent Advances*, in *Advances in Experimental Medicine and Biology*. 1998, Springer New York LLC. p. 109-121.
26. Jarowenko, W., *Acetylated starch and miscellaneous organic Esters*, in *Modified Starches Properties and Uses*, O.B. Wurzburg, Editor. 1986, CRC Press. p. 55-78.
27. Shogren, R.L., *Rapid preparation of starch esters by high temperature/pressure reaction.* Carbohydrate Polymers, 2003. **52**(3): p. 319-326.
28. Raquez, J.M., et al., *In situ compatibilization of maleated thermoplastic starch/polyester melt-blends by reactive extrusion.* Polymer Engineering and Science, 2008. **48**(9): p. 1747-1754.
29. Raquez, J.-M., et al., *Maleated thermoplastic starch by reactive extrusion.* Carbohydrate Polymers, 2008. **74**(2): p. 159-169.
30. Narayan, R., J. Stagner, and V. Dias Alves, *Biodegradable thermoplasticized starch-polyester reactive blends for thermoforming applications*, WIPO, Editor. 2009.
31. González Seligra, P., et al., *Influence of incorporation of starch nanoparticles in PBAT/TPS composite films.* Polymer International, 2016. **65**(8): p. 938-945.
32. Lendvai, L., A. Apostolov, and J. Karger-Kocsis, *Characterization of layered silicate-reinforced blends of thermoplastic starch (TPS) and poly(butylene adipate-co-terephthalate).* Carbohydrate Polymers, 2017. **173**: p. 566-572.
33. Reis, M.O., et al., *Influence of microcrystalline cellulose in thermoplastic starch/polyester blown films.* Polímeros, 2017. **27**(2): p. 129-135.
34. Zhang, J.F. and X. Sun, *Mechanical properties of poly(lactic acid)/starch composites compatibilized by maleic anhydride.* Biomacromolecules, 2004. **5**(4): p. 1446-1451.
35. Sun, Z., W. Liu, and Y.J. Wang, *Biodegradable Materials from Starch-Grafted Polymers*, U.S. Patent, Editor. 2009.
36. Wang, N., J. Yu, and X. Ma, *Preparation and characterization of thermoplastic starch/PLA blends by one-step reactive extrusion.* Polymer International, 2007. **56**(11): p. 1440-1447.
37. Shujun, W., Y. Jiugao, and Y. Jinglin, *Preparation and characterization of compatible thermoplastic starch/polyethylene blends.* Polymer Degradation and Stability, 2005. **87**(3): p. 395-401.

38. Stagner, J., et al., *Thermoplasticization of High Amylose Starch by Chemical Modification Using Reactive Extrusion.* Journal of Polymers and the Environment, 2011. **19**(3): p. 589-597.
39. McGlashan, S.A. and P.J. Halley, *Preparation and characterisation of biodegradable starch-based nanocomposite materials.* Polymer International, 2003. **52**(11): p. 1767-1773.
40. Cheng, J., et al., *The composites based on plasticized starch and carbon nanotubes.* International Journal of Biological Macromolecules, 2013. **59**: p. 13-19.
41. Peng, B.L., et al., *Chemistry and applications of nanocrystalline cellulose and its derivatives: A nanotechnology perspective.* Canadian Journal of Chemical Engineering, 2011. **89**(5): p. 1191-1206.
42. (NRC), N.R.C., *Nanocrystalline Cellulose (NCC) technology*. 2013, Natural Resource Canada (NRC).
43. Siqueira, G., J. Bras, and A. Dufresne, *Cellulosic bionanocomposites: A review of preparation, properties and applications.* Polymers, 2010. **2**(4): p. 728-765.
44. Muthuraj, R., M. Misra, and A.K. Mohanty, *Biodegradable compatibilized polymer blends for packaging applications: A literature review.* Journal of Applied Polymer Science, 2018. **135**(24).
45. Li, Z. and F. Zhao, *An analytical hierarchy process-based study on the factors affecting legislation on plastic bags in the USA.* Waste Management & Research, 2017. **35**(8): p. 795-809.
46. Thompson, A.A., et al., *Degradation Rate of Bio-based Agricultural Mulch is Influenced by Mulch Composition and Biostimulant Application.* Journal of Polymers and the Environment, 2019. **27**(3): p. 498-509.
47. Brodhagen, M., et al., *Biodegradable plastic agricultural mulches and key features of microbial degradation.* Applied Microbiology and Biotechnology, 2015. **99**(3): p. 1039-56.
48. Wortman, S.E., I. Kadoma, and M.D. Crandall, *Assessing the potential for spunbond, nonwoven biodegradable fabric as mulches for tomato and bell pepper crops.* Scientia Horticulturae, 2015. **193**: p. 209-217.
49. Miles, C., et al., *Deterioration of potentially biodegradable alternatives to black plastic mulch in three tomato production regions.* HortScience, 2012. **47**(9): p. 1270-1277.
50. Hernandez, R.J., *Plastics in Packaging*, in *Handbook of Plastics, Elastomers, and Composites*. 2004, McGraw-Hill. p. 627-692.
51. Morschbacker, A., *Bio-ethanol based ethylene.* Polymer Reviews, 2009. **49**(2): p. 79-84.
52. Echlin, P., *Handbook of Sample Preparation for Scanning Electron Microscopy and X-Ray Microanalysis*. 2009: Springer.
53. Amelinckx, S., et al., *Electron Microscopy: Principles and Fundamentals*. 2008: VCH.
54. International, A., *ASTM D790 Standard Test Methods for Flexural Properties of Unreinforced and Reinforced Plastics and Electrical Insulating Materials*. 2010.

55. Haupert, F. and B. Wetzel, *Reinforcement of Thermosetting Polymers by the Incorporation of Micro- and Nanoparticles*, in *Polymer Composites*. 2005, Springer. p. 45-62.
56. Leong, Y.W., et al., *Comparison of the Mechanical Properties and Interfacial Interactions Between Talc, Kaolin, and Calcium Carbonate Filled Polypropylene Composites.* Journal of Applied Polymer Science, 2004. **91**(5): p. 3315-3326.
57. International, A., *ASTM D1708 Standard Test Method for Tensile Properties of Plastics by Use of Microtensile Specimens*. 2010.
58. Ward, I.M. and J. Sweeney, *Mechanical Properties of Solid Polymers*. 2012: Wiley.
59. Standard, A., *ASTM D256 Standard Test Methods for Determining the IZOD Pendulum Impact Resistance of Plastics*. 2010.
60. International, A., *ASTM D5420 Standard Test Method for Impact Resistance of Flat Rigid Plastic Specimen by Means of a Striker Impacted by a Falling Weight (Gardner Impact)*. 2010.
61. Beauvalet, M., *Application of Cellulose Nanomaterials in Thermoplastic Composites*, in *Chemical Engineering*. 2016, University of Waterloo: Waterloo, ON, Canada.
62. Tizzotti, M.J., et al., *New (1)h NMR procedure for the characterization of native and modified food-grade starches.* Journal of Agricultural Food Chemistry, 2011. **59**(13): p. 6913-9.
63. Nilsson, G.S., et al., *Determination of the degree of branching in normal and amylopectin type potato starch with 1H-NMR spectroscopy: Improved resolution and two-dimensional spectroscopy.* Starch/Staerke, 1996. **48**(10): p. 352-357.
64. Praznik, W., H. Schillinger, and R.H.F. Beck, *Changes in the Molecular Composition of Maize Starch During Kernel Development.* Starch - Stärke, 1987. **39**(6): p. 183-187.
65. Olivato, J.B., et al., *Elaboration, morphology and properties of starch/polyester nano-biocomposites based on sepiolite clay.* Carbohydrate Polymers, 2015. **118**: p. 250-6.
66. Nayak, S.K., *Biodegradable PBAT/Starch Nanocomposites.* Polymer-Plastics Technology and Engineering, 2010. **49**(14): p. 1406-1418.
67. Aggarwal, P. and D. Dollimore, *The combustion of starch, cellulose and cationically modified products of these compounds investigated using thermal analysis.* Thermochimica Acta, 1997. **291**(1-2): p. 65-72.
68. Teramoto, N., et al., *Synthesis, thermal properties, and biodegradability of propyl-etherified starch.* European Polymer Journal, 2003. **39**(2): p. 255-261.
69. Liu, X., et al., *Thermal degradation and stability of starch under different processing conditions.* Starch/Staerke, 2013. **65**(1-2): p. 48-60.
70. Soliman, A.A.A., N.A. El-Shinnawy, and F. Mobarak, *Thermal behaviour of starch and oxidized starch.* Thermochimica Acta, 1997. **296**(1-2): p. 149-153.
71. Soares, R.M.D., et al., *Thermal degradation of biodegradable edible films based on xanthan and starches from different sources.* Polymer Degradation and Stability, 2005. **90**(3): p. 449-454.
72. Vasques, C.T., et al., *Effect of thermal treatment on the stability and structure of maize starch cast films.* Starch/Staerke, 2007. **59**(3-4): p. 161-170.

73. Muniyasamy, S., et al., *Biodegradable green composites from bioethanol co-product and poly(butylene adipate-co-terephthalate).* Industrial Crops and Products, 2013. **43**(1): p. 812-819.
74. Lekube, B.M., et al., *Influence of processing on the mechanical properties and morphology of starch-based blends for film applications.* Journal of Applied Polymer Science, 2019. **136**(39).
75. Forssell, P.M., et al., *Phase and glass transition behaviour of concentrated barley starch-glycerol-water mixtures, a model for thermoplastic starch.* Carbohydrate Polymers, 1998. **34**(4): p. 275-282.
76. Marten, E., R.-J. Müller, and W.-D. Deckwer, *Studies on the enzymatic hydrolysis of polyesters. II. Aliphatic–aromatic copolyesters.* Polymer Degradation and Stability, 2005. **88**(3): p. 371-381.
77. Mitrus, M., *Glass transition temperature of thermoplastic starches.* International Agrophysics, 2005. **19**(3): p. 237-241.
78. De Graaf, R.A., A.P. Karman, and L.P.B.M. Janssen, *Material properties and glass transition temperatures of different thermoplastic starches after extrusion processing.* Starch/Staerke, 2003. **55**(2): p. 80-86.
79. Ureña-Benavides, E.E. and C.L. Kitchens, *Wide-angle X-ray diffraction of cellulose nanocrystal-alginate nanocomposite fibers.* Macromolecules, 2011. **44**(9): p. 3478-3484.
80. Meesorn, W., J.O. Zoppe, and C. Weder, *Stiffness-Changing of Polymer Nanocomposites with Cellulose Nanocrystals and Polymeric Dispersant.* Macromolecular Rapid Communications, 2019. **40**(9).
81. Dufresne, A., *Nanocellulose: a new ageless bionanomaterial.* Materials Today, 2013. **16**(6): p. 220-227.
82. Khan, A., et al., *Optimization of microfluidization for the homogeneous distribution of cellulose nanocrystals (CNCs) in biopolymeric matrix.* Cellulose, 2014. **21**(5): p. 3457-3468.
83. Warren, F.J., M.J. Gidley, and B.M. Flanagan, *Infrared spectroscopy as a tool to characterise starch ordered structure--a joint FTIR-ATR, NMR, XRD and DSC study.* Carbohydrate Polymers, 2016. **139**: p. 35-42.
84. Wildi, R.H., E. Van Egdom, and S. Bloembergen, *PROCESS FOR PRODUCING BIOPOLYMER NANOPARTICLES*, U.S. Patent, Editor. 2017: U.S.
85. Khan, I., *Hybrid Biocomposites with Starch Derived Nanoparticles and Cellulose Fibers*, in *Chemical Engineering*. 2017, University of Waterloo: Waterloo, ON, Canada.
86. Sailaja, R.R.N. and M. Chanda, *Use of poly(ethylene-co-vinyl alcohol) as compatibilizer in LDPE/thermoplastic tapioca starch blends.* Journal of Applied Polymer Science, 2002. **86**(12): p. 3126-3134.
87. Wei, D., et al., *Morphology and mechanical properties of poly(butylene adipate-co-terephthalate)/potato starch blends in the presence of synthesized reactive compatibilizer or modified poly(butylene adipate-co-terephthalate).* Carbohydrate Polymers, 2015. **123**: p. 275-282.

88. Yatigala, N.S., D.S. Bajwa, and S.G. Bajwa, *Compatibilization improves physico-mechanical properties of biodegradable biobased polymer composites.* Composites Part A: Applied Science and Manufacturing, 2018. **107**: p. 315-325.
89. Kyrikou, I. and D. Briassoulis, *Biodegradation of agricultural plastic films: A critical review.* Journal of Polymers and the Environment, 2007. **15**(2): p. 125-150.
90. Taguet, A., M.A. Huneault, and B.D. Favis, *Interface/morphology relationships in polymer blends with thermoplastic starch.* Polymer, 2009. **50**(24): p. 5733-5743.
91. Bikiaris, D. and C. Panayiotou, *LDPE/starch blends compatibilized with PE-g-MA copolymers.* Journal of Applied Polymer Science, 1998. **70**(8): p. 1503-1521.
92. Taghizadeh, A., P. Sarazin, and B.D. Favis, *High molecular weight plasticizers in thermoplastic starch/polyethylene blends.* Journal of Materials Science, 2013. **48**(4): p. 1799-1811.
93. Guzman, A., et al., *Pilot study of the influence of thermoplastic starch based polymer packaging material on the growth of diatom population in sea water environment.* Polish Journal of Chemical Technology, 2011. **13**(2): p. 57-61.
94. Thongtan, R. and K. Sriroth, *Physical properties of thermoplastic cassava starches extruded from commercial modified derivatives in a pilot scale*, in *2011 International Conference on Applied Mechanics, Materials and Manufacturing, ICAMMM 2011*. 2012: Shenzhen. p. 1007-1013.
95. Olsson, E., et al., *Montmorillonite for starch-based barrier dispersion coating - Part 2: Pilot trials and PE-lamination.* Applied Clay Science, 2014. **97-98**: p. 167-173.

Appendix

TGA thermograms on TPS copolymer resin

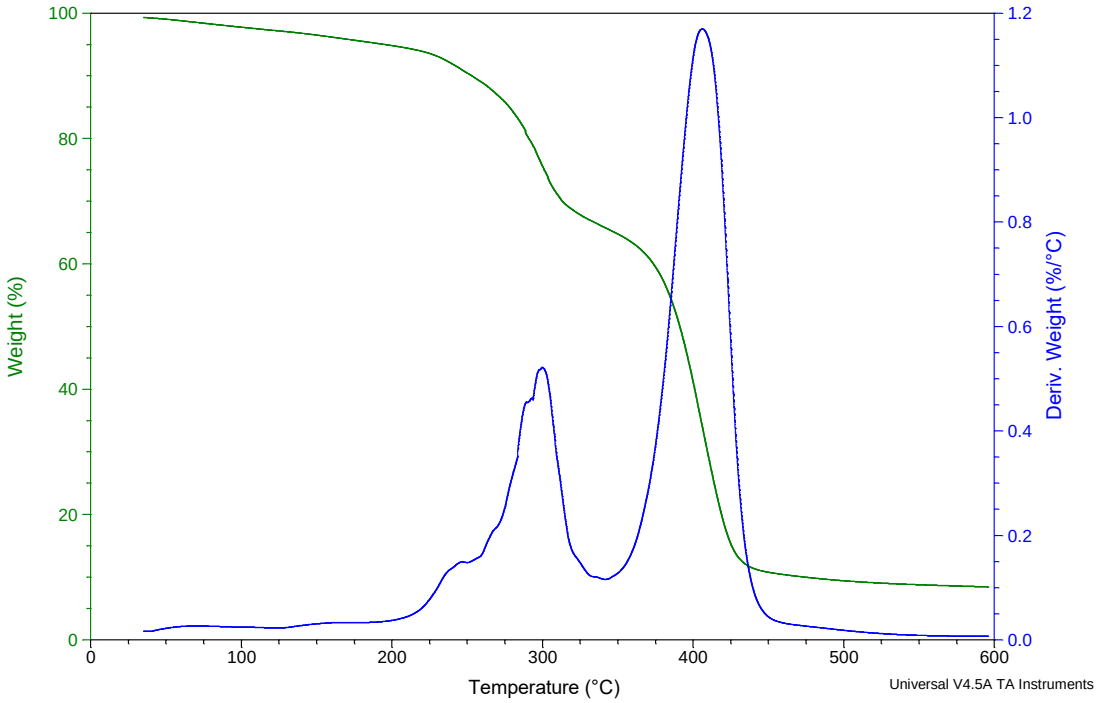

Figure 0.1 TGA: weight loss and DTG on TPS copolymer resin prior to processing

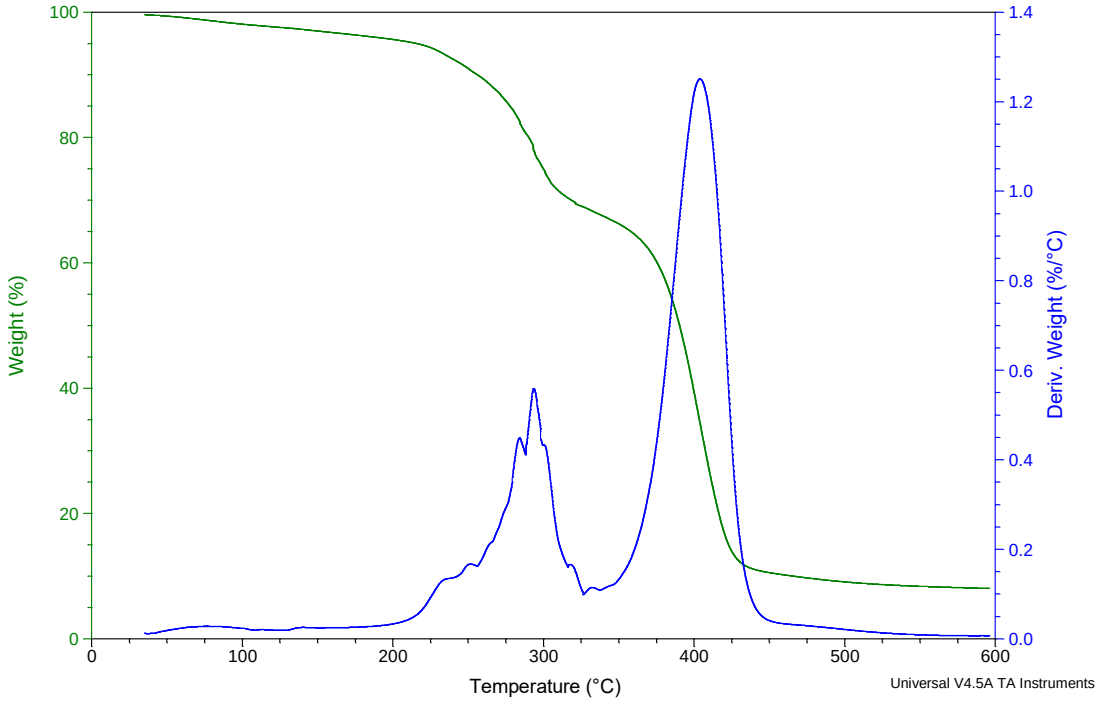

Figure 0.2 TGA: weight loss and DTG on TPS copolymer resin processed at 150 °C

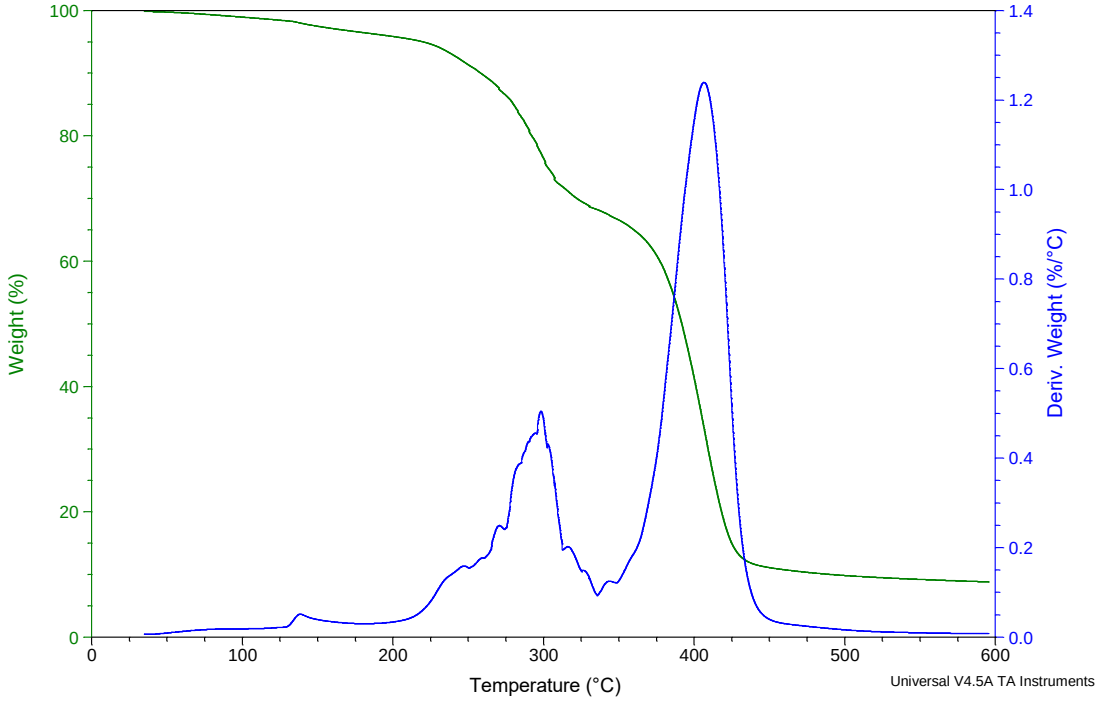

Figure 0.3 TGA: weight loss and DTG on TPS copolymer resin processed at 155 °C

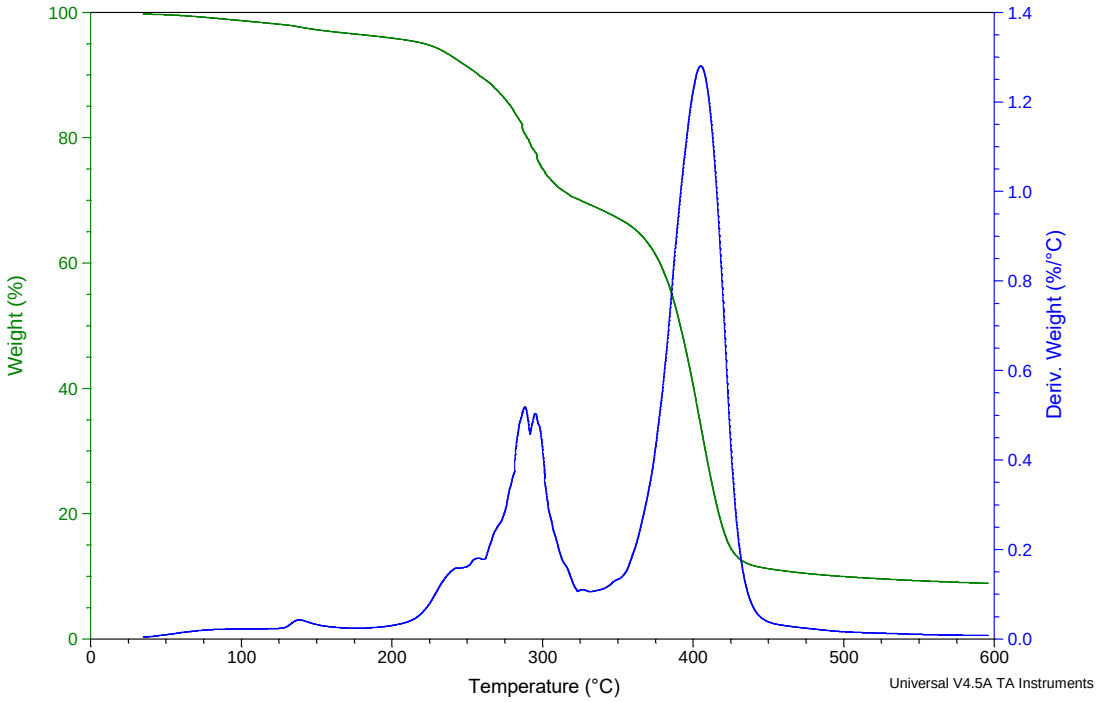

Figure 0.4 TGA: weight loss and DTG on TPS copolymer resin processed at 165 °C

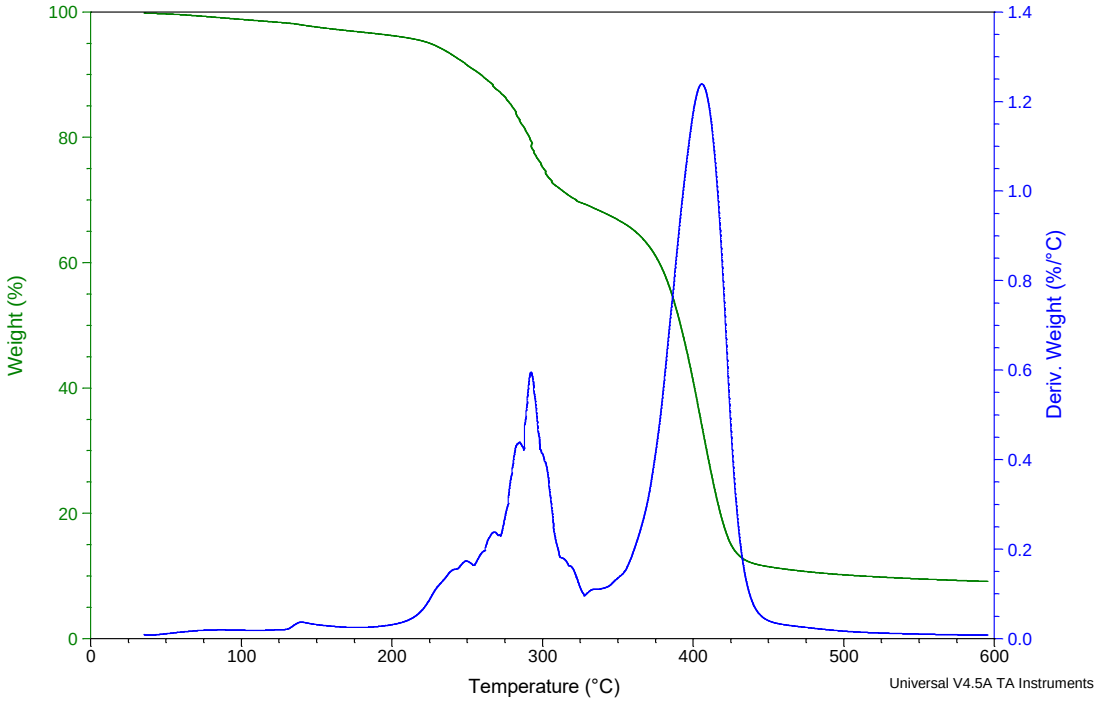

Figure 0.5 TGA: weight loss and DTG on TPS copolymer resin processed at 175 °C

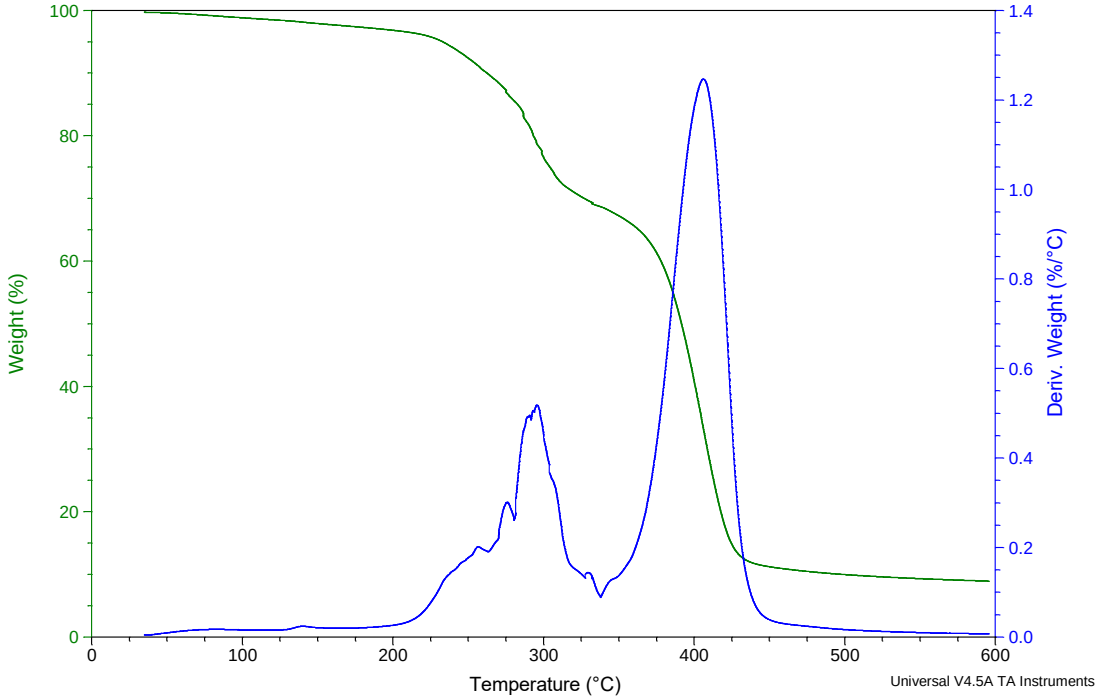

Figure 0.6 TGA: weight loss and DTG on TPS copolymer resin processed at 185 °C

Maleation of starch

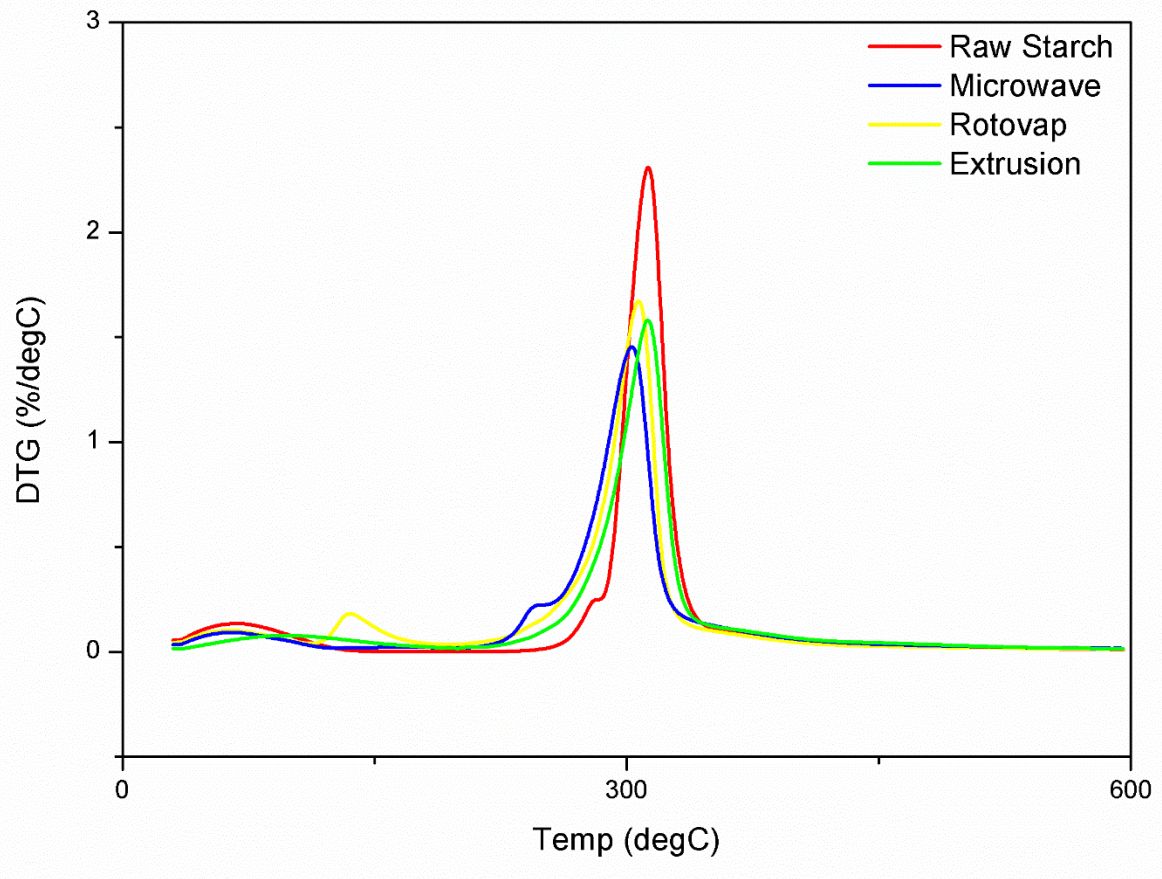

Figure 0.7 DTG curves of unmodified (raw) starch and modified starches

Quantification of free glycerol in SNP

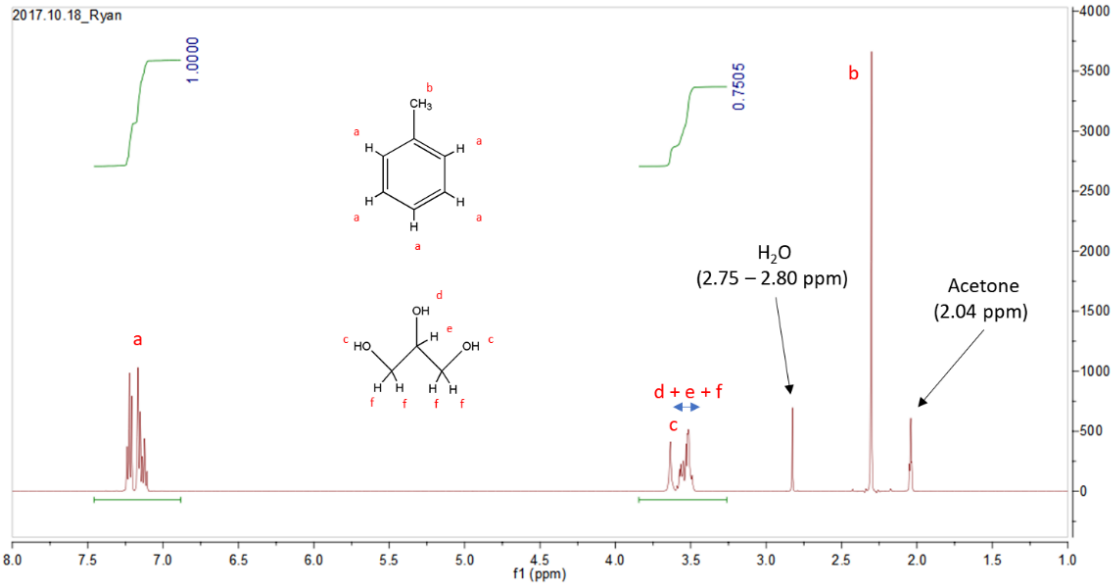

Figure 0.8 ^{1}H NMR: Toluene + Glycerol in Acetone

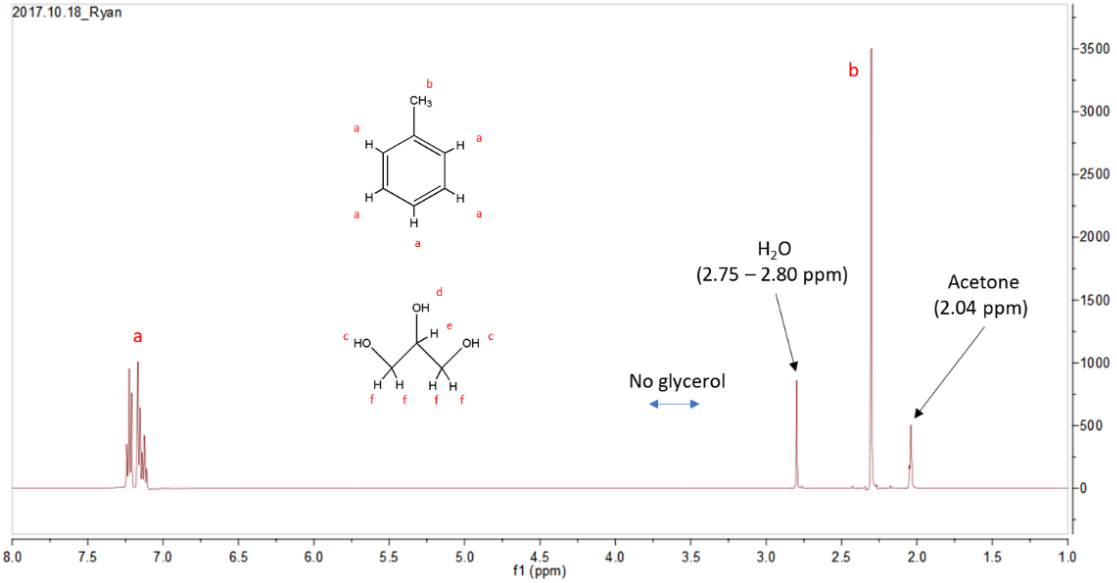

Figure 0.9 ^{1}H NMR: SNP (0 % glycerol) + Toluene in Acetone

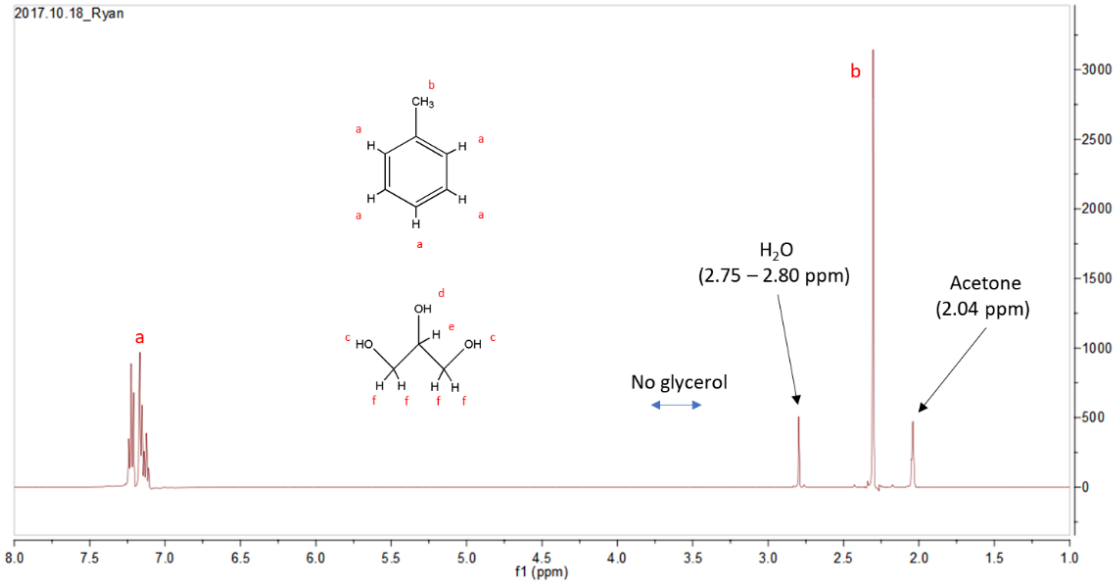

Figure 0.10 ^{1}H NMR: SNP (9 % glycerol) + Toluene in Acetone

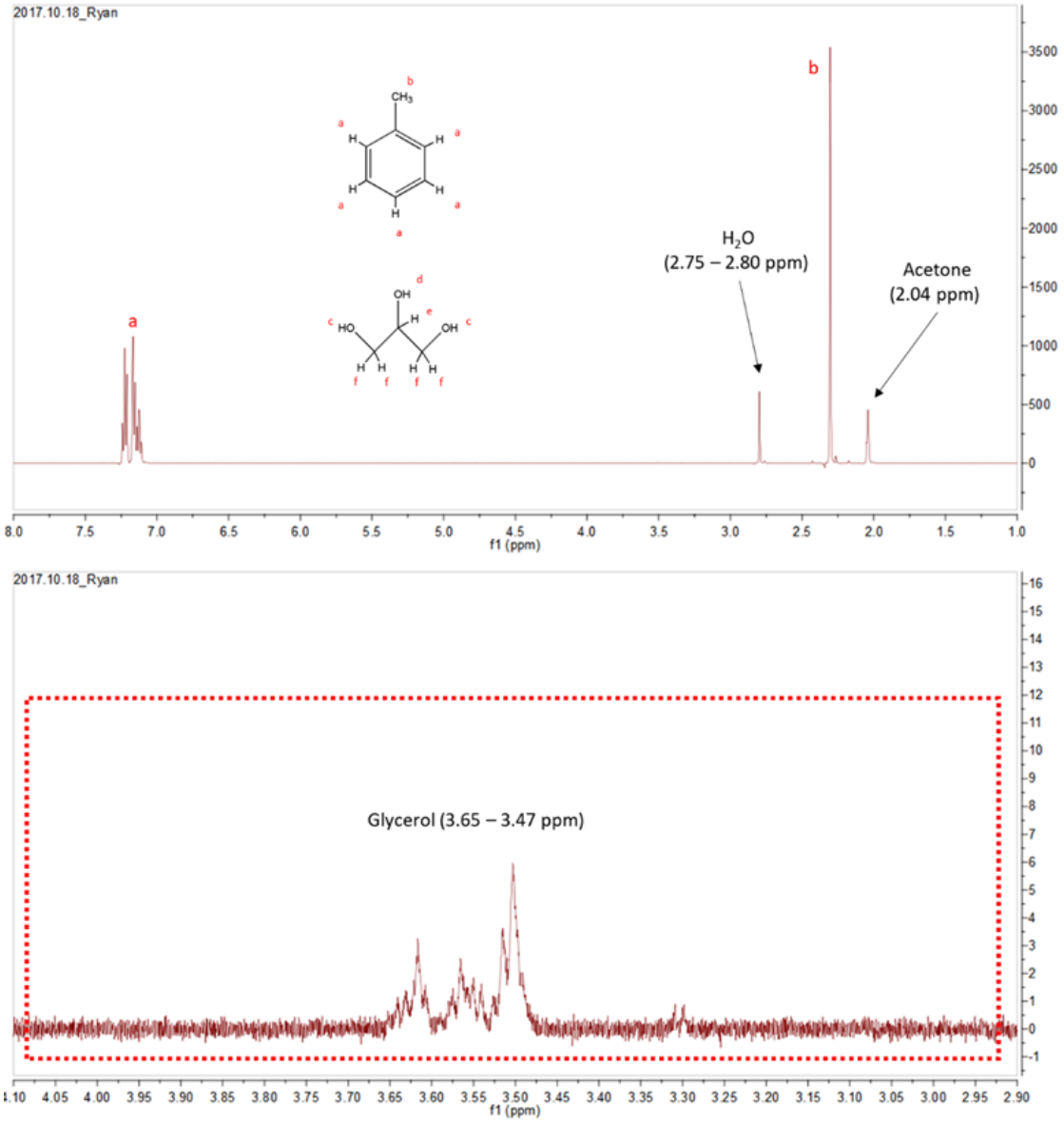

Figure 0.11 ^{1}H NMR: SNP (17 % glycerol) + Toluene in Acetone

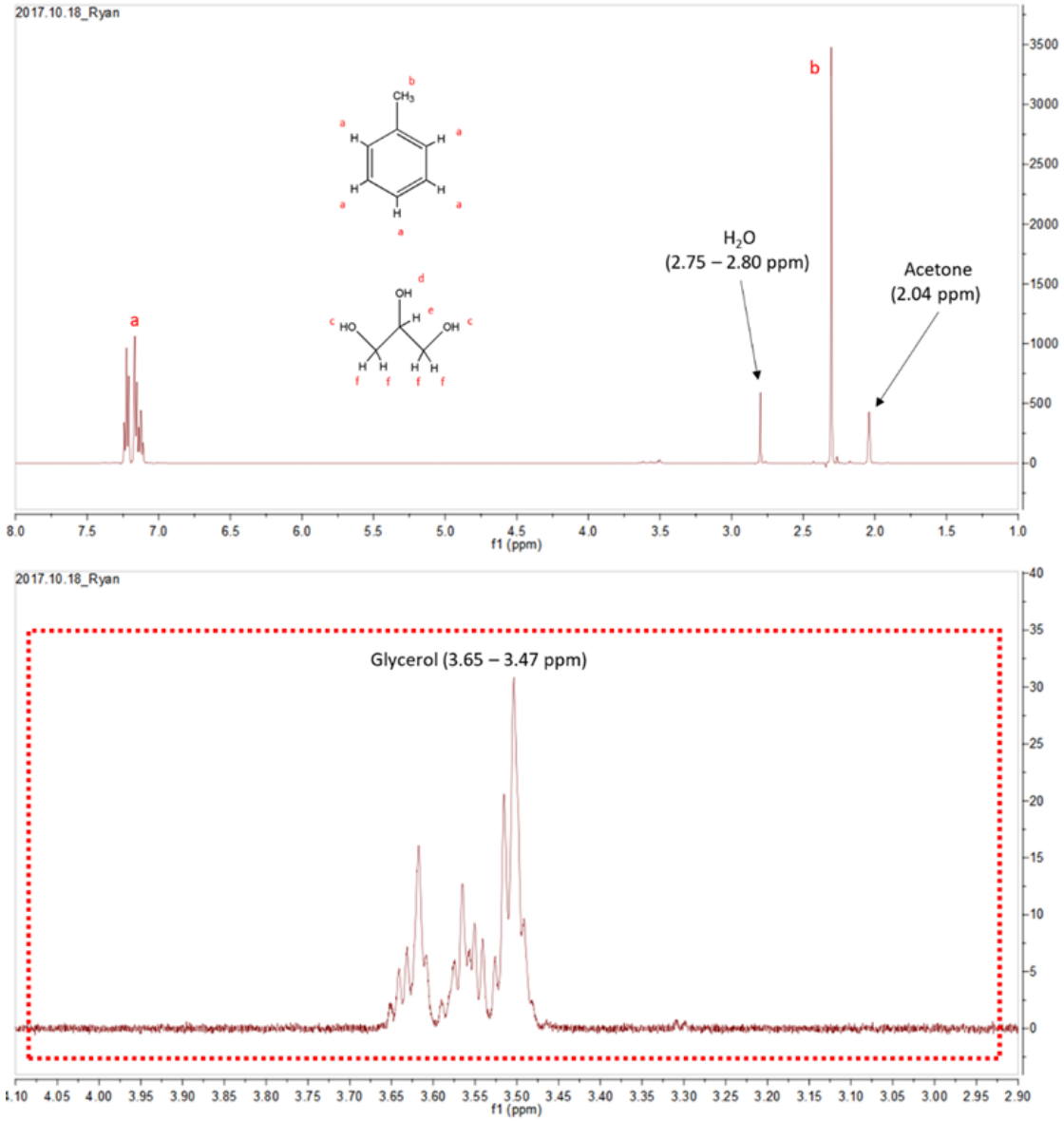

Figure 0.12 ^{1}H NMR: SNP (24 % glycerol) + Toluene in Acetone

SNP-LLDPE composites

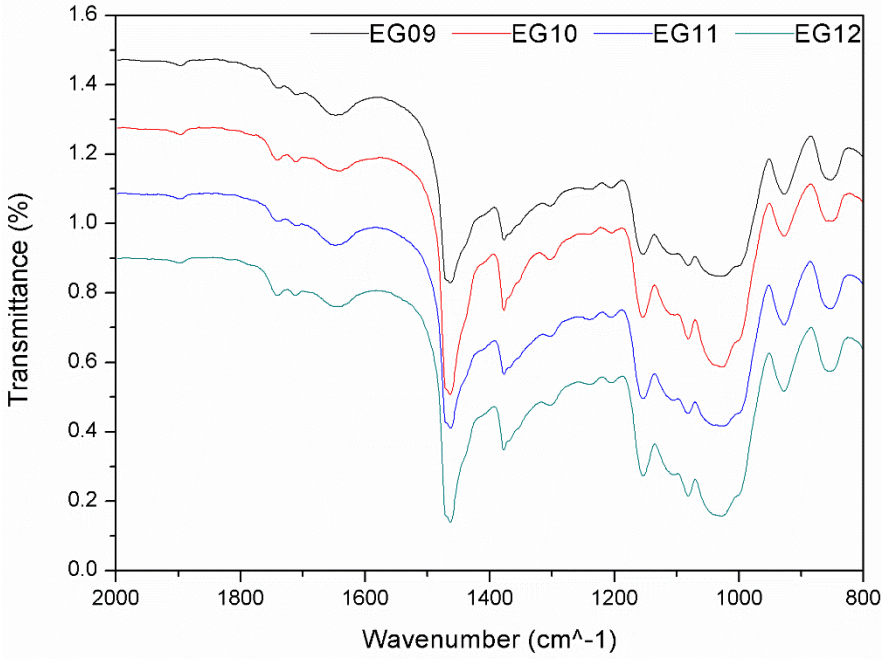

Figure 0.13 FTIR spectra of SNP-LLDPE composites (refer to Table 5.2)

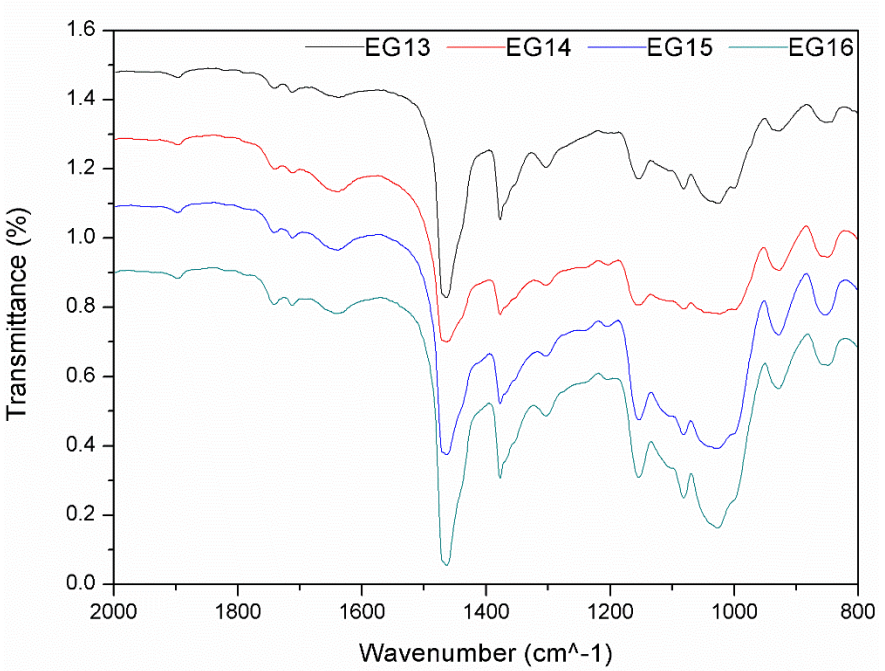

Figure 0.14 FTIR spectra of SNP-LLDPE composites (refer to Table 5.2)

*SNP filler particle size distributions (*Figure 0.15 *through* Figure 0.26*)*

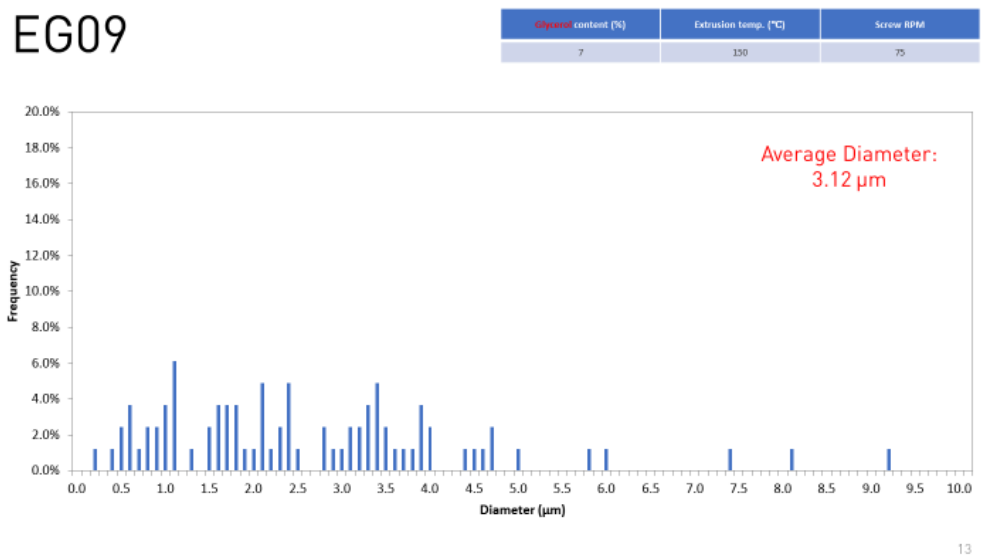

Figure 0.15

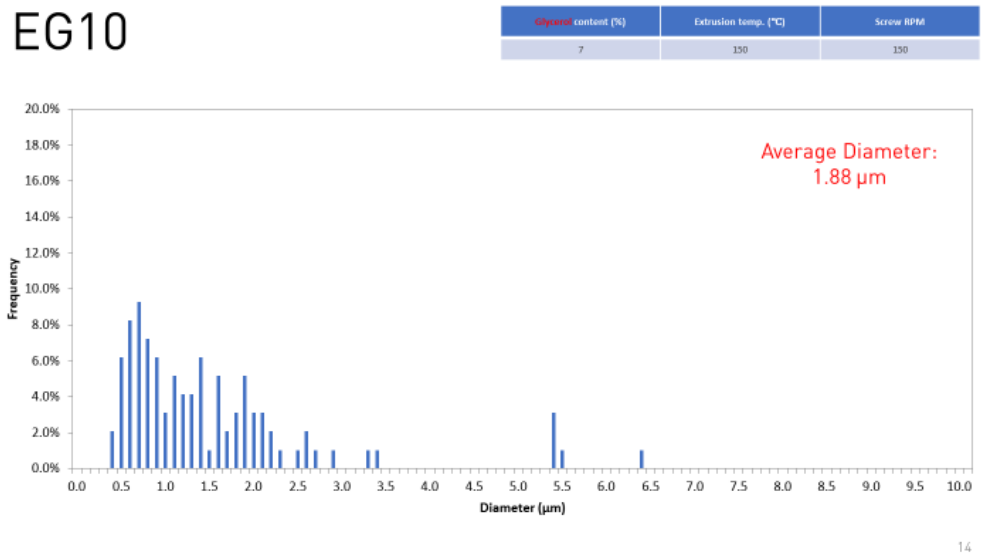

Figure 0.16

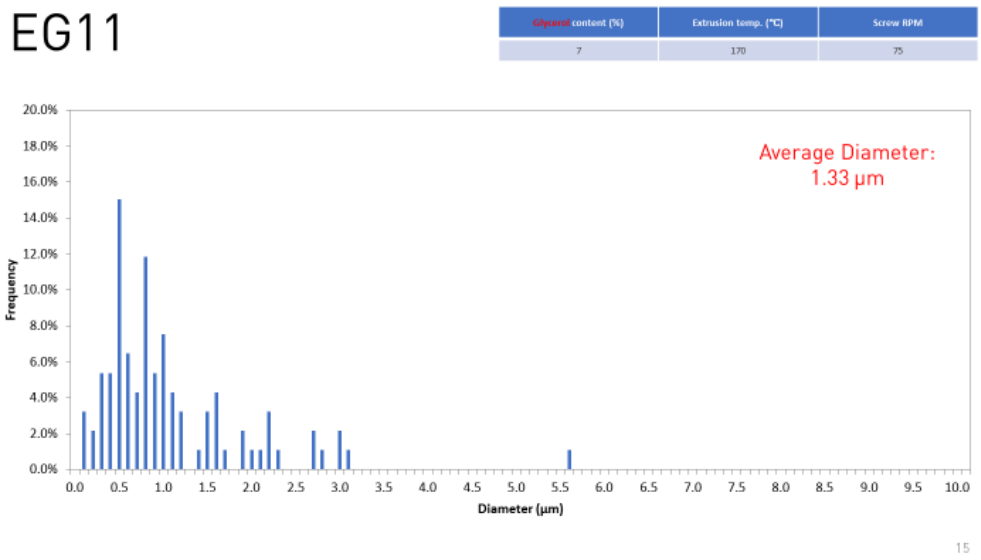

Figure 0.17

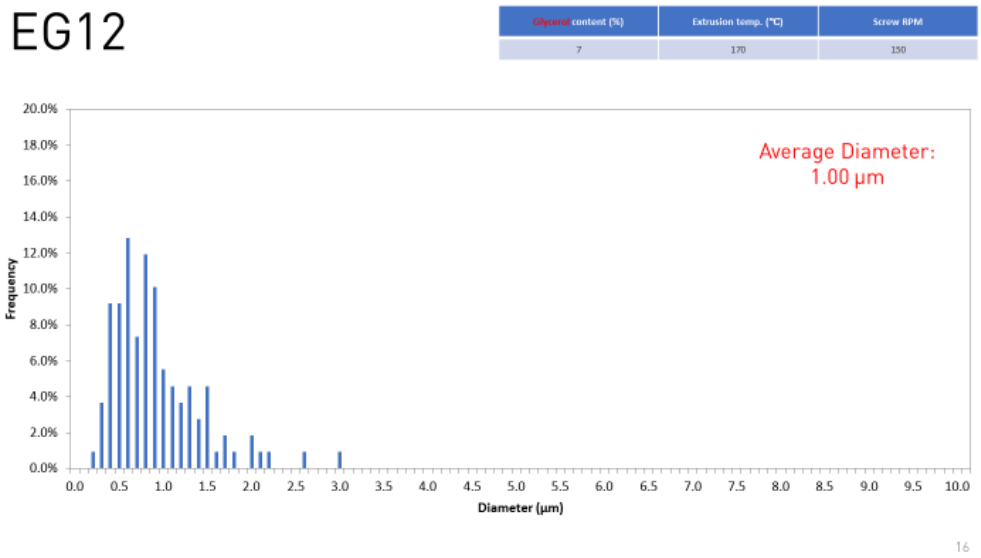

Figure 0.18

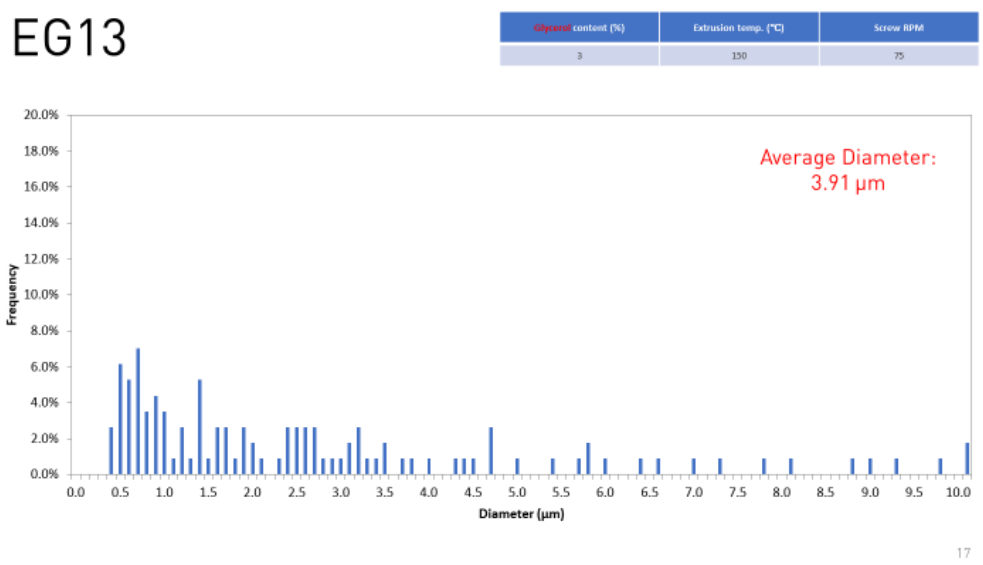

Figure 0.19

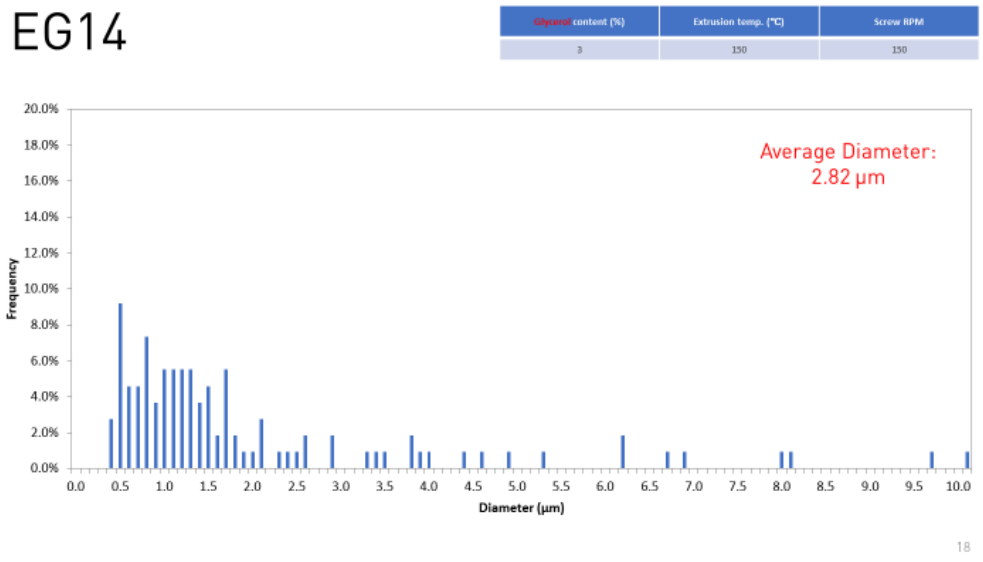

Figure 0.20

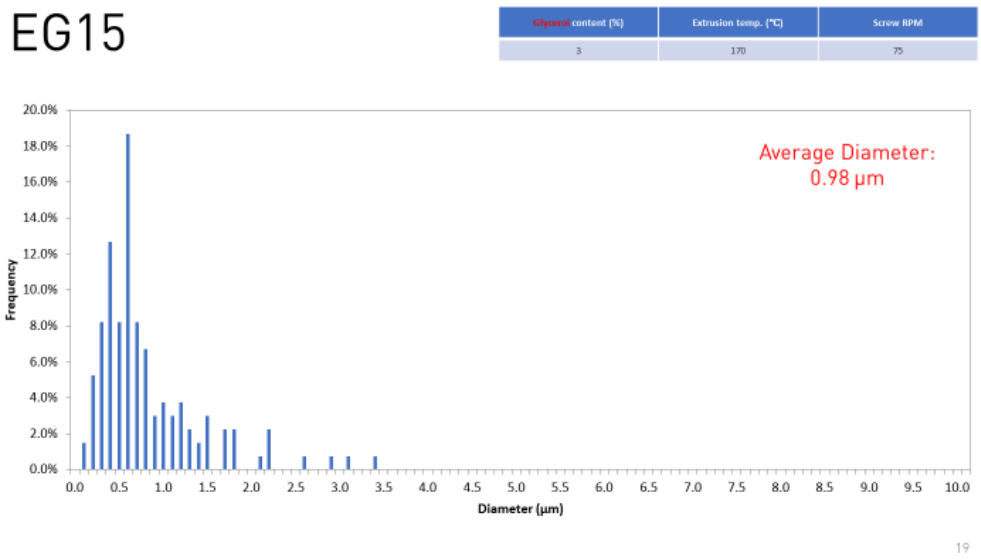

Figure 0.21

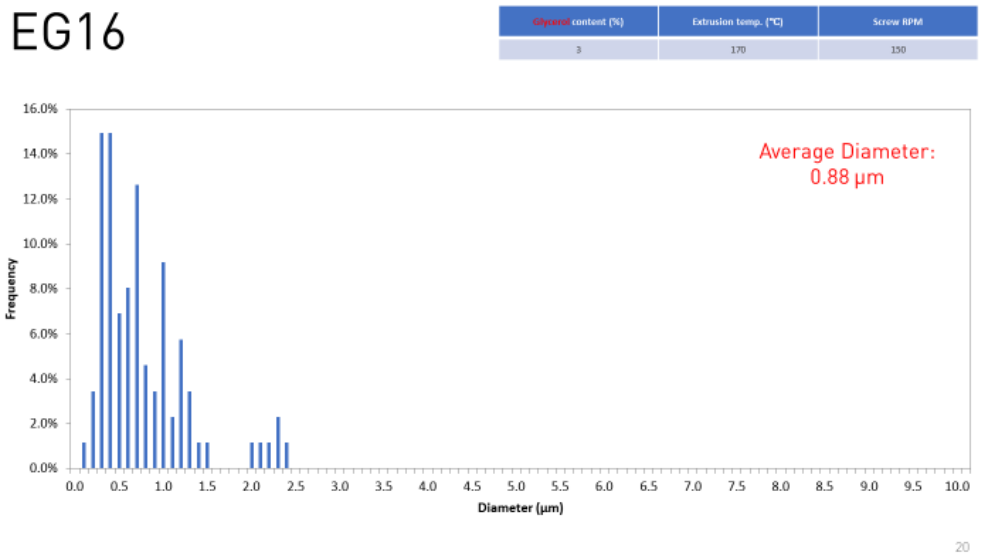

Figure 0.22

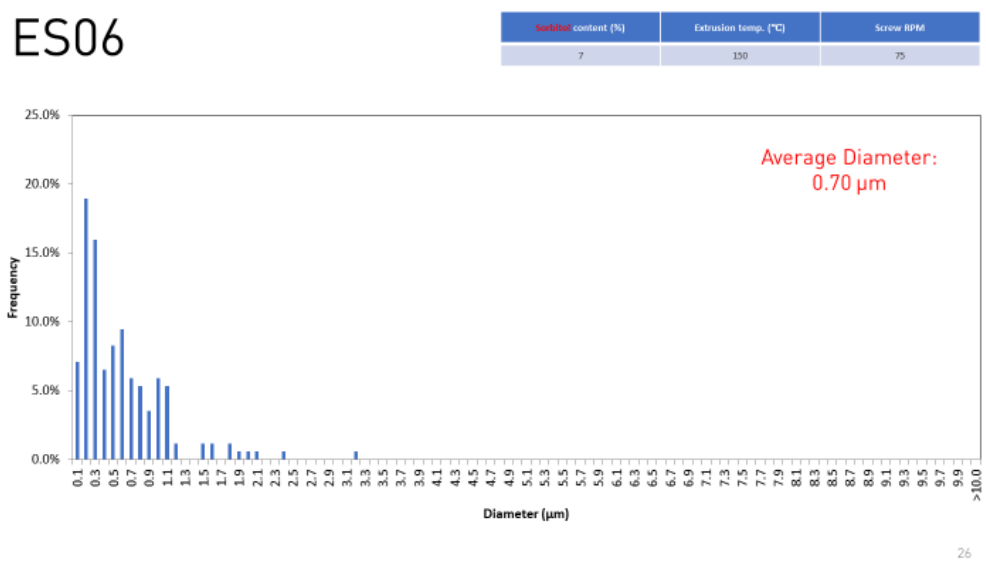

Figure 0.23

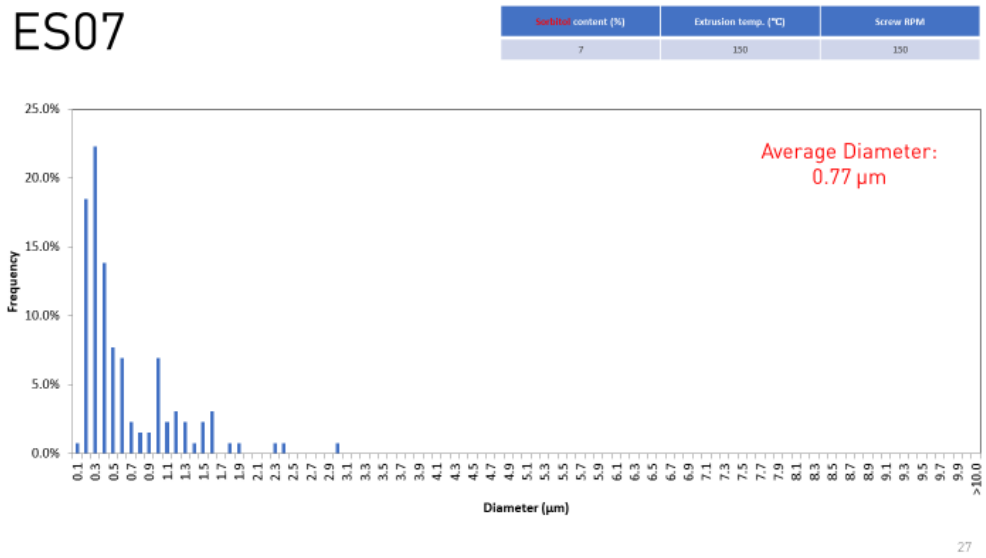

Figure 0.24

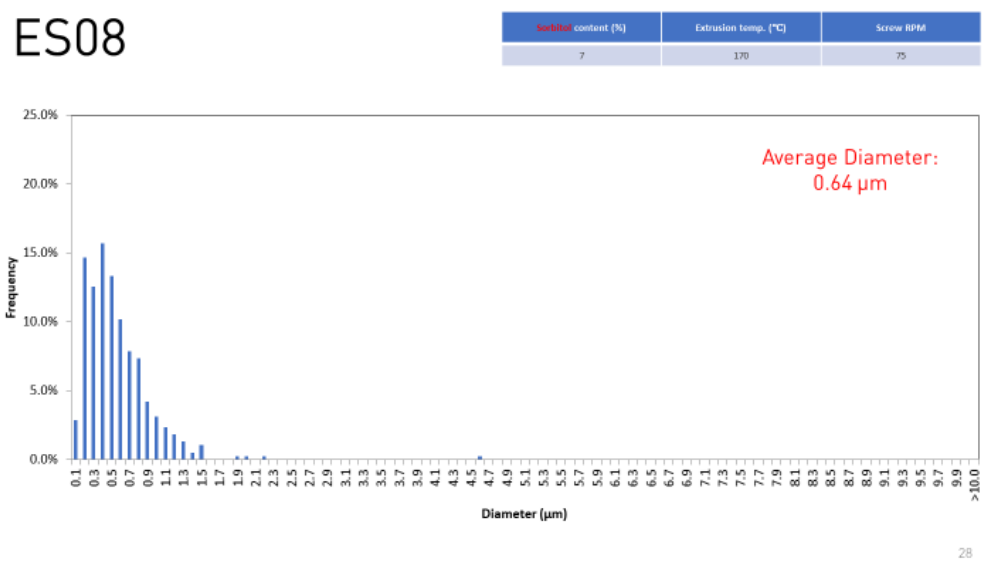

Figure 0.25

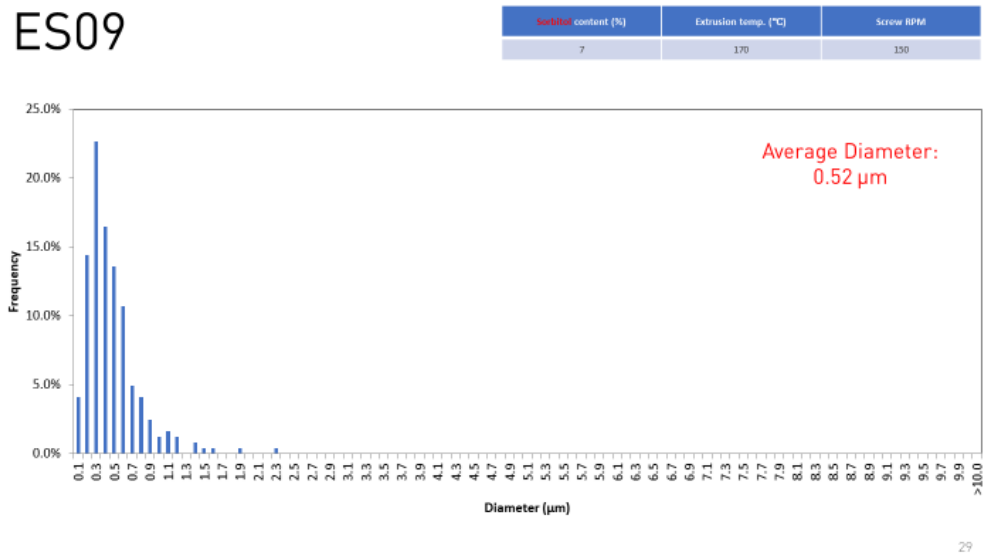

Figure 0.26

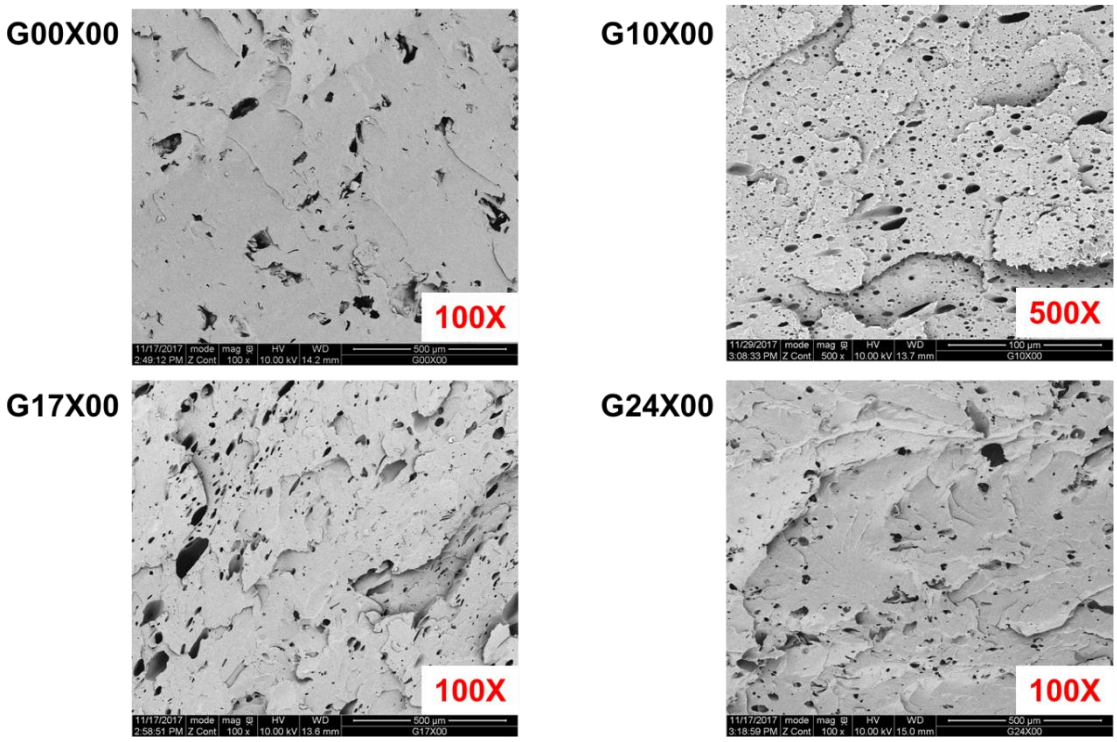

Figure 0.27 SEM images of SNP-LLDPE composites with various original glycerol concentration added in SNP

AIB-VINÇOTTE International s.a. / n.v.
SAFETY, QUALITY, ENVIRONMENT
Member of the Group AIB-VINÇOTTE
Head office : Boulevard A. Reyers 80 - B-1030 Brussels / Belgium

VINÇOTTE - CERTEST PRODUCTS
Everest - Leuvensesteenweg 248 / B-1800 Vilvoorde / Belgium
Tel. : +32(0)2 674.57.50 - Fax : +32(0)2 674.57.85
E-Mail : okbiobased@vincotte.be

OK biobased VINÇOTTE

CERTIFICATE FOR AWARDING AND USE OF THE 'OK BIOBASED' CONFORMITY MARK

No. B 11-082-A

Issued by AIB-VINÇOTTE International

For the product(s) described hereafter :

Product Domain :	Biobased Products
Product Group :	Raw material
Product Family :	Bio material
Product Type :	Granulates
Trade mark :	I'm green™
Product description / Particularities :	HDPE grades : SGF 4950, SGF4960, SHA7260, SHC7260, SHB7255LSL, SHE150, SGM9450F Color : natural translucent
Class (between 1 & 4):	The product is assigned to class 4, meaning: 80 % ≤ Biobased Carbon Content of the product ≤ 100 % ★★★★
Conformity examination applied for by :	**BRASKEM SA** **Centro Prod. PP/PE Triunfo** **BR 386 – Rodovia Tabaí-Canoas, lote 04, 850** **Triunfo – RS – CEP 95853-000** **Brazil**
Criteria for certification :	• AVI Test Program 'OK biobased' with reference OK 20 edition A • Methodology conform to ASTM D 6866 "Standard Test Methods for Determining the Biobased Content of Solid, Liquid, and Gaseous Samples Using Radiocarbon Analysis"
Validity of the certificate :	From 28 April 2011 till 28 April 2014
Conclusions of the examination :	The products comply with the above mentioned certification criteria, as confirmed by the test report of AVI no .09/ 60309554/ 104171p
Applicable certification system :	Type examination followed by supervision through verification tests on samples from the distributor's stocks and/or of the market. The conformity of the product is guaranteed by the procedures for awarding and use of the 'OK biobased' conformity mark. This only applies for specimen bearing the 'OK biobased' mark.

Caution : *The use of OK biobased-certified polymers / materials is not a guarantee that intermediate or finished product into which it is incorporated complies with the requirements of the OK biobased programme.*

This certificate is issued in English.

Brussels, 28 April 2011

For the Certification Committee

L. TORDEUR
Contract Manager

Ph. DEWOLFS
President of the Committee

Annex

09-CERTOKR-e

Figure 0.28 Polyethylene bio-based carbon content analysis report